NUCLEAR STRUCTURE INVESTIGATIONS OF SOME MEDIUM-WEIGHT ISOTOPES

by

Gavin Wallace

A Thesis submitted for the

Degree of Doctor of Philosophy

Victoria University of Wellington,
Wellington, NEW ZEALAND.

September, 1971

ABSTRACT

This thesis describes the methods and results of investigations made to determine the decay schemes of three short-lived isotopes ^{112}Ag, ^{114}Ag and ^{116}Ag.

A total of 76 γ-rays was observed with a Ge(Li) detector in the γ-radiation which follows the β-decay of ^{112}Ag to levels of ^{112}Cd. γ-γ coincidence and angular correlation measurements were made with Ge(Li)-NaI(Tl) and NaI(Tl)-NaI(Tl) systems. A decay scheme consistent with the present data is proposed. Cross sections for the reactions $^{112}Cd(n,p)^{112}Ag$ and $^{115}In(n,\alpha)^{112}Ag$ were measured, and the half-life of the ^{112}Ag decay was found to be 3.14 ± 0.01 hr.

The decay scheme of ^{114}Ag was studied with Ge(Li) γ-ray detectors and plastic β-ray detectors. 9 of the 11 γ-rays observed in the decay were incorporated into ^{114}Cd level structure previously determined by conversion electron measurements on the $^{113}Cd(n,\gamma)^{114}Cd$ reaction. The endpoint energy of the β-decay was determined as 4.90 ± 0.26 MeV; no branching was evident in the β-spectrum. A decay scheme is proposed for which the β-branching was deduced from the measured γ-ray yield and a calculated cross section value for the $^{114}Cd(n,p)^{114}Ag$ reaction. The ^{114}Ag half-life was determined as 4.52 ± 0.03 sec; a search for a previously reported isomeric state of ^{114}Ag was unsuccessful.

Ge(Li) and NaI(Tl) γ-ray detectors were used to study the direct and coincidence spectra that result from the decay of ^{116}Ag, the half-life of which was found to be 2.50 ± 0.02 min. 53 γ-rays were observed from this decay. The β-branching to the 17 excited states of ^{116}Cd in the

proposed decay scheme was derived from the measured γ-ray yield and a calculated cross section value for the $^{116}Cd(n,p)^{116}Ag$ reaction. Spin and parity assignments for the energy levels of ^{116}Cd are made.

An investigation of the applicability of two collective models to nuclear structure typical of the Cd nuclei studied demonstrated that one of the models was misleading when applied to vibrational nuclei. A potential function was developed in the other model to extend the investigation to include a study of the transition between extremes of collective motion. This was used to examine the correspondence between nuclear level schemes representative of rotational and vibrational excitations.

CONTENTS

Chapter One

INTRODUCTION

1.1 General

This thesis describes the application of some experimental and theoretical methods to determine the nuclear structure and properties of three Ag isotopes that are typical of the medium weight region of the periodic table. Attention has been focussed on the triad of odd-odd Ag isotopes with A = 112, 114 and 116, all of which have short half-lives, and the Cd nuclei that are the respective decay daughters. The choice of these isotopes was made primarily because of the lack of experimental knowledge of the decay schemes of ^{114}Ag and ^{116}Ag. Although, in the former case, the level structure of the daughter nucleus is well-known through excitations by different modes, there have been no observations of their decay reported since 1962. The decay of ^{112}Ag has been thoroughly studied with NaI(Tl) detectors, but the advent of Ge(Li) detectors with their superior energy resolution warranted a reinvestigation of the γ-rays following the β-decay. Another reason for including ^{112}Ag arises from an interesting deviation in half-lives of the three odd-odd isotopes which are approximately 3.2 hr, 5 sec and 2.5 min in order of increasing A. As the vibrational nature of the Cd daughters is little changed with A, and because the β-decay energy W_o should steadily increase with A, the Fermi theory of β-decay would predict that the half-lives become shorter if the Ag isotopes were similar. The indicated inconsistency therefore points to changes in the nuclear configurations which should be apparent from the ground states of the Ag isotopes. From the experimentally devised decay schemes, one would hope that the ground state spins and parities can be found so that the systematics of the Ag triad can be explained in terms of the single particle model.

The study of decaying nuclides includes, of course, a study of the level structure of the daughters. By a comparison of log ft values characterising the β-decay, one should gain insight into the nature of levels which are populated. The manner in which the γ-ray decay proceeds from these levels is also governed by selection rules and observation of the γ-rays should help to reveal spins and parities of the levels. The low-energy levels of the Cd nuclei are well-known to be typical of vibrational types of excitation but there are some serious departures from the simple vibrational model. It was therefore thought worth while to investigate the low-energy level structure of the Cd nuclei with a model which had been successfully applied to deformed nuclei and was capable of extension to vibrational nuclei without gross approximations to the framework of collective motion.

Except for the $^{115}In(n,\alpha)^{112}Ag$ reaction, there are only two low-energy methods of producing the required Ag isotopes: as fission products and by (n,p) reactions. The former method, because it requires chemical separations, is not easily applied to short-lived products. Fast neutron irradiation of Cd isotopes, which was therefore employed, also presents experimental difficulties that mainly arise from the low production cross sections for the Ag nuclides. Cross section calculations for (n,p) reactions[1], based on a statistical model, indicate a value of less than 6 mb for ^{112}Ag production with 14.5 MeV neutrons, and this falls to $\sim$1.4 mb for ^{116}Ag. The technique is therefore made more difficult by the undesired products of competing reactions (mainly (n,γ), (n,2n) and (n,α)) and, as there are several naturally occurring isotopes of the target element Cd, the study of the short-lived Ag isotopes requires isotopically-

enriched targets. The anticipated low yields also imply that to gain statistically significant data, the irradiation-detection process must be repeated many times and that the time durations involved should be carefully selected to minimise a build-up of contaminant radiation. Precautions must be taken to reduce background radiation while counting is in progress. Limits are obviously inherent in the method, and experiments such as the determination of γ-γ angular correlations were considered impractical for isotopes with half-lives of the order of seconds.

1.2 Outline of Contents

The next five chapters of this thesis discuss in detail the methods and objectives indicated in the preceding section. Chapter 2 describes the necessary experimental equipment and its operation as applied to short-lived isotope study, and chapter 3 is concerned with the analysis of data and its application in the elucidation of nuclear properties. The investigations on the decay of the odd-odd Ag isotopes are reported in chapter 4, and each section on an isotope is written to be complete in itself. A conclusion in this chapter re-examines the systematics of the Ag isotopes with regard to their position in the periodic table. The fifth and sixth chapters are concerned with the daughters of the Ag isotopes, and attempts are made to synthesise Cd level structures and nuclear properties in terms of collective models of the nucleus. Chapter 5 lays the framework of the models, and chapter 6 examines the results obtained by their application. A brief summary and discussion of the results of the thesis is given in chapter 7.

References for each chapter are to be found at the end of the

chapter. Computer programs used throughout the study are not listed in this thesis but are included in the Institute of Nuclear Sciences program library and are available on request.

REFERENCES

1) D.G. Gardner and S. Rosenblum, Nucl. Phys. A96 (1967), 121.

Chapter Two

EXPERIMENTAL METHODS AND EQUIPMENT

Investigations of the decay of short-lived isotopes require special instrumentation and experimental techniques. This chapter describes the methods and equipment employed to study the Ag isotopes. Much of the equipment peculiar to this work was already in existence[9,1] at the Institute of Nuclear Sciences, where this study was carried out, and although some of it has been upgraded, the detailed description given in ref.[1] is still valid.

2.1 Irradiation System

Fast neutrons were obtained for irradiation purposes by utilising the $T(d,n)^4He$ reaction. The titanium titride targets (TRT-101; obtained from U.K.A.E.A., Amersham, England) were placed in the straight-on position to the I.N.S. 3 MV Van de Graaff accelerator (High Voltage Engineering Corp. model KN), enabling deuteron currents of up to 250 μA to be used. The target, vacuum sealed with the use of Cd O-rings, was cooled by a continuous flow of water against one face; the depth of water in the target assembly was kept shallow ($\sim$2.5 mm) to minimise scattering and energy loss of neutrons. The coolant water was useful for rough calibration of β-spectra (see section 3.3C) and for monitoring neutron flux. Typically, with a 200 μA target current of 0.8 MeV deuterons, fluxes of about 1.4×10^8 neutrons $cm^{-2}.sec^{-1}$ were obtained. However, this value which was calculated from the yield of the $^{19}F(n,2n)^{18}F$ reaction, varies according to the use and age of the target. The tritium, of activity 8-10 curies, is occluded in a 2.2 mg/cm^2 layer of titanium on a 0.025 cm thick copper backing 2.85 cm in diameter. The expected energy loss of 1 MeV deuterons due to passage through the titanium will therefore be $\sim$ 440 keV[2] and most of the neutrons produced by the $T(d,n)^4He$ reaction will have energies in the range 16.0 $\pm$ 0.5 MeV[3].

Thermal neutrons were generated by the $^{9}Be(d,n)^{10}B$ reaction with paraffin used as a moderator. The thermal neutron flux resulting from a 2.0 MeV deuteron beam of 200 μA was estimated to be 3×10^{8} neutrons cm^{-2}. sec^{-1} from the yield of the $^{197}Au\ (n,\gamma)^{198}Au$ reaction.

As the process of irradiation-detection was repetitive and a minimum background rate was required while detecting short-lived products of irradiation, it was necessary to devise a beam stopper to avoid having to turn the accelerator off. This consisted of a water-cooled block of copper mounted on an eccentric shaft, perpendicular to the beam, which was rotated through 90^{o} (in 0.2s) by a double-acting air piston connected to the shaft through a simple lever. The face of the copper block upon which the beam was incident was capped by tungsten sheet (0.012" thick) in thermal contact only at the perimeter of the block. This was to ensure that the stopping surface was maintained at a high temperature, hence minimising any tendency for it to act as a drive-in target which would produce neutrons by the $D(d,n)^{3}He$ reaction. The beam stopper was earthed while operating. As well as being very effective in reducing the background radiation, it lengthened the lives of the tritium targets.

The target region was enclosed in a castle of blocks made from a mixture of paraffin (as a moderator of fast neutrons) and borax (to absorb neutrons by the $^{10}B(n,\alpha)^{7}Li$ reaction). 12" thick walls were generally employed, giving a reduction of about 80% in the neutron flux in the target room, and lowering the flux in the adjacent experimental area to below tolerance. A $\frac{1}{2}$" thick interior lining of borax was used to reduce the thermal neutron flux drifting back to the sample irradiation position.

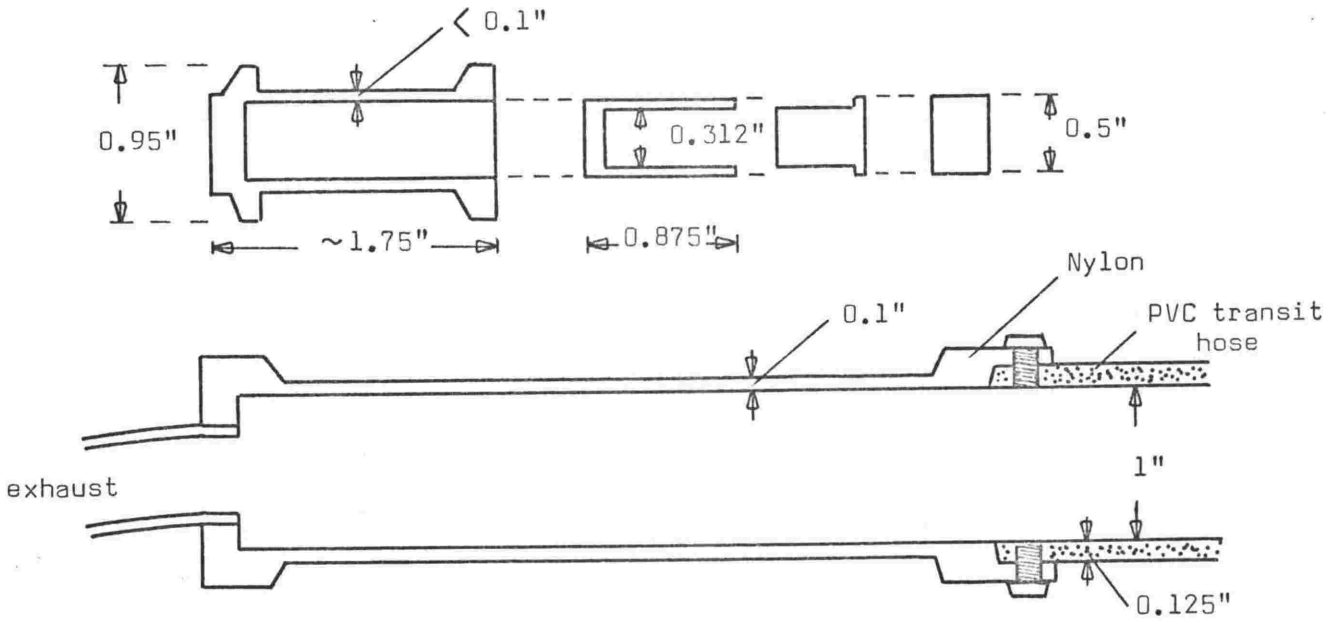

(a) γ-ray analysis

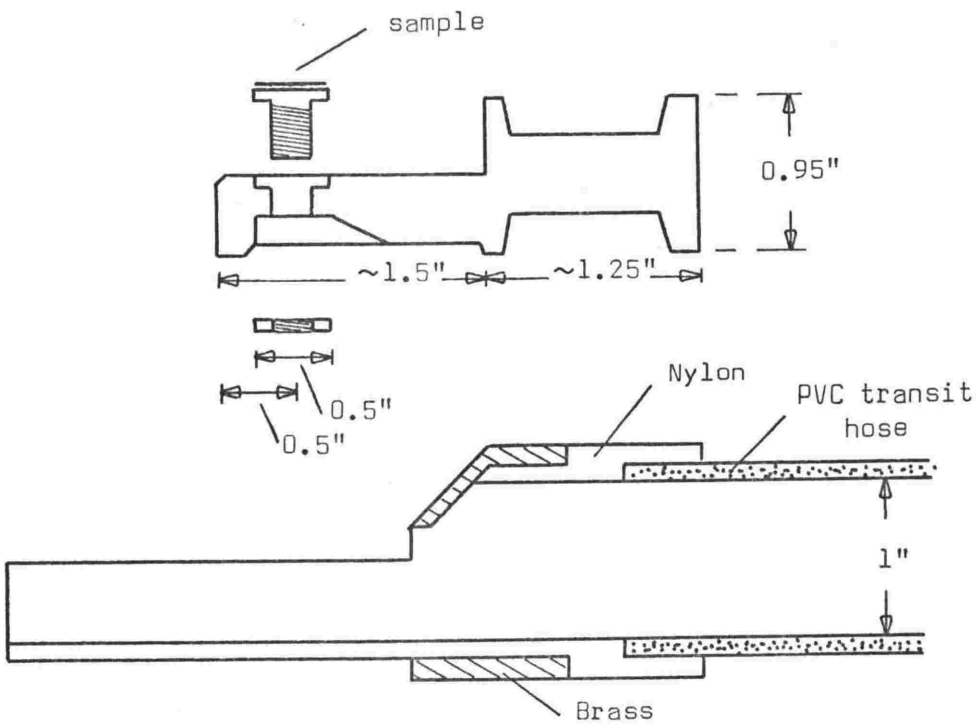

(b) β-ray analysis

Fig. 2.1 Dimensions and shapes of rabbits and heads.

2.2 Pneumatic Transport System

Samples to undergo activation to produce short-lived products were contained in or on polythene "rabbits" (see fig. 2.1). Polythene was chosen as it is the most suitable substance with necessary mechanical strength which does not give rise to interfering radiations. Capsules used for γ-ray analyses were thin-walled and contained about 18 gm of the natural element or, when enriched isotopes were used, a further cylindrical capsule which held the enriched sample. Samples and containers were sealed into the rabbits by melting in a polythene plug over a low gas flame. After trials with guidance systems for β-ray rabbits, it was found that the loss of part of the upper half of the rabbit, to create a flat surface for the sample, lowered the centre of gravity so that the rabbit did not rotate while in motion. Slurries of the sample and polystyrene, dissolved in benzene, were prepared in thin layers on the $\frac{1}{2}$" diameter heads of polythene bolts which could be inserted into recessed holes on the flat surfaces of rabbits and held with a polystyrene nut. On evaporation of the benzene, the sample is embedded in the polymer, and the attachment to the bolt will stand severe shock. Substances used for calibration purposes were prepared in the same manner. The rabbits, inserted in a 1" internal diameter PVC hose, could be moved between the detectors and the tritium target (a distance of about 30 ft, including through a 5 ft thick concrete wall) by the action of compressed air and a modified vacuum cleaner.

The irradiation and counting heads (fig. 2.1, 2.2) of the system, fitted at the ends of the PVC tube, were turned from $1\frac{1}{2}$" nylon rod. To the former, placed directly beneath the tritium target, was attached the

Fig. 2.2 Tritium target and irradiation head of pneumatic transport system. The tritium target is coupled to the beam tube but remains insulated from it.

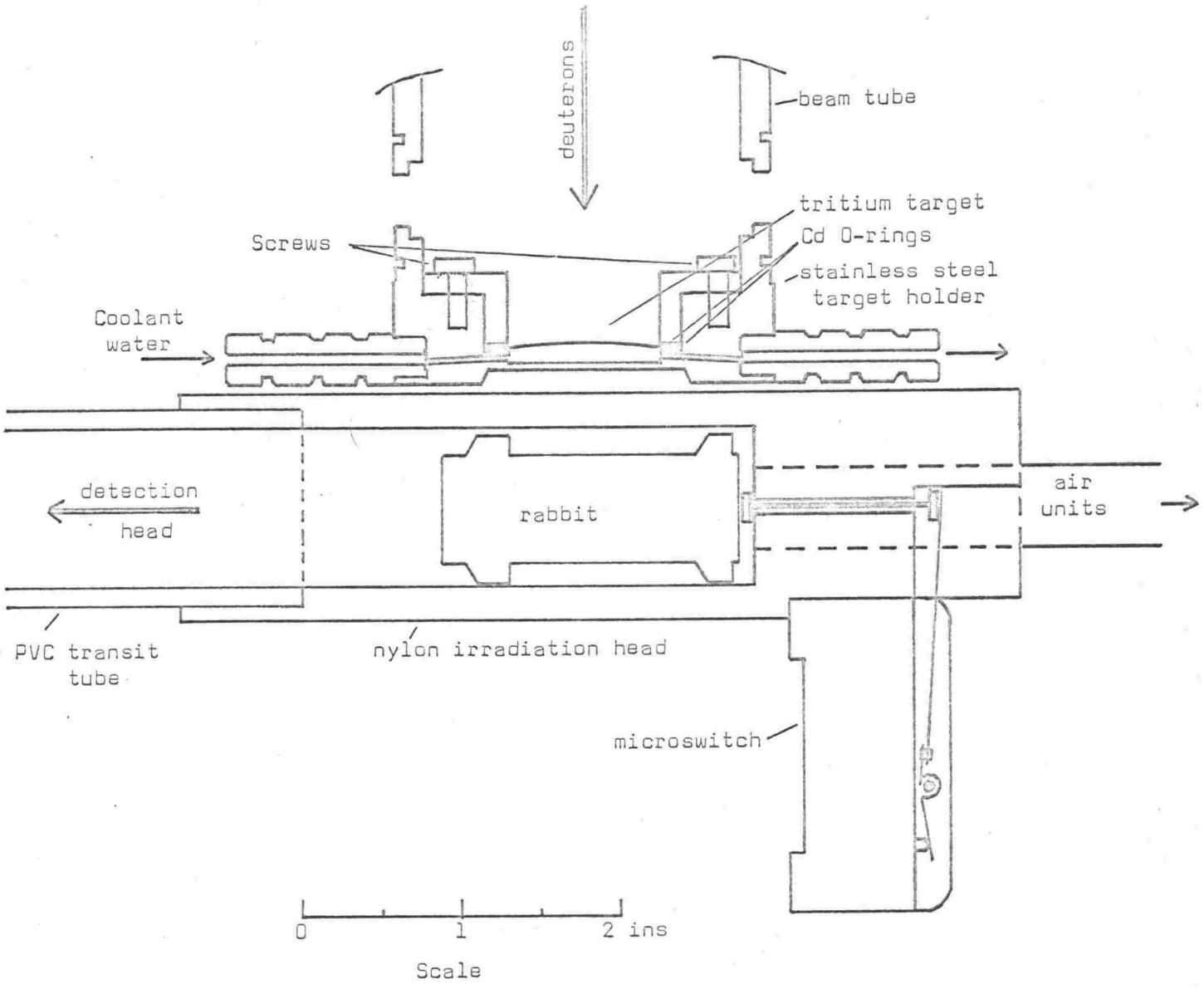

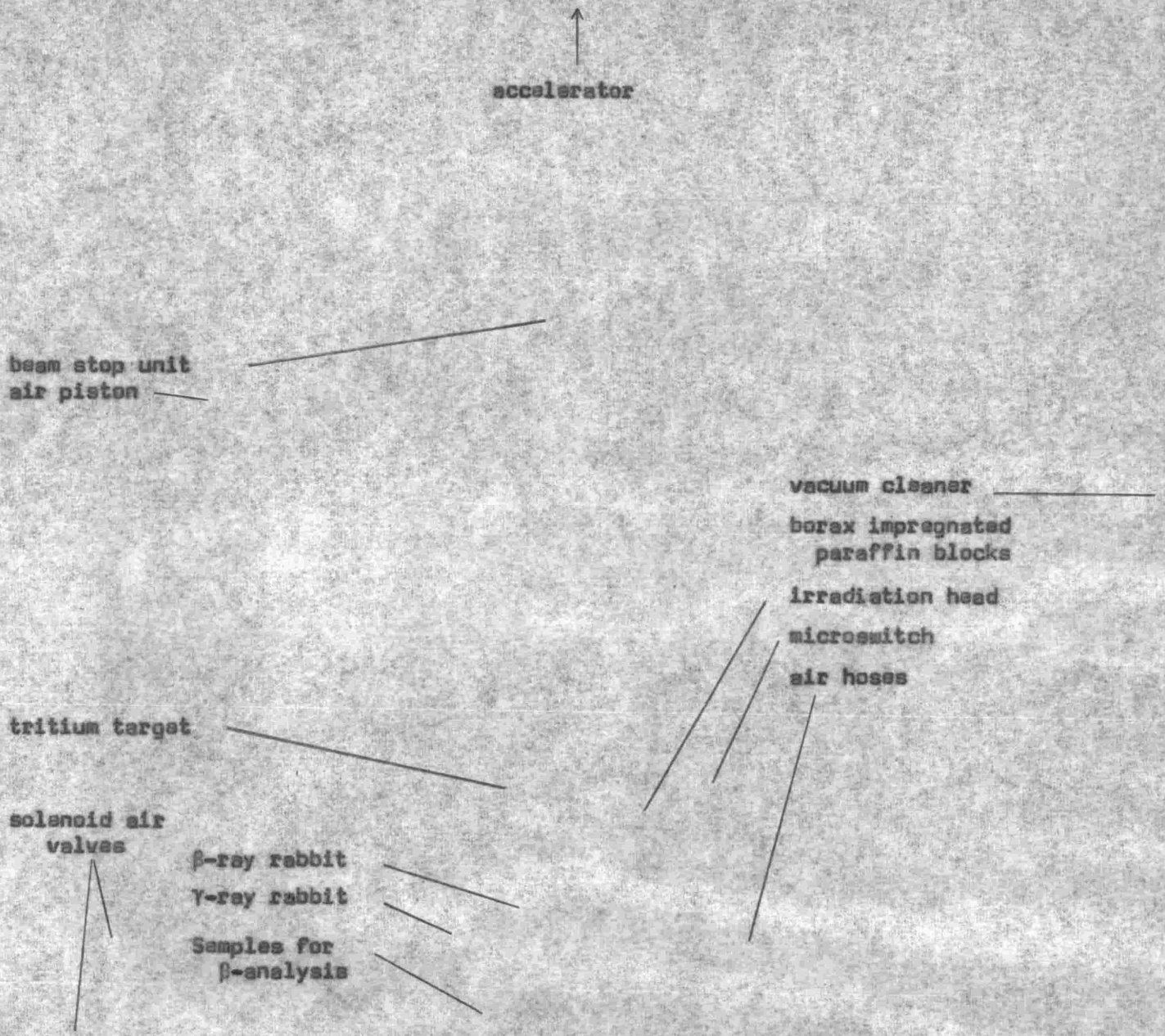

Plate 1. Tritium target assembly.

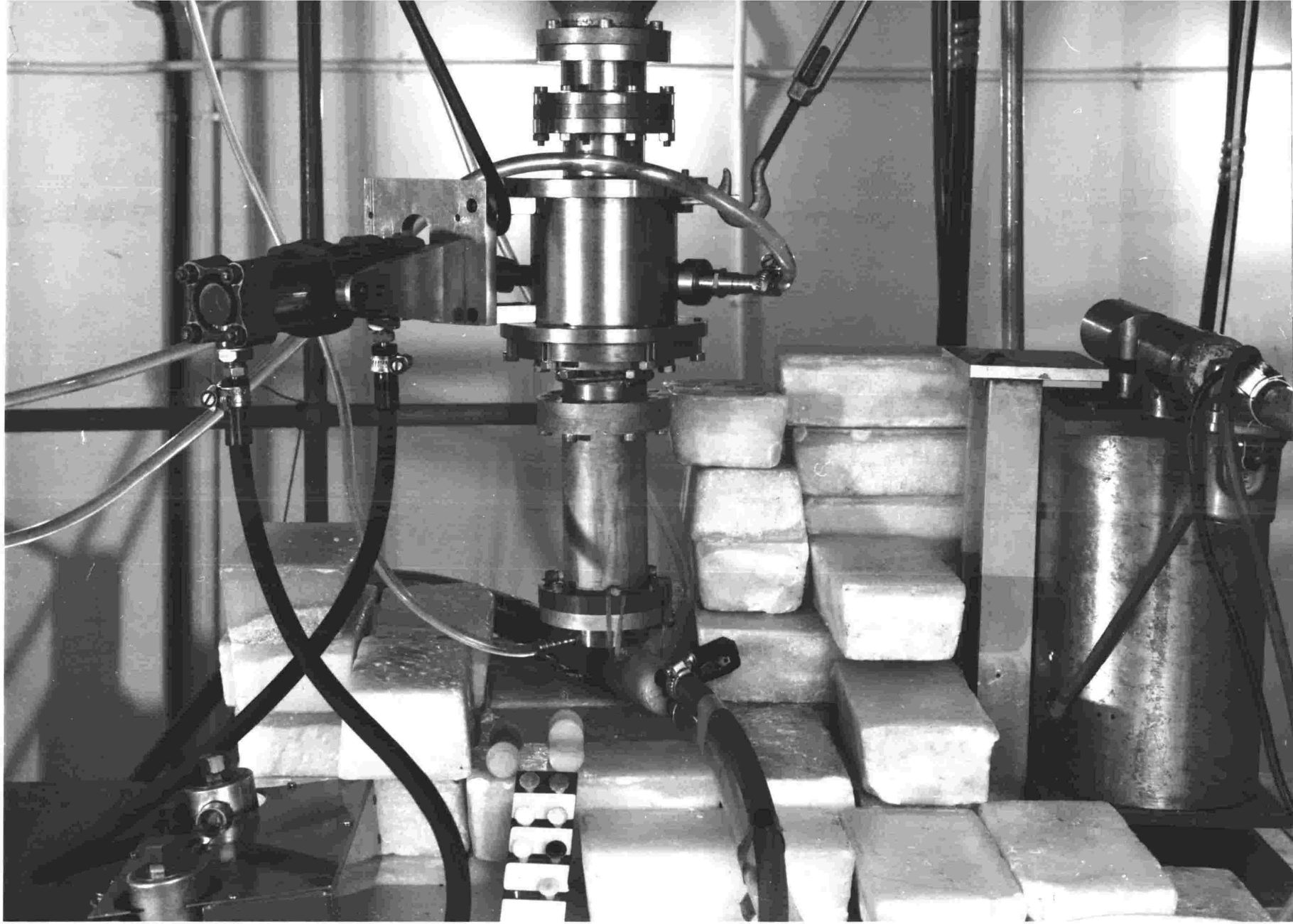

high pressure air hose and a hose from the vacuum cleaner. A microswitch mounted on this head indicated the arrival of the rabbit, thereby electronically defining the start of irradiation. A $\frac{1}{2}$" solenoid air valve allowed a blast of compressed air (at about 60 p.s.i.) into the head and blew the rabbit to the counting end. The duration of the blast was adjustable to prevent the rabbit from bouncing back from the head. Another air valve sealed off the vacuum cleaner inlet during this movement of the rabbit.

The transit times for the transport system were typically:

to detector (compressed air)	$\sim$1.0 sec
to T-target (vacuum cleaner)	$\sim$4 sec

The former transit time is of greater importance and could be shortened by increasing air pressure, but at the expense of rougher treatment of the rabbit.

Plate 1 shows the arrangement of equipment at the target end of the pneumatic system.

2.3 Cadmium Targets

Both natural and isotopically-enriched Cd metal samples were used as targets to produce Ag isotopes. No contaminant radiations were found to arise from expected elemental impurities. The enriched samples were obtained on loan from the Electromagnetic Separation Group, A.E.R.E., Harwell, on condition that they would not be subjected to more than 15,000s irradiation in a 14 MeV neutron flux of 10^9 neutrons $cm^{-2}.sec^{-1}$, and that the samples were not contaminated with any long-lived activities. The mass analyses of the samples are:

Isotope	Abundances %		
A	^{114}Cd sample(3 gm)	^{116}Cd sample(1 gm)	Natural
106	0.01	-	1.22
108	0.02	-	0.88
110	0.18	-	12.39
111	0.16	0.2	12.75
112	1.25	0.22	24.07
113	0.31	0.11	12.26
114	97.84	1.31	28.86
116	0.02	98.14	7.58

2.4 Detection Systems

The construction of a suitable environment to enable spectroscopy of low activities was carried out according to the suggestions of Heath[4]. Radiation from the activated samples was detected in a lead castle of internal dimensions 27" x 23" x 36". The walls and top of the castle were 4" thick, and were internally lined, first with 26 gauge copper sheets, and then with 1/4" thick perspex (in place of the more usually used cadmium lining[5]). The linings were used to inhibit the detection of fluorescent X-rays of lead which result from primary radiation in the shield wall. The castle was situated in a concrete pit about 6 ft below ground level.

Several Ge(Li) semiconductor detectors, ranging in active volumes from 5 to 30 cm^3, were fabricated at the Institute of Nuclear Sciences[6] but their long term stabilities varied considerably. Resolutions, generally from about 5 keV (fwhm) at 1.332 MeV photon energies, and peak-to-Compton ratios usually worsened within a period of months. These effects are believed to arise from a gradual deterioration of the surface conditions of the detector, resulting in increased leakage current, caused

by a slow build-up of pressure inside the cryostat. Near the end of this study, a 32.1 cm^3 Ortec Ge(Li) detector, with a 2.2 keV fwhm at 1.332 MeV and a peak-to-Compton ratio of 26:1, became available. Various NaI(Tl) crystals were also available for γ-ray spectroscopy and these were used in coincidence systems.

A 3" x 3" cylinder of plastic scintillator (NE102), painted white with a water-based reflector paint (NE560) and encased in earthed aluminium foil to reduce noise, was optically coupled to a 3" Dumont K1846 photomultiplier tube to serve as a β-detector. In a compromise between geometric efficiency and spectral response, incident radiation was partially collimated through $\frac{1}{2}$" aluminium plate such that the solid angle for a point source in the experimental configuration was $\sim$0.6 steradians. Further discussions on detector performance are given in the next chapter.

Standard NIM electronics were used for amplification and pulse detection. Pulse-height analysers available were a 256-channel RCL, a 512-channel Nuclear Data (ND130AT), a 4096-channel Kicksort (711) and a Digital Equipment Corp. PDP-8 computer with an associated Nuclear Data 1024-channel dual ADC (ND160F). The latter was used to obtain time-sequences of spectra[7]: a start pulse from one side of the dual parameter ADC commenced accumulation of pulses from the other side in a fixed sequence of memory regions of the computer for a preset time in each. It was possible to set multiples of from 3 x 1024 channels to 48 x 64 channels, and the cycle could be repeated so that spectra from the decay of short-lived isotopes could be built up to obtain results of statistical significance. The computer plus ADC could also be used in two-dimensional coincidence detection for up to 64K channels with the bulk storage

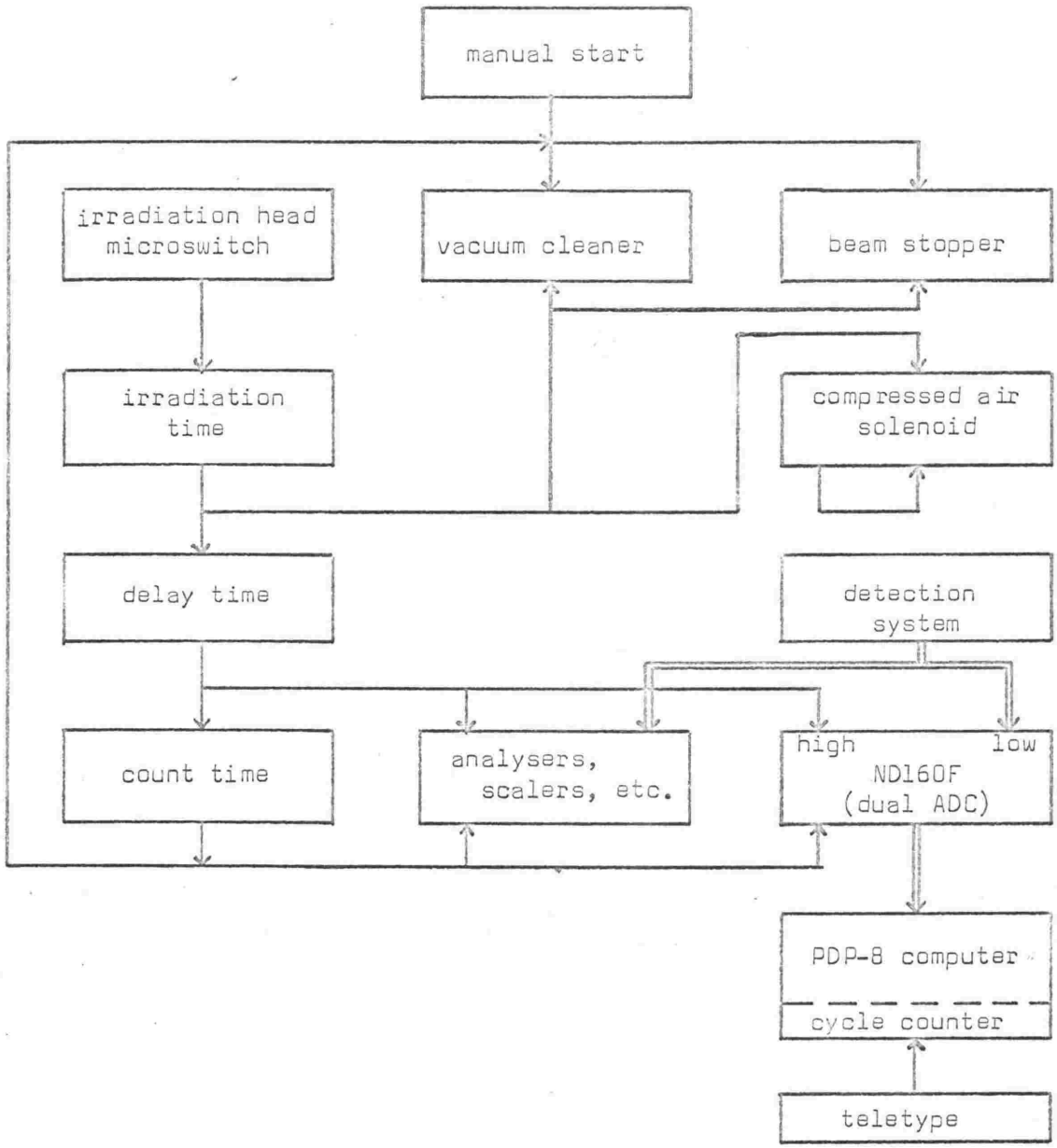

Fig. 2.3. Schematic control system and the sequence of events for short-lived isotope detection.

available[8]. Other pulse-height analysers were controlled by gating with suitable voltage levels.

2.5 Control System; Sequence of Events

The study of short-lived nuclides and the necessity to recycle the irradiation and counting process obviously required automation of the system. Equipment associated with the pneumatic transport system and most of the necessary detection units were interfaced to an autoprogrammer which had been built at I.N.S.[9]. This, together with an associated 6-channel timing unit, variable from 1 msec to 999 sec, could start, stop and reset equipment. The sequence of events, shown schematically in fig. 2.3, was preset by connections in a patchboard. The timing of the PDP-8 was derived from clock pulses of the ADC and not from a timing unit of the autoprogrammer.

REFERENCES

1) P.J. Mathew, Thesis, Victoria University of Wellington (1969).

2) J.B. Marion and F.C. Young, "Nuclear Reaction Analysis", North-Holland (1968).

3) N.G. Chapman and P.B. Johnson, VUW Phys. Report NP7 (1966).

4) R.L. Heath, AEC Report, IDO-16880-1 (1964).

5) K. Siegbahn, "α-, β- and γ-ray Spectroscopy", North-Holland (1966).

6) G.E. Coote, INS Report INS-R-42 (1967).

7) H.J. Hay, INS Report INS-R-59 (1968).

8) K.P. Pohl and M.R. Manning, to be published in Nucl. Inst. and Meth. (1971).

9) K.A. Bargh, INS Report INS-IM-A3 (1964).

Chapter Three

SPECTRUM ANALYSIS AND DATA REDUCTION

This chapter formulates the methods and analyses found necessary to relate experimental measurements to nuclear properties and structure. It is, of course, in no way complete, but does deal with some specific problems peculiar to short-lived isotope decay and the experimental methods applied in this work.

3.1 Computing Facilities

There are, at present, two computers at I.N.S. to facilitate data collection and analysis. The older of the two is a Digital Equipment Corp. PDP-8 which has a 4K, 12-bit word core memory. The other is a PDP-9/L, with an 8K, 18-bit word core memory. Although larger, the latter is not as flexible as the PDP-8 since the smaller machine has additional 64K bulk storage in the form of magnetic discs. CRO and plotting facilities are interfaced to both computers as well as high-speed paper tape handling units. Extended arithmetic elements (EAE) have also been installed. Pulse-height analysers are interfaced to the PDP-8 for dumping of spectra to the computer. Use also could have been made of an Elliott 503 computer with 24K memory of 39-bit words. However, the ready access to, and the on-line analysis by, the smaller machines outweighed the advantages of the larger and faster computer.

Several languages are available for use on the PDP- series computers, but programming is chiefly in MACRO or FORTRAN. The PDP-9/L uses FORTRAN-IV and a mnemonic language called MACRO-9. The equivalent PDP-8 languages are a disc version of FORTRAN-II and MACRO-8, and these are somewhat more limiting. FORTRAN-II is a one-pass compiler, the object programs being run with operating systems of fixed dimensions. PDP-8

programs are not relocatable and because of the limited capabilities of the assemblers, one can generally write more efficiently in MACRO.

2.2 γ-Ray Spectrum Analysis

2.2.A Spectral Shapes.

Discussions of the origin, detection and detectors of γ-rays are to be found in most elementary text books on nuclear physics, and will therefore not be included here in detail. With the advent of high-resolution Ge(Li) detectors, escape- and photopeaks have assumed primary importance while the presence of corresponding Compton responses in the γ-ray spectrum has become rather inconvenient, particularly as it is more difficult to predict the shape resulting from this multiscattering process. The Compton spectrum may be reduced by anti-coincidence detection systems, but it is more usual to fit a continuum and subtract this from the peaks in the total spectrum.

If several reaction products are present with different decay modes, then the resulting γ-ray spectrum will be complex, with possible overlapping peaks. It is then necessary to have either standard line shapes which can be adjusted to fit the experimental peaks, or to have analytical expressions describing the peaks. The inferior resolution of a scintillator spectrum demands the latter method of analysis, and it is normal to use the entire spectrum resulting from a single γ-ray for the fitting of complex spectra. The standard spectra may be synthesised or experimental, and one fits by linear least-squares methods to the unknown spectrum as a whole, or to each peak singly. In the latter case fitting begins at the high-energy end and each fitted standard is successively subtracted in a process known as spectrum peeling.

Peaks in a γ-ray spectrum result when the γ-ray loses its total energy in one interaction and the peak should therefore be a line. However, the charge or photon collection process within the detector is governed by Poisson statistics and, with random preamplifier noise, this results in the response having a Gaussian shape. As only 3 eV of energy is required to generate an electron-hole pair in Ge, compared with a typical value of 300 eV for a phosphor, the number of ion-pairs generated by a γ-ray photon is two orders of magnitude larger in Ge. Efficiency of conversion of holes into near-optical radiation and the photomultiplication process further increases this proportion so that the energy resolution of a phosphor is considerably inferior to that of semiconductors. It is only because of their much higher photopeak efficiency and adaptibility that the NaI(Tl) detectors have continued to be useful in γ-ray spectroscopy.

Since a photopeak can be represented by a Gaussian energy distribution, one could, by taking logarithms and appropriate weighting, perform a linear least-squares fit to an experimental photopeak to find its parameters. However, incomplete charge collection in the semiconductor, caused by trapping effects of impurities in the crystal lattice and bremsstrahlung energy losses in multiple Compton events, by reducing the size of some of the voltage pulses to be analysed, adds a low energy tail to the expected Gaussian. The adopted analytical expression for a photopeak is that suggested by Routti and Prussin[2)]

$$N_i = A \exp\left[f(z)\right] \tag{1}$$

where

$$\begin{aligned} f(z) &= -z^2/2\sigma^2 && -1 \leqslant z \leqslant h \\ &= (2z + 1)\, 1/2\sigma^2 && z < -1 \\ &= (-2z + h)\, h/2\sigma^2 && z > h \end{aligned} \tag{2}$$

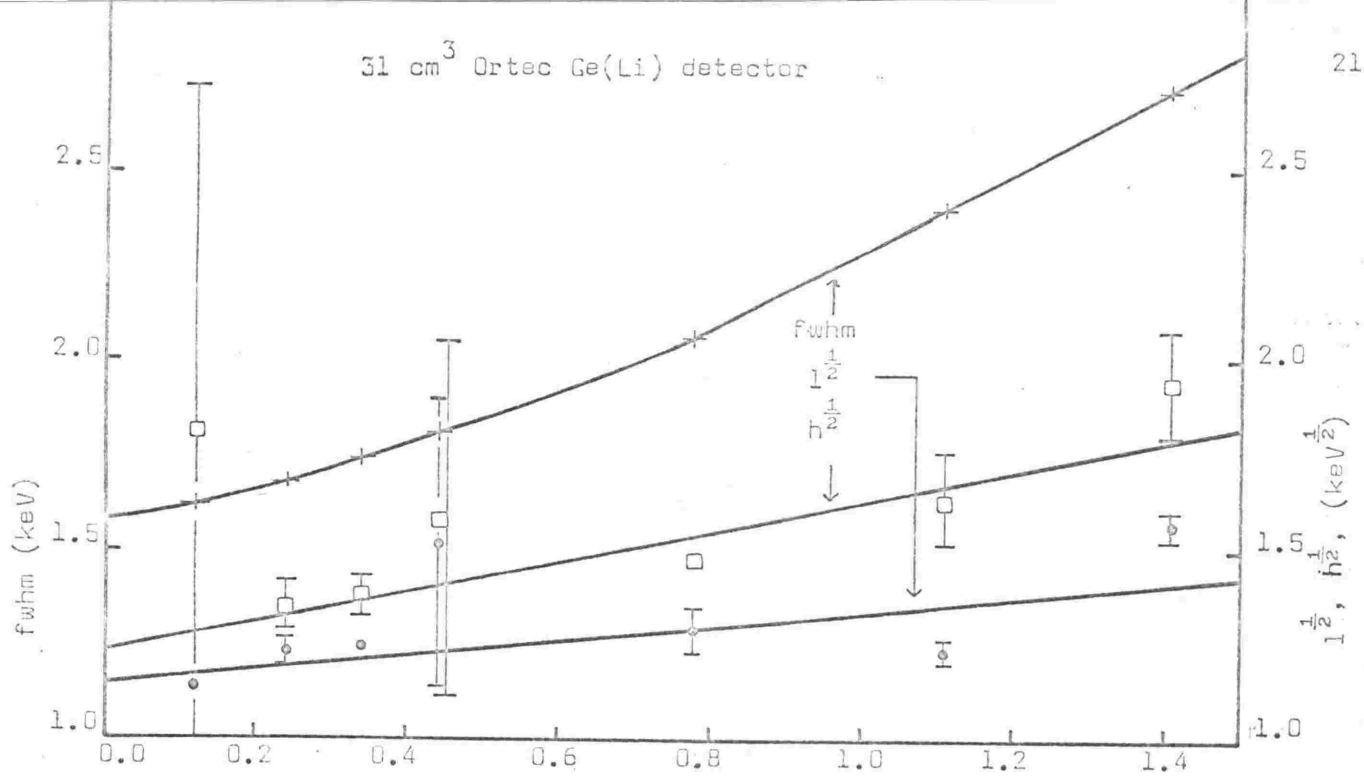

Fig. 3.1(a) Variation of photopeak shape parameters with energy (^{152}Eu)
fwhm=$\left[(0.361+1.327E)^2+1.537^2\right]^{\frac{1}{2}}$, $l=(1.15+0.19E)^2$, $h=(1.23+0.39E)^2$ keV

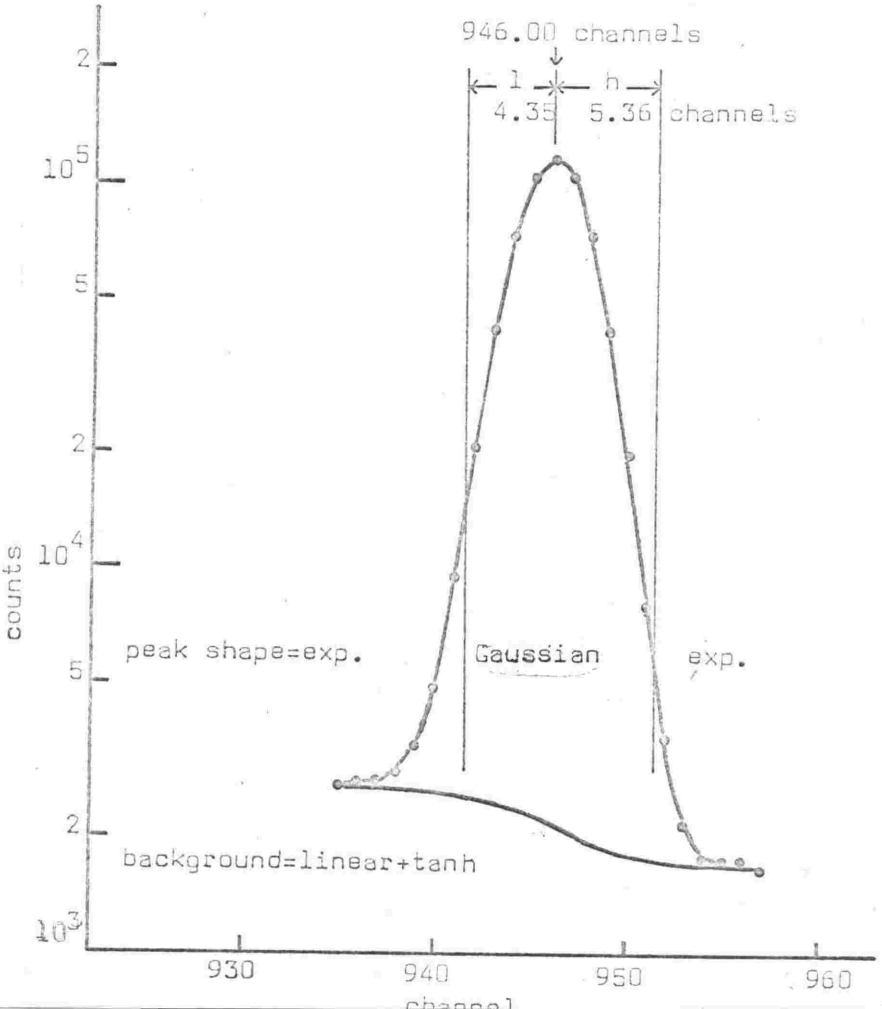

Fig. 3.1(b) Fit to 344.3 keV photopeak of ^{152}Eu, χ^2=3.65

for

$$\begin{aligned} z &= (i - \bar{i}) \\ \sigma &= \text{fwhm}/2\ (2\ \ln 2)^{\frac{1}{2}} \\ A &= \text{height of the peak} \\ \bar{i} &= \text{position of the peak in channels} \end{aligned} \tag{3}$$

The shape of the peak is described by a Gaussian in the central region, and the tails are assumed to be simple exponentials which join the Gaussian so that the function and its first derivative are continuous. l and h are the distance in channels from the centroid of the peak to the lower and upper junction points. These parameters and the fwhm are fixed by interpolation from values obtained for isolated peaks of the same spectrum. The following formulae give the best representation:

$$\begin{aligned} l &= (AL + BL*E)^2 \\ h &= (AH + BH*E)^2 \\ \text{fwhm} &= \left[(AF + BF*E)^2 + CF^2\right]^{\frac{1}{2}} \end{aligned} \tag{4}$$

where E is the energy of the peak in MeV. Note that the relation for fwhm is derived from the overlap of two Gaussian responses: detector and electronic noise. Attempts[3] have been made to predict these coefficients for a particular detector in terms of the energy parameters of a spectrum, but no firm relationships can, as yet, be made. A typical set of these parameters is shown in fig. 3.1(a).

To compensate for the discontinuity in a linear background under very large peaks it was found necessary to include a tanh-type background estimated from first approximations to the peak parameters:

$$B_i \alpha A' \tanh(-0.95\, z'/\mathrm{fwhm}) \quad (5)$$

This function greatly improved the stability of fitting as the boundaries of the fitting interval were changed. An example of a fit to a large peak is given in fig. 3.1.(b). Methods and programs using these analytical shapes are fully described in references[1,4].

3.2.B γ-Ray Calibration

The energy calibration of a γ-ray spectrum in the energy range 0.1 - 3 MeV is almost trivial as the photon energies of a large number of long-lived radioactive isotopes have been accurately determined for this purpose[5]. The detection system was calibrated before and after an experiment with common γ-ray sources and, particularly when counting over long durations of time, a gain stabiliser was used. The calibrations obtained were fitted to polynomials by least-squares procedures from which the energies of unknown photopeaks were obtained. When the relationships of γ-rays (such as escape peaks and energy level systematics) of a spectrum had been established, they were then used to bootstrap[6] a subsequent recalibration.

The efficiency calibration, relating the changes in cross sections for various detection processes, is more difficult to achieve and, as Ge(Li) detectors do not at present lend themselves to rigid calculations, it is usually carried out with sources of known intensities. The full-energy peak efficiency is then obtained by comparison of the experimentally determined photopeak intensity with the known intensity. There are several sources calibrated for this purpose[5,7]. The geometry of the rabbit source and the detector is complicated because the source is

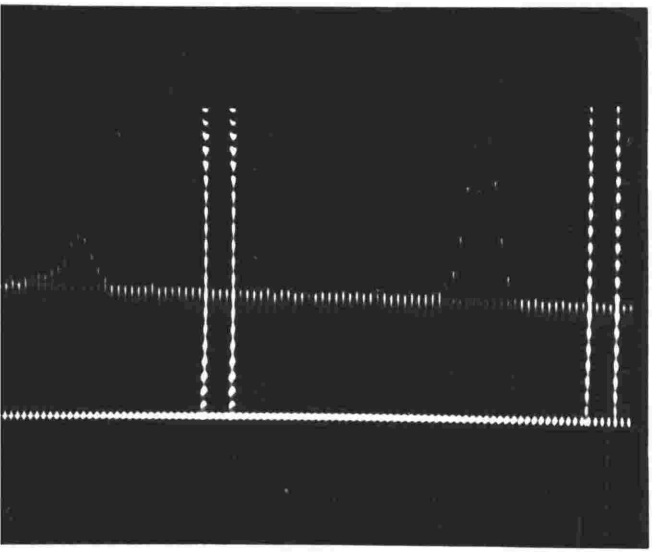

Background fit, data selected by pairs of markers.

χ^2 = 0.34/degree of freedom

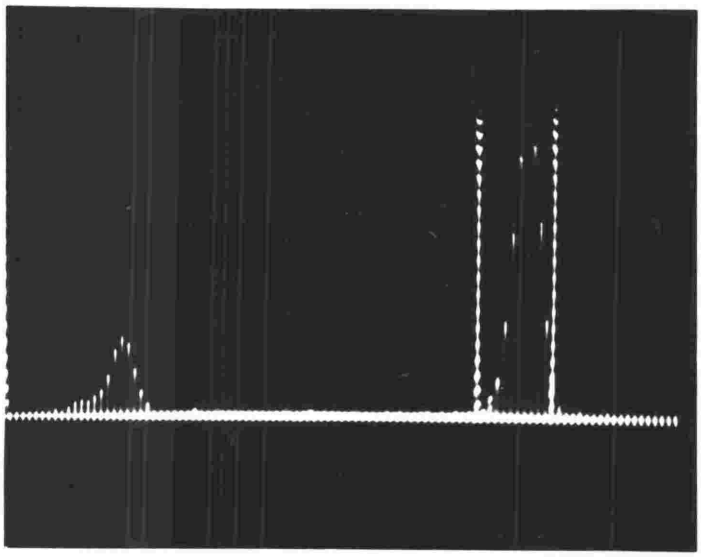

Background removed, fit to one peak defined by one pair of markers.

χ^2 = 7.45/degree of freedom

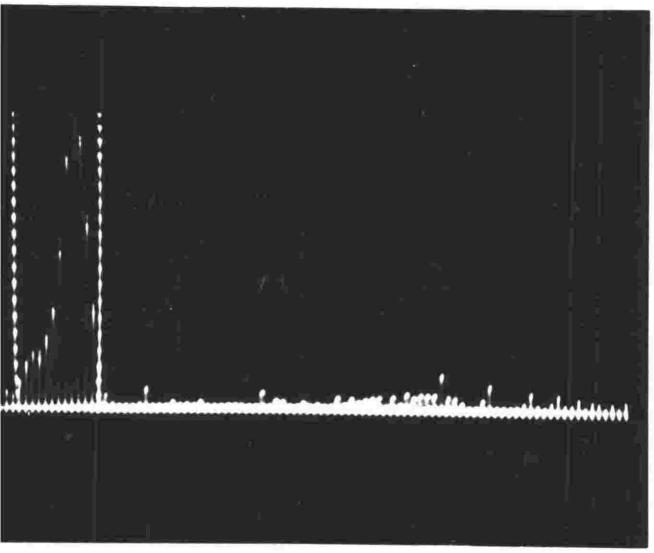

Single peak removed, fit to remaining doublet.

χ^2 = 1.46/degree of freedom

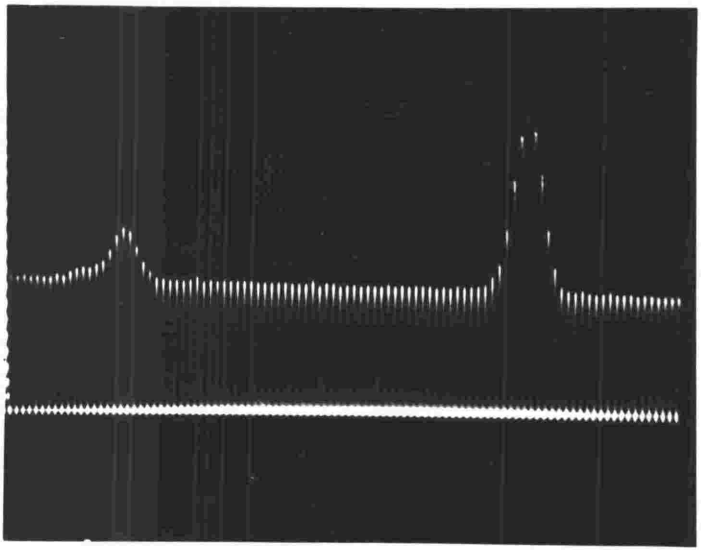

Total calculated spectrum overlaid on the original data.

Plate 2. Computer-assisted analysis of γ-ray spectra (interactive version on the PDP-8).

extended and as close to the detector as possible. Consequently, experiments were designed such that a knowledge of the relative, rather than the absolute, efficiency was required.

As it is preferable to express the efficiency as a function of γ-ray energy, and carry out a least-squares fitting procedure to get an unbiased estimate of errors, use was made of the fact that the full-energy peak efficiency of a Ge(Li) detector very nearly obeys a power law in the range 0.2 to 3.0 MeV, and that the relative efficiency can be fitted to [8]

$$\ln (\epsilon_m/\epsilon_n) = b (x_m - x_n) + c (x_m^2 - x_n^2) \quad (5)$$

where

$$x = \ln (1022/E_\gamma) \text{ and } E_\gamma > 150 \text{ keV} \quad (6)$$

Fig. 3.2 shows the relative photopeak efficiency curve and escape peak ratios for the 31 cm^3 Ortec detector. The parameters b and c for this detector are

$$b = 1.1828 \qquad c = 0.0479$$

3.3 β-Ray Spectrum Analysis

The detection of β-particles is similar in many ways to that for γ-rays, although, in the former case, the β-spectrum is continuous in energy. Decays with short half-lives imply allowed transitions with high endpoint energies (W_o), and the use of rabbits limits suitable β-ray detectors to Si(Li) semiconductors and plastic scintillators. Since the anticipated maximum energy of the β-rays to be studied was ~6 MeV, involving a range of ~1 cm in Si, plastic scintillators had to be used. Because of their poor resolution and incomplete absorption of the energy

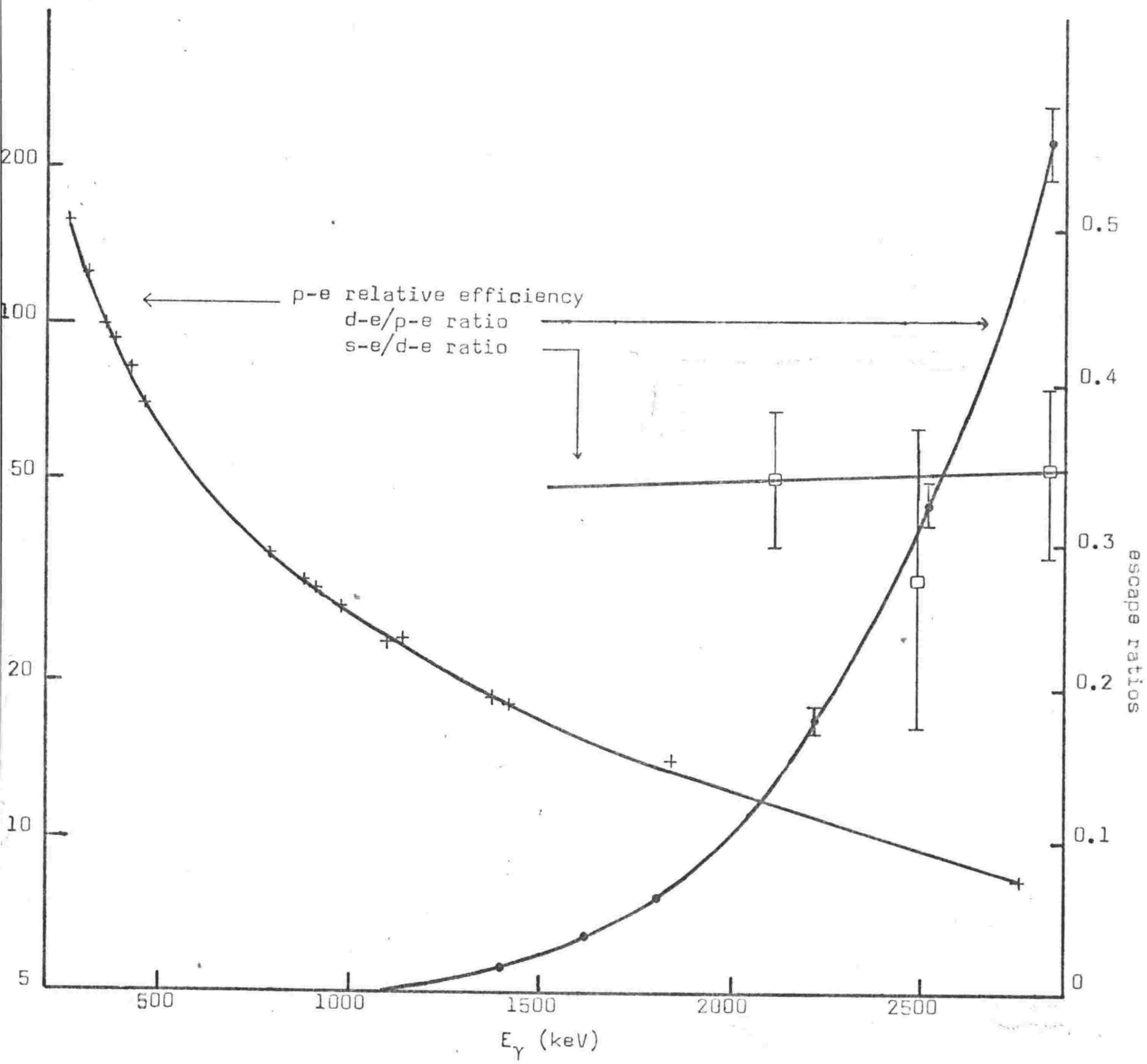

Fig. 3.2. Full-energy peak efficiency and peak intensity ratios of the 31 cm^3 Ortec Ge(Li) detector.

of the incident β-particles within the scintillator, corrections are necessary to conteract distortions of the spectral shape. The anticipated energy range of the β-particles allows neglection of screening effects and bremsstrahlung.

3.3.A Spectral Shapes

A β-ray spectrum is analysed basically by the comparison of the measurement with the results expected from theory. The Fermi theory of β-decay predicts an energy distribution of $\beta^{\pm}$-particles (positrons and electrons) which can be expressed

$$N_{\pm}(W)\,dW = \frac{g^2}{2\pi^3}\,F(\mp Z,W)\,pW\,(W_o - W)^2\,S_n(W)dW \qquad (7)$$

where $N_{\pm}(W)dW$ is the number of $\beta^{\pm}$-rays in the energy range $W \longrightarrow W + dW$, and g is a factor involving nuclear transition elements (constant for a particular decay). The term $pW\,(W-W_o)^2\,dW$ represents the statistical shape (with relatvistic β-ray energy W and momentum p in m_oc^2 and m_oc units respectively) and the shape factor, $S_n(W)$, signifies that the transition is n^{th} forbidden. For an allowed transition (n=o), $S_n(W)$ is independent of energy, and it can usually be expressed as a polynomial in W for forbidden spectra.

The Fermi function, $F(\mp Z,W)$, is the relativistic ratio of the electron density at the nucleus to the density at infinity (F=1 for Z=0) and represents the Coulomb interaction between nucleus and β-particle. When the nucleus is treated as a point charge, but with the density ratio evaluated at the nuclear radius R, then[9)]

$$F(\mp Z,W) = \frac{2(1+\gamma_o)\left[\frac{2pR}{\hbar/m_o c}\right]^{-2(1-\gamma_o)}}{\left[\Gamma(2\gamma_o+1)\right]^2}\left|\Gamma(\gamma_o+i\nu)\right|^2 e^{\pi\nu} \qquad (8)$$

where

$$\gamma_o = \left[1-(\alpha Z)^2\right]^{\frac{1}{2}}, \quad \alpha = \frac{e^2}{\hbar c} \doteq \frac{1}{137}, \quad \nu = \mp \alpha ZW/p \qquad (9)$$

The reduced Fermi function

$$g(\mp Z,p) = p^{2\gamma_o}\left|\Gamma(\gamma_o+i\nu)\right|^2 e^{\pi\nu} \qquad (10)$$

is tabulated[9,10], and therefore

$$F(\mp Z,W) = \frac{2(1+\gamma_o)\left[\frac{2R}{\hbar/m_o c}\right]^{-2(1-\gamma_o)}}{\left[\Gamma(2\gamma_o+1)\right]^2} \times \frac{W}{p} \times \frac{g}{p^2} \qquad (11)$$

The first factor can be calculated quite easily for a particular daughter nucleus (Z), and is independent of momentum. The factor $\frac{W}{p}$ is included for the transformation from a momentum distribution to one of energy. For ease in programming, an approximation[11] for the reduced Fermi function was used for which

$$\left|\Gamma(\gamma_o+i\nu)\right|^2 \doteq \left|\Gamma(1+i\nu)\right|^2 / (\nu^2+\tfrac{1}{4})^{1-\gamma_o} \qquad (12)$$

and $$\left|\Gamma(1+i\nu)\right|^2 = \pi\nu / \left|\sinh\pi\nu\right|$$

giving

$$g(\mp Z,p) \doteq 2\pi\nu\, p^{2\gamma_o} / (1-e^{-2\pi\nu})(\nu^2+\tfrac{1}{4})^{1-\gamma_o} \qquad (13)$$

The accuracy of this was checked with the tabulated values of Fano[9] and deviations were found to be less than 0.1%.

Hence, for an allowed transition, a plot of

$$\left[N_{\pm}(W)/F\ (\mp Z,W)\ pW \right]^{\frac{1}{2}} \text{ - vs - } W$$

is linear, and the intercept on the W-axis gives the total disintegration energy W_o. A linear plot for forbidden spectra can be obtained by applying a suitable function, $S_n(W)$. Obviously then, the above Fermi-Kurie plot will also reveal spin and parity changes in the β-transitions and, where there is more than one group of β's present, it will give the relative intensities and endpoints of the different groups. Determination of the latter transition properties is facilitated by a method of Ford and Hoffman[12].

The comparable half-life, ft, is widely used to indicate spin and parity changes involved in the transition. The total probability of decay for a given β-transition is

$$\lambda_{\pm} = \int_1^{W_o} N(W)\ dW = \ln 2/t$$

$$= (g^2/2\pi^3) \int_1^{W_o} F(\mp Z,W)\ pW\ (W_o-W)^2\ S_n(W)\ dW \qquad (14)$$

where t is the half-life for the decay. For the allowed spectrum

$$S_o \int_1^{W_o} F(\mp Z,W)\ pW\ (W_o-W)^2\ dW = S_o f_o(\mp Z,W) \qquad (15)$$

giving the Fermi integral function f, which is tabulated; hence it can be seen that the product $f_o t$ only involves nuclear matrix elements for the transition. When the transition is forbidden, the correct shape factor must be applied[13], and if there is branching then the partial half-life and corresponding $f(Z,W_{o_i})$ must be used. Nomograms for calculation of

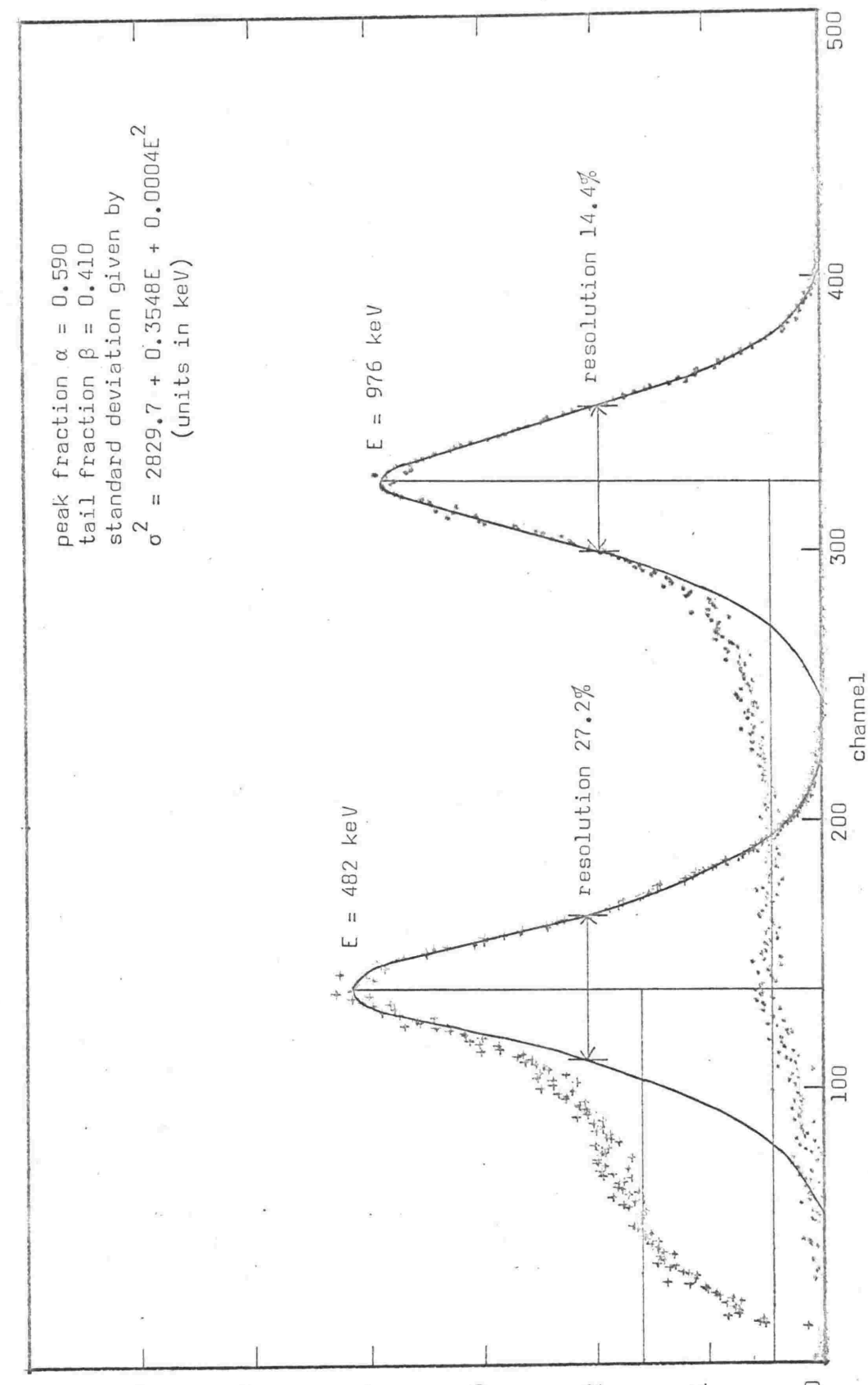

Fig. 3.3. Conversion electron peaks of ^{207}Bi showing the assumed Gaussian plus tailing response. The drop in counts at low energy is due to the coincidence system used.

ft values are given by Verrall et al.[14], and Gleit et al.[15] place limits upon their interpretation.

3.3.B Corrections for β-Ray Spectra

The response of a plastic scintillator to mono-energetic electrons, examples of which are shown in fig. 3.3, is a Gaussian peak associated with the totally absorbed β-rays plus a constant-height tail which arises from partial energy losses due to scattering from the crystal[16]. The ratio of intensities of the tail and peak appears to be independent of the incident electron energy[17]. Obviously, such a response will distort the shape of the accumulated β-spectrum, and efforts should be made to counteract the distortions. Some improvement can be obtained by good collimation of the incident β-particles but the effect cannot be completely removed by arrangement of the experimental configuration. Before applying the analysis of the preceding section, attempts should be made to correct the β-spectrum.

Palmer and Laslett[18] derived a resolution correction for β-spectra using a truncated Taylor expansion but as this involves the assumption of an analytical form for the undistorted spectrum and as it is likely that only the first two derivatives can be evaluated with precision, this method is unsatisfactory. A numerical method is more attractive, i.e., the distorted spectrum, a column vector M, is given by

$$M = RS \tag{16}$$

where S is the undistorted or true spectrum and R is the response of the system. Dixon and Aitken[19] have shown that the existence of the inverse matrix R^{-1} for a Gaussian response is doubtful, and Slavinskas et al.[20],

assuming its existence, have proved that its use would lead to greatly enhanced errors in the practical case. The latter workers extended an iterative method for resolution correction[17] such that fewer iterations were required and tailing corrections could be included. It is this procedure which has been adopted in the work reported here.

If S^1 is the first estimate of the true spectrum, then a second estimate, S^2, can be obtained from the relation

$$S^2 = S^1 + M - RS^1 \tag{17}$$

and after m iterations

$$S^{m+1} = S^m + M - RS^m$$
$$= (I - R^m)\, S^1 + R^{-1} \left[I - (I - R)^m \right] M$$

where I is the identity matrix. In the limit, provided $(I - R^m) \longrightarrow 0$, then

$$\lim_{m \to \infty} (S^{m+1}) = R^{-1}M \tag{18}$$

Freedman et al.[17] found this process to converge within 2-4 iterations to S^{m+1} where RS^{m+1} reproduced M to within 2% accuracy. R^{-1}, although assumed to exist, is not used and does not have to be evaluated directly. The statistical deviations show a linear increase with each iteration, thus requiring that the number be kept to a minimum. To do this[20], the full response matrix is approximated as a product of a triangular matrix (for tailing corrections) and a Gaussian matrix (for resolution correction), since the former can be inverted in closed form. The application of the tailing correction gives a good first guess S^1 of the true spectrum, with very little increase in error, and with only one iteration required to

correct for the remaining Gaussian resolution.

The response function shown in fig. 3.3 can be approximated to a convolution of a Gaussian $G(E,E_o)$ with a tailing function $L(E,E_o)$,

$$\text{i.e.} \quad R(E,E_o) = \int L(E,E')\, G(E',E_o)\, dE' \tag{19}$$

$$\text{where} \quad L(E,E_o) = \frac{k_o + \delta(E-E_o)}{k_o E_o + 1} \qquad E \leqslant E_o \tag{20}$$

$$= \qquad 0 \qquad\qquad E > E_o$$

$$\text{and} \quad G(E,E_o) = (1/\sqrt{2\pi}\,\sigma) \exp\left[-(E-E_o)^2/2\sigma^2\right] \tag{21}$$

Since spectra are digitised, the response functions are replaced by matrices. Then

$$M = LGS \quad \text{and} \quad L^{-1} M = GS = S^1 \tag{22}$$

and the first guess S^1 is good because the spectrum is continuous and has a "width" very large compared with G.

If α_i, β_i are the areas under the peak and tail respectively, then

$$\beta_i = k_i E_i / (k_i E_i + 1), \qquad \alpha_i = 1 - \beta_i \tag{23}$$

and with these definitions and the assumption that α, β are independent of energy

$$\begin{aligned} L_{ii} &= \alpha \\ L_{ij} &= 0 \quad \text{for} \quad i > j \\ L_{ij} &= \beta / (i-1) \quad \text{for} \quad i < j \end{aligned} \tag{24}$$

The element of the first estimate are then

$$S_i^1 = \frac{M_i}{\alpha} - \frac{\beta}{\alpha^2} \sum_{j=i+1}^{N} \frac{M_j}{(j-1)} \left[\prod_{k=i+1}^{(j-1)} \left(1 - \frac{\beta}{(k-1)\alpha}\right) \right] \qquad (25)$$

for an N-channel spectrum.

The elements of the Gaussian response are

$$G_{ij} = (1/\sqrt{2\pi}\,\sigma_i) \exp\left[- (j-i)^2/2\sigma_i^2 \right] \qquad (26)$$

where σ_i is treated as a function of channel number i, and σ^2 is assumed to obey a quadratic variation in energy. The latter may be evaluated from conversion electron spectra. The effect of other channels j is assumed negligible outside the range $j = i \pm 3\sigma_i$. Hence

$$(GS^1)_i = (1/\sqrt{2\pi}\,\sigma_i) \sum_{j=i-3\sigma_i}^{i+3\sigma_i} \exp\left[- (j-i)^2/2\sigma_i^2 \right] S_j^1 \qquad (27)$$

The effect these corrections have upon a β^- -spectrum is demonstrated in figs 3.4 and 3.5.

3.3.C β-Ray Calibration

An energy calibration for β-detectors can be made with Compton edges of γ-rays, with conversion electrons and with endpoint energies of standard β-spectra. The first method is undesirable as it uses electrons generated within the phosphor; the second and third methods were used under identical experimental conditions to the detection of unknown β-rays. Table 3.1 lists the nuclides found suitable for use as calibration sources. It was necessary to count in coincidence to obtain clear conversion lines, which were also used for resolution corrections.

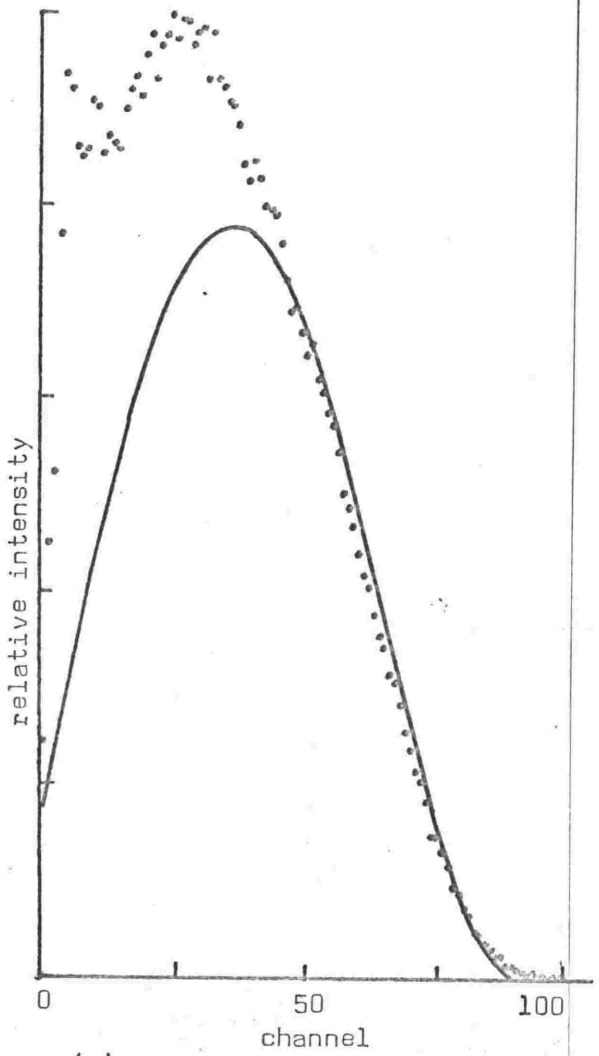

(a) raw data

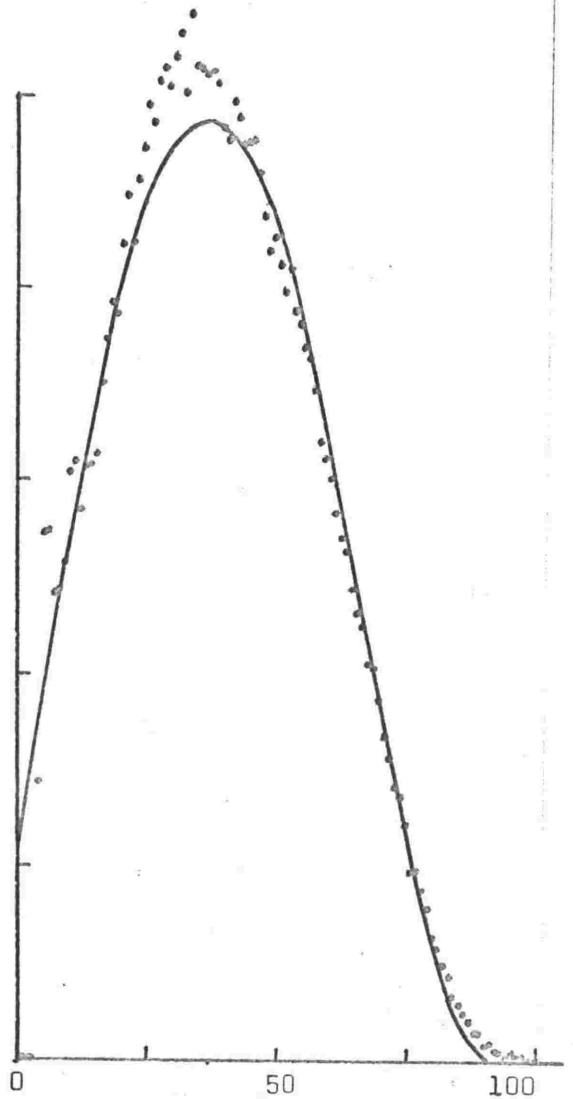

(b) tail-corrected data

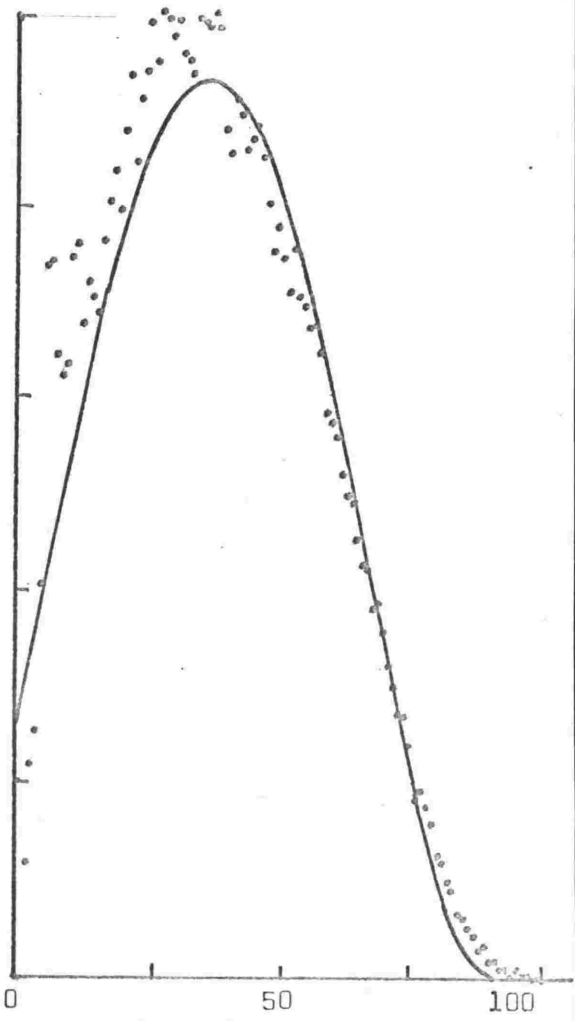

(c) tail and resolution-corrected data

Fig. 3.4 β-spectra of ^{28}Al showing the effect of various corrections. The curve in each case is constructed from the corresponding linear fit to the Fermi-Kurie plot (fig. 3.5).

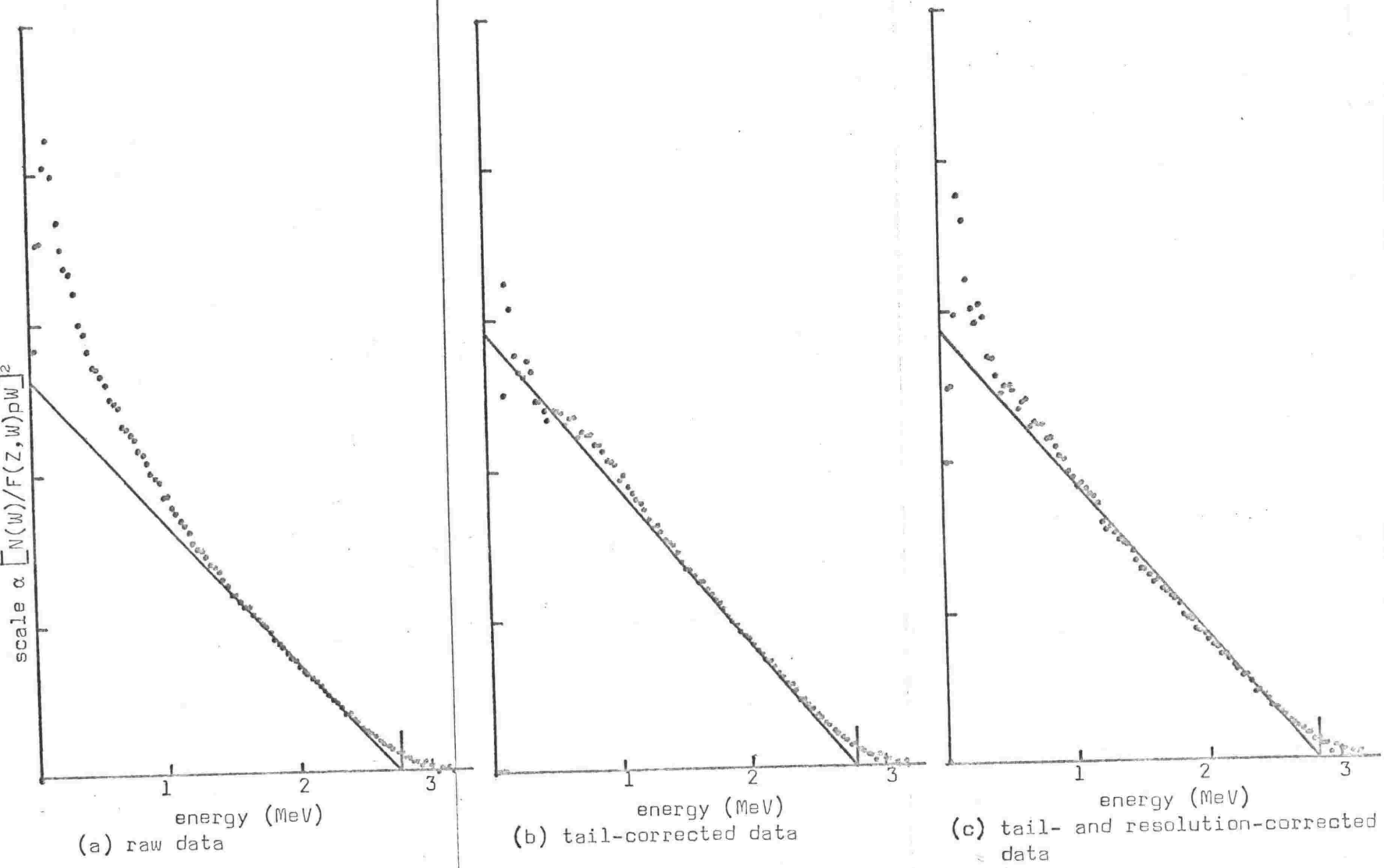

Fig. 3.5 Fermi-Kurie plots of ^{28}Al β-spectra showing the effect of various corrections. Constructed β-spectra from the linear fits are shown in fig. 3.4.

source	mode	electron energy (MeV)	half-life	production	c	γ's present (MeV)
^{28}Al	β^-	2.87	2.31min	$^{28}Si(n,p)^{28}Al$	1.652	1.78
^{16}N	β^-	4.291 10.291	7.2 sec	$^{16}O\ (n,p)^{16}N$	1.784 1.875	6.134, 7.112
^{34m}Cl	β^+	4.460	1.6 sec	$^{35}Cl(n,2n)^{34m}Cl$	1.796	2.8
^{24}Na	β^-	1.393	15 hr	$^{27}Al(n,\alpha)^{24}Na$	1.334	1.368, 2.754
^{32}P	β^-	1.710	14.3 d	$^{32}S(n,p)^{32}P$	1.495	-
^{207}Bi	ce_K	0.976 0.482	30 yr	-	-	0.569, 1.063

Table 3.1. Sources found useful for the calibration of β-ray spectra. The Compton electrons from γ-rays should be subtracted from the total spectrum.

To obtain greater accuracy in a calibration by endpoint energy, use was made of the fact that, at high energies, the reduced Fermi function[21]

$$f(Z,W) \alpha W^{c} \qquad (28)$$

where c is a constant. Since the relation between pulse amplitude and incident energy has been found to be linear to within 2%[21,31] over the range 0.5 to 13.5 MeV, a plot of

$$\left[N_i / i^{c} \right]^{\frac{1}{2}} - \text{vs} - i$$

for channel number i would be linear at high energies with the required endpoint. The value of the constant c has been found graphically and is tabulated with the appropriate calibration standards.

The β-ray efficiency of organic phosphors is essentially independent of energy[22].

Methods described in this section were programmed in MACRO for use on the PDP-8 computer[32].

3.4 γ-Ray Angular Correlations

The use of the Wigner-Eckhart theorem on the theoretical formula describing the angular distributions of γ-radiation allows it to be factorised into two parts. One depends only on quantities which characterise the nuclear transition (reduced matrix elements) and the other is dependent on quantities describing the nuclear alignment. This orientation can be chosen by particle absorption or observation, or by γ-ray observation.

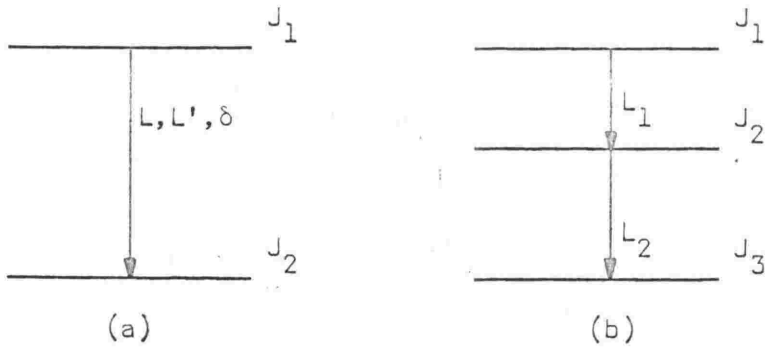

If the axis of cylindrical symmetry is defined by the experimental arrangement, and if there are at most two multipoles, L and L' (generally L' = L + 1), contributing to the transition shown in (a), then the angular distribution of the γ-radiation for the decay $J_1 \longrightarrow J_2$ can be written in the form[23]

$$W(\theta) = \sum_{k \text{ even}} \left\{ B_k(J_1) \left[R_k(LLJ_1J_2) + 2\delta R_k(LL'J_1J_2) + \delta^2 R_k(L'L'J_1J_2) \right] P_k(\cos\theta)/(1+\delta^2) \right\} \tag{29}$$

where the mixing ratio of the two multipoles is

$$\delta = \frac{\langle J_1 \,||\, T_{L'}^{\langle\pi'\rangle} \,||\, J_2 \rangle / (2L'+1)^{\frac{1}{2}}}{\langle J_1 \,||\, T_L^{\langle\pi\rangle} \,||\, J_2 \rangle / (2L+1)^{\frac{1}{2}}} \tag{30}$$

The symbols $\langle\pi\rangle$, $\langle\pi'\rangle$ stand for electric or magnetic, and the coefficients R_k are defined

$$R_k(LL'J_1J_2) = (-)^{1+J_1-J_2+L'-L-k} \left[(2J_1+1)(2L+1)(2L'+1)\right]^{\frac{1}{2}} \times (LL'1-1 \,|\, k0)\, W(J_1J_1LL', kJ_2) \tag{31}$$

The nuclear alignment of the state of spin J_1 is described by $B_k(J_1)$ which, by definition, is

$$B_k(J_1) = \sum_{m=-J_1}^{J_1} w(m)(-)^{J_1-m} (2J_1 + 1)^{\frac{1}{2}} (J_1 J_1 m-m \mid k0) \qquad (32)$$

and $B_o(J_1) = 1$. The positive numbers $w(m)$ are the population parameters of the magnetic substates of the initial state J_1 with the properties

$$\sum_m w(m) = 1$$
$$0 \leqslant w(m) \leqslant \tfrac{1}{2}(1 + \delta_{m0}) \qquad (33)$$

The following conditions apply to formula (29):

(i) J_1, J_2 have definite parity

(ii) $|J_1 - J_2| \leqslant L,L' \leqslant J_1 + J_2$; $L,L' \neq 0$

(iii) since the circular polarisation of the γ-ray angular distribution is not observed, the sum is made over even values of k only.

(iv) because of time reversal properties of $T_L^{\langle\pi\rangle}$, the mixing ratios are real.

Considering the transitions shown in (b) for which state J_1 is randomly populated, the observation of a γ-ray of multipolarity L_1 associated with the transition $J_1 \longrightarrow J_2$, chooses a quantisation axis and the state J_2 is effectively aligned when the circular polarisation of the populating γ-ray is unobserved. Assuming definite parities, B_k can be written[23)]

$$B_k(J_2) = \left[R_k(L_1L_1J_2J_1) + (-)^{L_1-L_1'} 2\delta_1 R_k(L_1L_1'J_2J_1) + \delta_1^2 R_k(L_1'L_1'J_2J_1)\right] /(1+\delta_1^2) \tag{34}$$

with

$$\delta_1 = \frac{\langle J_1 \| T_{L_1'} \langle \pi_1' \rangle \| J_2 \rangle /(2L_1'+1)^{\frac{1}{2}}}{\langle J_1 \| T_{L_1} \langle \pi_1 \rangle \| J_2 \rangle /(2L_1+1)^{\frac{1}{2}}} \tag{35}$$

and the angular distribution of the γ-ray corresponding to the transition $J_2 \longrightarrow J_3$ can be obtained from (29).

Values of the coefficients R_k are tabulated[23]. Alternative treatments of this problem give rise to different coefficients and, in particular, the Z_1 coefficients of Sharp et al.[24] are useful because of their prime number format.

The coefficients of the Legendre polynomials in the angular distribution formula require correction for finite detector size as the angular resolution smooths the distributions predicted for ideal detectors. Tables of these attenuation coefficients are available[23,25,26].

The method adopted for analysis[33] comprised the insertion of trial spin values into a search for the mixing ratio, δ, based on χ^2-minimisation.

3.5 Half-Life Determination; Least Squares Procedures

The application of statistical processes to nuclear decay imposes stringent conditions upon experimental procedures used in the determination of half-lives. This is made clear on examination of the binomial distribution which is the fundamental frequency distribution governing random events.

If the probability of occurrence of a random event (such as the decay of a nucleus) is p, then in a random group of z independent trials, the probability, P_k, that the event will occur x times is[27)]

$$P_x = \frac{z!}{x!\ (z-x)!}\ p^x\ (1 - p)^{2-x} \qquad (36)$$

The well-known exponential rate of decay of a group of identical nuclei clearly implies that the z trials and the probability will not be independent unless z is effectively constant (i.e., $x \ll z$). To ensure this, data must be collected in intervals much smaller than the mean life of the nuclei under study.

Under limiting cases, P_x can be expressed in two forms of greater use:

(i) if z is large, then the probability dP_x that x lies in a range $x \rightarrow x + dx$ is

$$dP_x = (1/(2\pi)^{\frac{1}{2}}\sigma)\ \exp\left[- (x-m)^2/2\sigma^2 \right]\ dx \qquad (37)$$

where $m = pz$ and σ is the standard deviation. This is the normal or Gaussian distribution.

(ii) if z is very large and $p \ll 1$ such that $m = pz$ remains finite, (36) can be approximated to give the Poisson distribution

$$P_x = (m^x/x!)\ \exp(- m) \qquad (38)$$

for which $\sigma = \sqrt{m}$.

In curve fitting, one typically has data n_k which is to be reproduced by values of some function $m_k(a_i)$. Clearly, the best method of deducing the parameter a_i is to maximise the overall joint probability, L, for the k intervals, a technique known as maximum likelihood

$$\text{i.e.,}\quad L = \prod_k P_k$$

or putting $W = \ln L$

$$W_p = \sum_k \left[n_k \ln m_k - m_k - \ln(n_k!) \right] \qquad \text{POISSON} \tag{39}$$

$$W_N = -\sum_k \left\{ \tfrac{1}{2} (n_k - m_k)^2 / \sigma_k{}^2 + \ln \left[(2\pi)^{\frac{1}{2}} \sigma_k \right] \right\} \qquad \text{NORMAL} \tag{40}$$

and a_i is found by solution of $\partial W / \partial a_i = 0$

From this, it is apparent that the least squares minimisation and the maximum likelihood technique are identical for processes governed by normal statistics (including most applications of nuclear decay).

The number of decaying nuclei detected in an experiment can be expressed as[34]

$$m = N_o \left[\exp(-\lambda t_1) - \exp(-\lambda t_2) \right] + B \tag{41}$$

where B represents the background rate. If the counting interval $(t_2 - t_1 = T)$ is constant, and there is a constant time δ between each period of counting then $m_k = N_o \left[1 - \exp(-\lambda T) \right] \exp \left[-\lambda (k - 1) (T + \delta) \right] + B$

$$= A \exp \left[-\lambda (k - 1) T' \right] + B \tag{42}$$

m_k is non-linear and so further analysis with this expression requires iterative methods such as Taylor expansion or χ^2-minimisation. Robinson[28] has investigated the effect of weighting $(1/\sigma_k{}^2)$ used in such procedures and has found $\sigma_k = (m_k')^{\frac{1}{2}}$ (where m_k' is the best value of the previous interation) to be most stable.

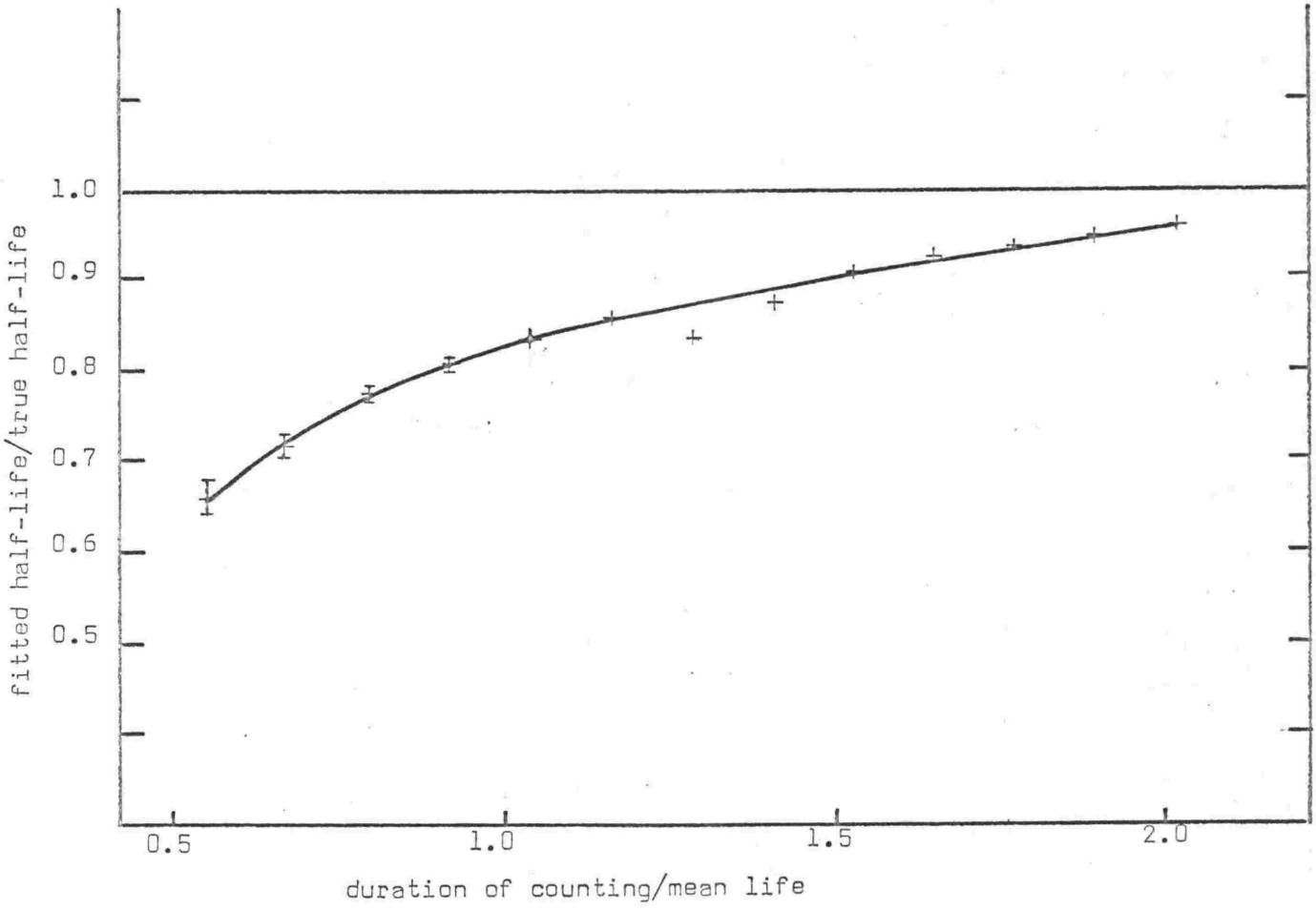

Fig. 3.6. Effect of short-duration counting on the fitted half-life. Note that this effect is absent in data for which the statistical errors are very small or zero. The initial count-rate for the above data was about 10^4 counts/interval.

Simpler methods exist, such as Peierls[27], but all require that the data be accumulated in intervals ideally about a tenth of a mean life and over three to five mean-lives, consistent with counting statistics. Fig. 3.6 illustrates the effect of short duration counting on the fitted half-life. This effect is due to the statistical variations in counting rate since synthesised data, or data in which n_k is very large, gives the same half-life independently of the duration of counting.

3.6 Measurement of Cross Sections

After a single irradiation of duration t, the number of counts accumulated in a photopeak of a γ-ray spectrum in a time t_c is

$$D_1 = \frac{P\theta C}{1+\alpha} \cdot \frac{\sigma \phi N}{\lambda} \cdot \left[1-\exp(-\lambda t)\right]\left[1 - \exp(-\lambda t_c)\right] \exp(-\lambda t_w) \qquad (43)$$

if there is a delay of t_w between completion of irradiation and the start of detection. The following definitions apply

P : absolute photopeak efficiency for selected γ-ray
θ : branching ratio of decay
C : source absorption factor
α : total internal conversion coefficient
σ : total cross section for the reaction
Ø : incident particle flux on target
N : total number of target nuclei.

If, in the application of the above to short-lived nuclides, the cycle time is T and the flux Ø is assumed to be constant, the cumulative detector response after n cycles is[29]

$$D_{nT} = D_1 \left[\frac{n}{(1-e^{-\lambda T})} - \frac{e^{-\lambda T}(1-e^{-n\lambda T})}{(1-e^{-\lambda T})^2} \right] \qquad (44)$$

$$\longrightarrow nD_1 \quad \text{for} \quad T >> T_{\frac{1}{2}}.$$

Rather than rely on accurate determinations of P, $\emptyset$ and C, all of which prove difficult for the extended source, measured quantities of substances, with known cross sections and reaction products with comparable decay modes, were mixed with elements of unknown cross sections. Cross sections were then evaluated by ratio of eq. (44).

3.7 Calculation of (n,p) Cross Sections

Gardner and Rosenblum[30] have developed a statistical model to yield semi-empirical equations which give good agreement with available experimental data. The ratio of (n,p) cross sections for isotopes are

$$\frac{\sigma(Z,A)}{\sigma(Z,A-1)} \doteq \exp 2\left\{ \left[a(E_m - \beta_p^*) \right]_A^{\frac{1}{2}} - \left[a(E_m - \beta_p^*) \right]_{A-1}^{\frac{1}{2}} \right\} \qquad (45)$$

where $E_m = E_n + Q_{n,p} - \delta$ and

E_n = neutron energy in CM system $\left(= \left[\frac{A}{1+A}\right]^2 E_n^L\right)$

δ = pairing energy of daughter nucleus

= 0 for odd-odd nucleus

= δ_n for odd-even "

= δ_p for even-odd "

= $\delta_n + \delta_p$ for even-even "

and $\delta_n = \delta_p = 1.7$ MeV for $Z \geqslant 40$

a = level density parameter = $\frac{A}{25}$

$$\beta_p^* = \frac{1.029(Z-1)}{1 + A^{1/3}} \cdot (1 - 1.13/A^{1/3})$$

It is the ratios rather than the absolute values which appear to be most reliable[30].

REFERENCES

1) G. Wallace, I.N.S. Report INS-P-69 (1970)

2) J.T. Routti and S.G. Prussin, Nucl. Inst. and Meth. 72 (1969), 125

3) G.J. McCallum, I.N.S. Report INS-LN-33 (1971)

4) G. Wallace, I.N.S. Report INS-P-70 (1970)
I.N.S. Report INS-P-61 (1970)

5) C.M. Lederer, J.M. Hollander and I. Perlman, "Table of Isotopes" (6th ed.), John Wiley and Sons (1967)

6) B.J. O'Brien (1970), unpublished

7) G. Aubin, J. Barrette, M. Barrette and S. Monaro, Nucl. Inst. and Meth. 76 (1969), 93

8) W.R. Kane and M.A. Mariscotti, Nucl. Inst. and Meth. 56 (1967), 289

9) U. Fano, National Bureau of Standards, Applied Math. Series 13 (1952)

10) A.H. Wapstra, G.J. Nijgh and R. Van Lieshout, "Nuclear Spectroscopy Tables", North-Holland (1959)

11) H.A. Bethe and R.F. Bacher, Rev. Mod. Phys. 8 (1937), 194

12) G.P. Ford and D.C. Hoffman, Nucl. Data 1 (1966), 411

13) J.P. Davidson, Phys. Rev. 82 (1951), 48

14) R.I. Verrall, J.C. Hardy and R.E. Bell, Nucl. Inst. and Meth. 42 (1966), 258

15) C.E. Gleit, C.W. Tang and C.D. Coryell, Nucl. Data Sheets 5-5-109 (1963)

16) T.J. Kennet and G.L. Leech, Nucl. Inst. and Meth. 24 (1963), 142

17) M.S. Freedman, T.B. Novey, F.T. Porter and F. Wagner, Rev. Sci. Inst. 27 (1956), 716

18) J.P. Palmer and L.T. Laslett, U.S.A.E.C. Report AECU-1220 (1951)

19) W.R. Dixon and J.H. Aitken, Can. J. Phys., 36 (1958), 1624

20) D.D. Slavinskas, T.J. Kennet and W.V. Prestwich, Nucl. Inst. and Meth. 37 (1965), 36

21) J.G. Cramer, B.J. Farmer and C.M. Class, Nucl. Inst. and Meth. 16 (1962), 289

22) K. Siegbahn, "α-, β- and γ-Spectroscopy", North-Holland (1965)

23) O. Hausser, J.S. Lopes, H.J. Rose and R.D. Gill, "Methods of Analysis of γ-Angular Distributions", Nucl. Phys. Lab. Report, Oxford (1966)

24) W.T. Sharp, J.M. Kennedy, B.J. Sears and M.G. Hoyle, AECL Report CRP-556 (1957)

25) A.R. Rutledge, AECL Report CRP-851 (1959)

26) D.C. Camp and A.L. Van Lehn, Nucl. Inst. and Meth., 76 (1969), 192

27) R.D. Evans, "The Atomic Nucleus", McGraw-Hill (1955)

28) D.C. Robinson, Harwell Report AERE-R5911

29) W.W. Givens, W.R. Mills and R.L. Caldwell, Nucl. Inst. and Meth. 80 (1970), 95

30) D.G. Gardner and S. Rosenblum, Nucl. Phys. A96 (1967), 121

31) R.L. Craun and D.L. Smith, Nucl. Inst. and Meth. 80 (1970), 239

32) G. Wallace, I.N.S. Report INS-P-62 (1970)

33) G.J. McCallum, B.J. O'Brien and M.J. Kelly, I.N.S. Report INS-P-84 (1971)

34) G. Wallace, I.N.S. Report INS-P-85 (1971)

Chapter Four

EXPERIMENTAL RESULTS

I THE DECAY OF ^{112}Ag

1. Introduction

Since the present work was initiated, considerable attention has been devoted to the study of the decay of ^{112}Ag[1,2,3] and the latest published results, those of Macdonald and Sharma[3] (MS), rigorously incorporate 92 γ-rays into a structure of 31 excited levels of ^{112}Cd. The level schemes deduced from these decay studies are in good agreement with the results of charged particle activation[4,5,6] and Coulomb excitation[7]. However, some minor inconsistencies are to be found in the γ-ray studies and, although the level scheme of MS is upheld, the results of the work reported here indicate slight disagreement in level energies. Some spin and parity assignments are confirmed by observation of γ-γ angular correlations, and measurements have been made of neutron cross sections for production of ^{112}Ag.

2. Experiments and Results

2.1 Source Preparation

Sources of ^{112}Ag were produced through the $^{112}Cd(n,p)^{112}Ag$ and the $^{115}In(n,\alpha)^{112}Ag$ reactions by the bombardment of natural Cd and In metals with 16 MeV neutrons from the I.N.S. 3 MV Van de Graaff accelerator. Silver activity was chemically separated by dissolving the targets in HNO_3 solution and, after the addition of Ag^+, Pd^{++} and Cd^{++} carriers, precipitating the silver as AgCl. Because only two stable isotopes are present in the In element, the (n,α) reaction produced ^{112}Ag activities which were virtually free of any competing Ag activities.

2.2 Cross Section Measurements

Cross sections for the production of ^{112}Ag were measured relative to the neutron cross sections of Fe and Al. Quantities of the two standards, in powdered metallic form, were mixed with samples of finely-divided In and Cd metals so that the irradiation and counting processes involved were identical. The incident neutron energy was estimated to be 16.3 ± 0.4 MeV and the standard cross sections at this energy were taken from ref.[8]. The results are given in table I-1.

The cross section for the $^{112}Cd(n,p)^{112}Ag$ reaction is of interest as Gardner and Rosenblum[9] have commented that the (n,p) cross section values for Cd isotopes present difficulties when attempts are made to fit them to an empirical formula. The results reported here, which are in general agreement with a value of 11 ± 3 mb[10] measured at a neutron energy

reaction	cross sections (mb)		mean
$^{112}Cd(n,p)^{112}Ag$	15.6 ± 2.1	15.0 ± 1.9	15.3 ± 2.0
$^{115}In(n,\alpha)^{112}Ag$	4.01 ± 0.52	4.07 ± 0.56	4.04 ± 0.54
reference reaction[8]	$^{56}Fe(n,p)^{56}Mn$ σ = 77 ± 6	$^{27}Al(n,\alpha)^{24}Na$ σ = 88 ± 6	

Table I-1. Production cross sections for ^{112}Ag at a neutron energy of 16.3 ± 0.4 MeV.

of 14 MeV, are considerably greater than the predicted value (5.3 mb at a neutron energy of 14.5 MeV). However, much better agreement is obtained by using the ratio equation[9] as the extrapolation of the (n,p) cross section of ^{111}Cd[8] gives a value of 18 ± 2 mb for the $^{112}Cd(n,p)^{112}Ag$ reaction. The $^{115}In(n,\alpha)^{112}Ag$ cross section is consistent with previous measurements[8] made at 14 MeV neutron energies.

2.3 Half-Life Measurement

After the production of a ^{112}Ag source by the (n,p) reaction, a time sequence of γ-ray spectra covering the energy range 500 to 670 keV was collected from which the analysed 606 + 617 keV peak intensities were fitted to a decay with a half-life of 3.14 ± 0.01 hr. The variation with time of the ^{112}Ag β-activity produced by the (n,α) reaction was also monitored and, on fitting, this gave a half-life of 3.13 ± 0.01 hr corresponding to 99.97% of the initial activity. Both values are in excellent agreement with those found by other investigators[1,11].

2.4 Direct and Coincidence γ-Ray Spectroscopy

The direct γ-ray spectra were taken with a 32cm^3 coaxial Ortec Ge(Li) detector and standard low noise amplifiers. The data were accumulated in a 4096-channel Kicksort analyser; the typical resolution obtained in an experiment was 3.1 keV (fwhm) at 1332 keV.

A 3" x 3" NaI(Tl) scintillator (Harshaw type 12S12) was added as a gating detector for Ge(Li)-NaI(Tl) coincidence measurements, and standard fast-slow coincidence circuitry was used with resolving times (2τ) of 70-100 ns. Coincidence spectra were analysed by a 1024-channel ADC (Nuclear Data ND160-F) and recorded on a PDP-8 computer. Typical γ-ray

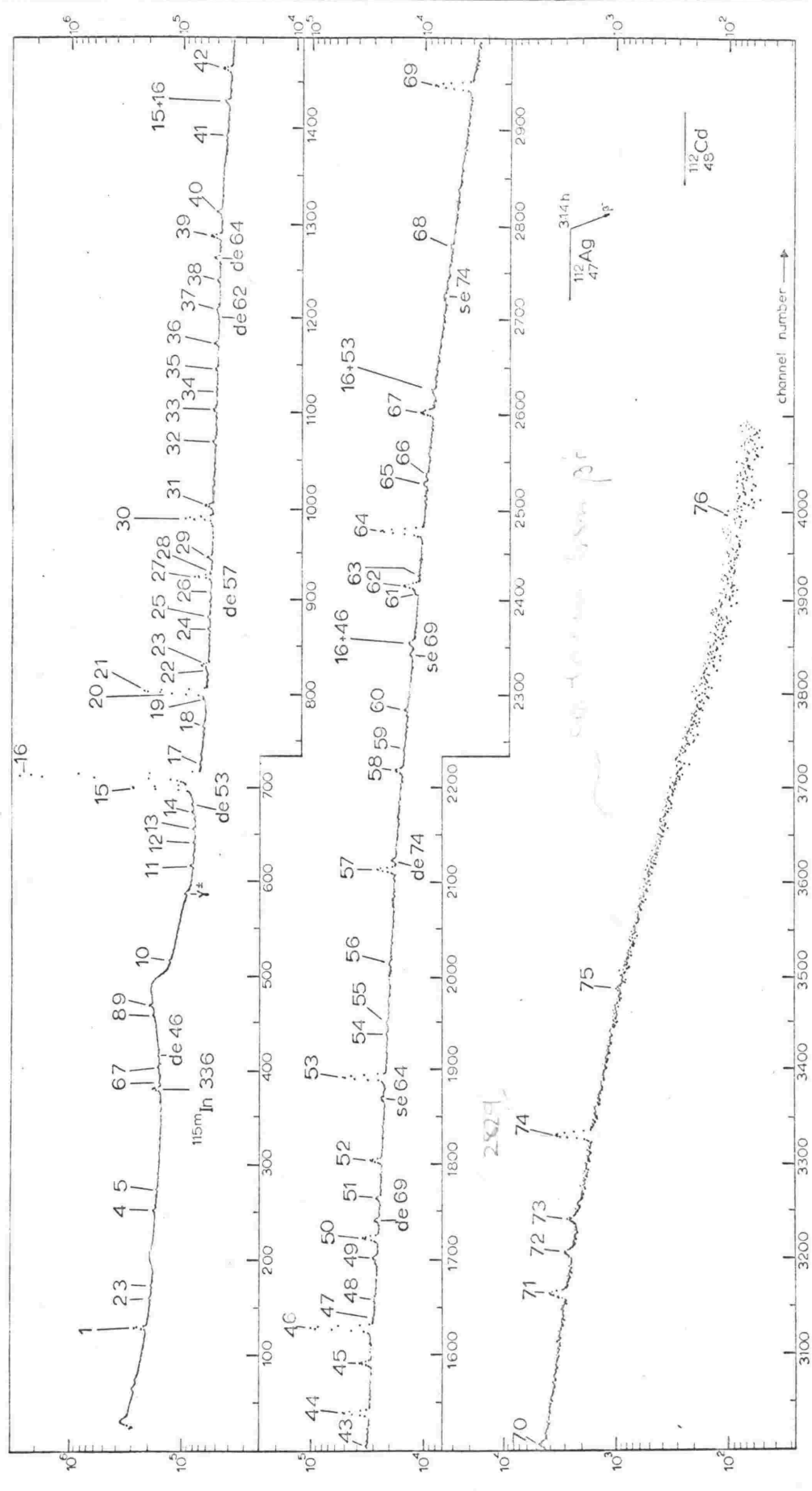

Fig. I-1. A γ-ray spectrum of the decay of ^{112}Ag measured with a 32 cm^3 coaxial Ge(Li) detector. The photopeaks are identified by numbers corresponding to those given in table I-2.

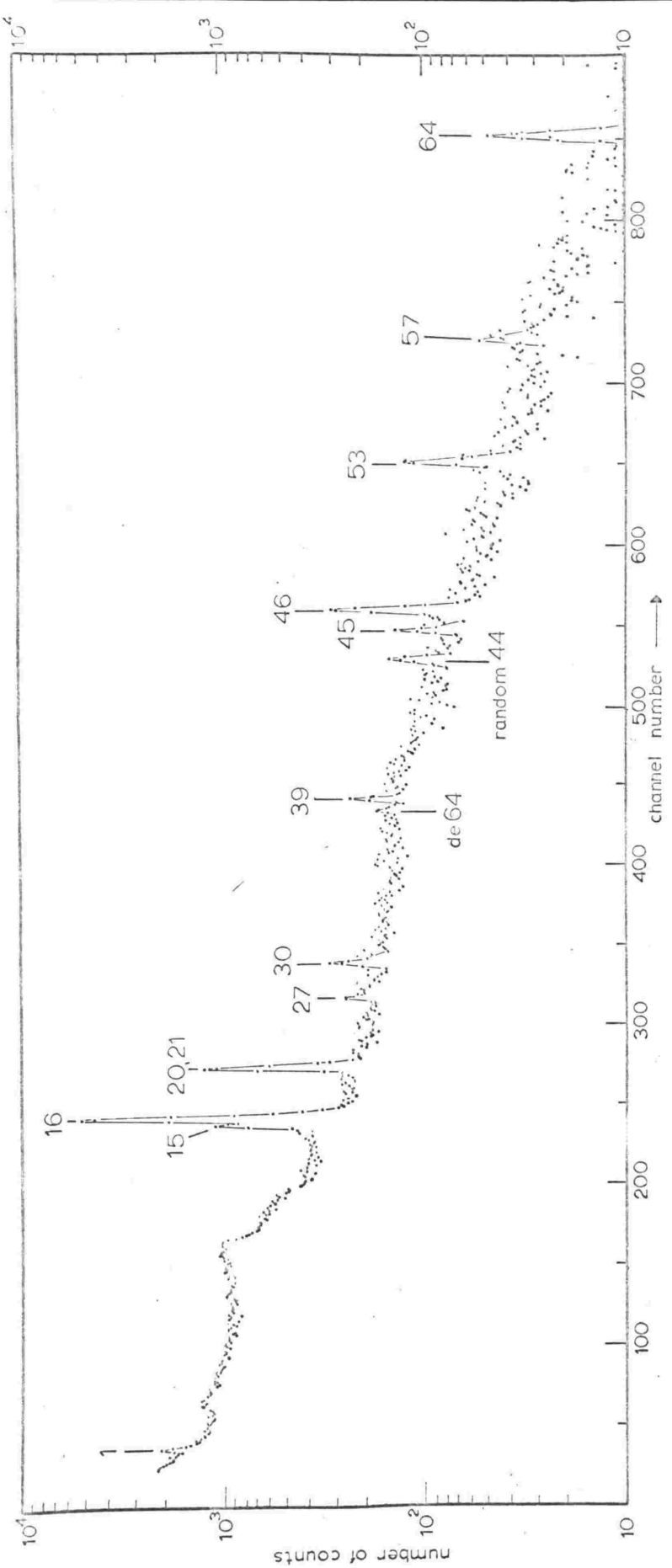

Fig. I-2. A γ-ray spectrum with a Ge(Li) detector in coincidence with the energy region 590-630 keV of a spectrum obtained with a NaI(Tl) detector.

spectra are given in figs I-1 and I-2.

The spectra obtained were analysed on a PDP-9/L computer using the techniques described by Routti and Prussin[12]. The energy calibration was initially derived from standard sources. When the relations between γ-rays were apparent from the level structure of ^{112}Cd, an internal recalibration was performed and this was bootstrapped to the level energy systematics. The resulting cubic polynomial gave γ-ray cascade sums which were in good agreement with each other. The γ-ray energies generally concurred with those of Saskai et al.[1] who had calibrated by accumulating standard spectra with ^{112}Ag γ-rays. Relative intensity measurements agreed with those obtained by MS to within 10%. The γ-rays are listed in table I-2.

2.5 Angular Correlations

The angular correlations of prominent γ-rays with the 617 keV transition following the decay of ^{112}Ag were determined with a 5" x 6" NaI(Tl), which was used for gating, and two 3" x 3" NaI(Tl) detectors. The latter two detectors were standardised against each other with the 4^+-2^+-0^+ angular correlation of ^{60}Ni, and, as several sources of ^{112}Ag were needed to gain sufficient data, each irradiation-detection process was normalised with respect to the number of gating pulses detected. The gate corresponded to the energy range 580-630 keV and no attempt was made to differentiate between the 606 and 617 keV peaks. As the 606 keV γ-ray has, apart from the 617 keV γ-ray, only γ-rays of minor intensities in coincidence with it, this had no effect on other angular correlations. A

No.	E_γ (keV)	I_γ	assignment	No.	E_γ (keV)	I_γ	assignment
1	121.0±0.2	0.18	FD	39	1103.6±0.2	0.98	MD
2	147.9±0.2	0.03		40	1125.9±0.2	0.41	WI
3	159.5±0.3	0.03		41	1194.1±0.5	0.07	ND
4	226.0±0.3	0.04	LI	42	1253.6±0.2	0.87	HB
5	244.8±0.3	0.03	GC	43	1282.9±0.5	0.09	NC
6	342.3±0.3	0.04		44	1312.3±0.2	2.8	DA
7	355.9±0.3	0.07		45	1356.6±0.2	1.1	OD
8	402.0±0.3	0.10	HG	46	1387.7±0.2	12.5	IB
9	410.7±0.2	0.27	MI	47	1397.4±0.6	0.07	TG
10	450.9±0.3	0.08	TM	48	1411.8±0.8	0.08	QD
11	536.4±0.3	0.12	IG	49	1451.4±0.3	0.35	TE
12	558.0±0.5	0.03	HD	50	1468.8±0.2	1.5	GA
13	569.8±0.3	0.10		51	1503.9±0.3	0.38	
14	585.4±0.3	0.09		52	1538.6±0.2	1.2	KB
15	606.7±0.2	7.2	CB	53	1613.6±0.2	6.6	LB
16	617.4±0.2	100	BA	54	1652.4±0.8	0.07	VE
17	629.2±0.4	0.04	YP	55	1683.7±0.7	0.10	
18	663.5±0.3	0.07	OI	56	1714.7±0.6	0.10	WE
19	688.9±0.4	0.10	KG	57	1798.4±0.2	2.1	MB
20	692.7±0.2	2.5	ID	58	1888.8±0.2	0.73	NB
21	694.8±0.2	6.9	DB	59	1909.2±0.6	0.10	
22	714.8±0.3	0.12	WM	60	1944.7±0.4	0.20	XC
23	718.4±0.2	0.39	QI	61	2051.5±0.3	0.28	OB
24	751.8±0.3	0.09	JD	62	2056.5±0.2	1.4	PB
25	762.3±0.3	0.12	LG	63	2066.0±1.6	0.03	JA
26	784.6±0.6	0.04		64	2106.2±0.2	5.6	QB
27	797.9±0.2	1.2	EB	65	2148.1±0.3	0.23	RB
28	802.3±0.4	0.07	TJ	66	2156.0±0.5	0.16	KA
29	815.8±0.2	0.31	FB	67	2211.6±0.2	1.0	SB
30	851.2±0.2	2.4	GB	68	2362.4±0.6	0.09	
31	861.6±0.2	0.51	TI	69	2506.8±0.2	2.5	NA
32	918.7±0.3	0.16	LD	70	2551.9±0.3	0.25	XB
33	947.3±0.3	0.19	MG	71	2686.0±0.2	0.59	YB
34	957.1±1.0	0.02	UI	72	2723.6±0.3	0.23	QA
35	983.8±0.3	0.12	MF	73	2752.8±0.3	0.22	ZB
36	1007.0±0.3	0.24	LC	74	2829.4±0.2	1.0	SA
37	1037.9±0.3	0.17	NG	75	2961.7±1.0	0.04	UA
38	1063.7±0.3	0.18		76	3393.0±1.2	0.01	A'A

Table I-2. Energies and relative intensities of γ-rays occurring in the decay of ^{112}Ag. Intensities above 0.1 are with an accuracy of about 10%. Below 0.1 the accuracy falls to 25%.

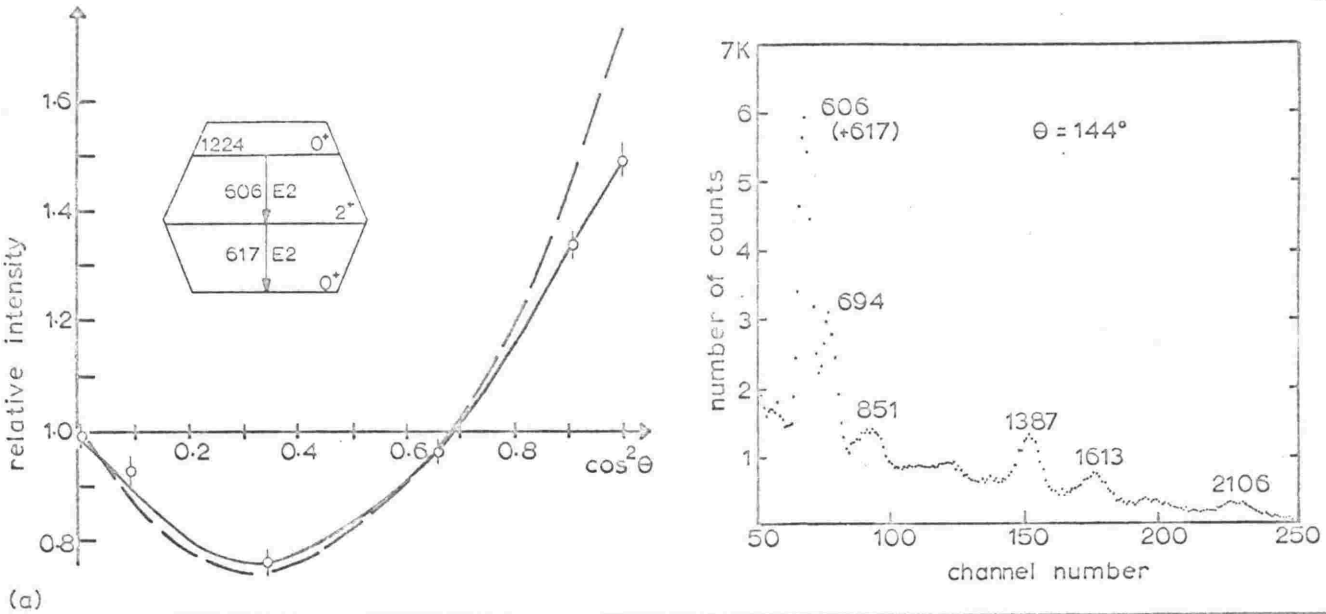

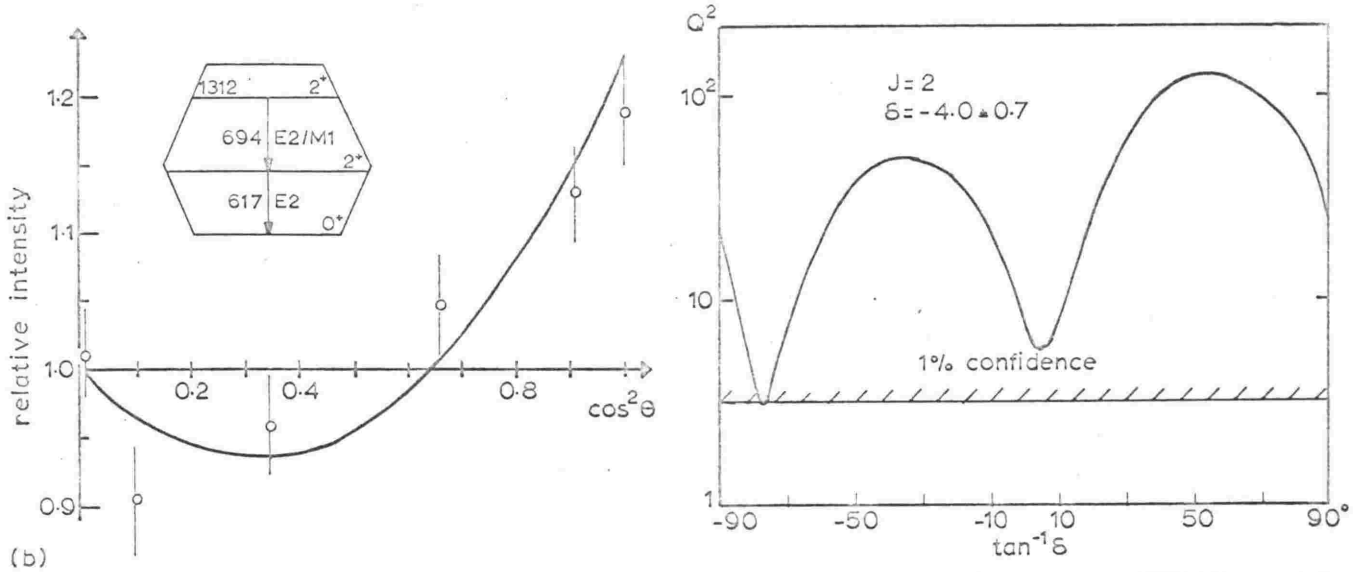

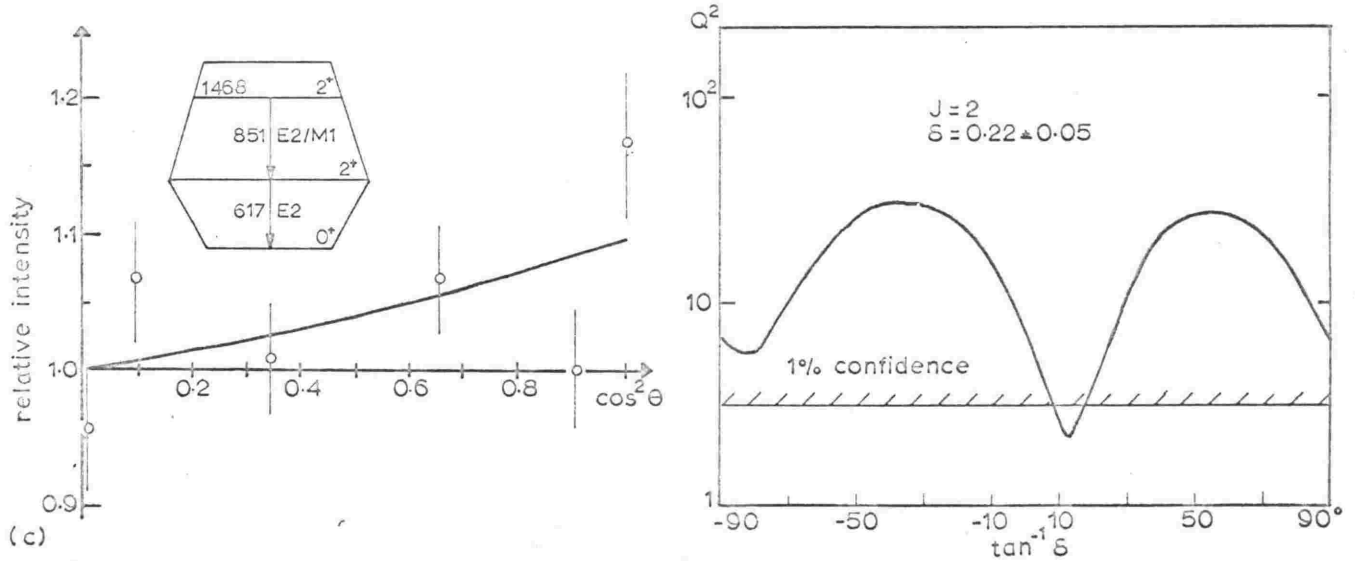

Fig. I-3. Angular correlations of major γ-rays from ^{112}Ag decay.

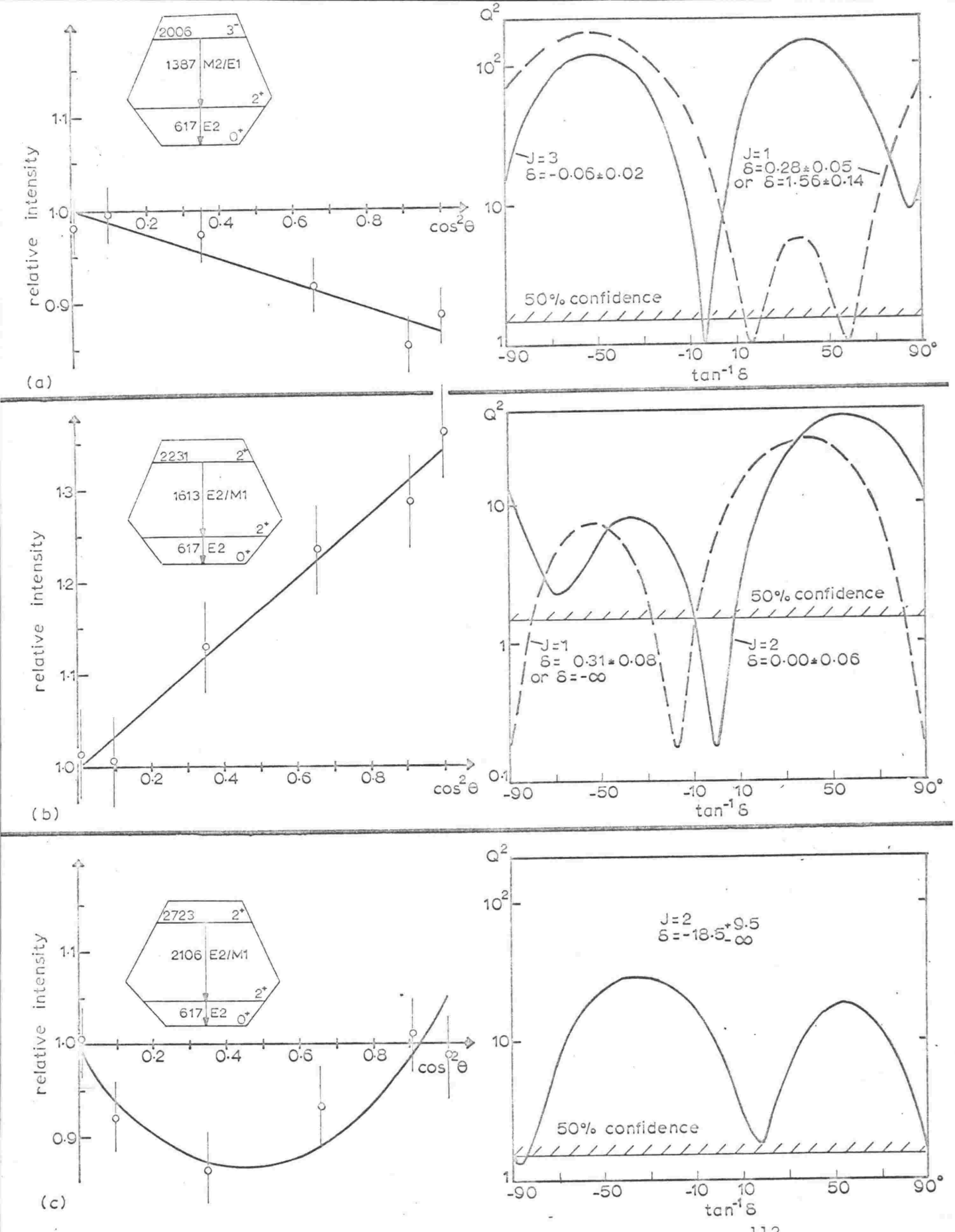

Fig. I-4. Angular correlations of major γ-rays from ^{112}Ag decay.

typical γ-ray spectrum detected by one of the 3" x 3" NaI(Tl) crystals for one irradiation is shown in fig. I-3(a), and least-squares analyses from these spectra are presented in figs I-3 and I-4. The parameter Q^2 (where $Q^2 = \chi^2/\text{degrees of freedom}$) is defined

$$Q^2 = (N-2)^{-1} \sum_{i=1}^{N} \left[W_{exp}(\theta_i) - W_{th}(\theta_i, \delta) \right]^2 \left[\sigma^2(\theta_i) \right]^{-1}$$

for the mixing ratio δ and the number of data points N. σ^2 are the variance associated with the experimental angular distribution W_{exp}.

3. Discussion

3.1 Direct and Coincidence γ-Ray Spectroscopy

A total of 76 γ-rays (table I-2) was observed in the γ-radiation following the decay of ^{112}Ag. Although less in number than those obtained from fission sources[2,3], this is a considerable increase over the 20 γ-rays reported[1] using the same production methods. 12 of these γ-rays remain unplaced in the level scheme, but only the one of 1503.9 keV energy is of significant intensity, and 8 represent new transitions between established levels.

Coincidence measurements with a gate set over the 606 and 617 keV peaks were consistent with the results of MS, and, because of the latter's thorough investigation of coincidence relationships, these experiments were not extended.

3.2 Angular Correlations

The spins and parities of levels at 1224, 1312 and 1468 keV have

been firmly established and mixing ratios for transitions of the latter two to the first excited state have been determined by Coulomb excitation[7]. The present measurement for the 694 keV transition agrees surprisingly well even although it is contaminated by the strong 692 keV γ-ray. The mixing ratio obtained for the 851 keV transition concurs qualitatively only as it indicates a predominant M1 character. The 606/617 keV angular correlation was analysed primarily as a test of the system, and, initially, bad agreement was found when the experimental points were compared with the theoretical distribution (broken line of fig. I-3(a)). However, this was resolved as it arises solely because of an enhancement of the random number of coincidences: if γ-rays of intensities I_1 and I_2 are detected in both systems, the ratio of random-to-true coincidences, assuming an isotropic angular correlation between γ_1 and γ_2, is increased by a factor $(I_1 + I_2)^2/2I_1I_2$ which, for ^{112}Ag decay, is 8.0. Using this simplified treatment, the angular distribution given by the continuous line in fig. I-3(a) was obtained in good agreement with the experimental points.

The Q^2 variation of the 1387/617 keV angular correlation shows that the level at 2005 keV may have spin 1 or 3, but a spin of 3 is consistent with the decay character of the state[3]. As the 1387 keV transition is almost pure in multipolarity, single particle estimates of transition probability favour a pure E1 transition from a negative parity state rather than a pure M1 transition. The assignment of 3^- agrees with the first octupole state found by (p,p') excitation[13], at an energy of 2000 ± 10 keV, and with the claim of Inoue et al.[11] that the β-spectrum to a level at 2.01 MeV has an allowed shape. The spin and parity of the

ground state of ^{112}Ag has previously been established as 2^- by Chan et al.[14].

The angular correlation of 1613/617 suggests spins of 1 or 2 for the level at an excitation energy of 2231 keV. This is consistent with a previous assignment[3] of 2^+ deduced from the branching ratios of γ-ray decay from the level. A similar assignment of 2^+ for the level at 2723 keV is upheld.

3.3 The Decay Scheme of ^{112}Ag

The decay scheme is presented in fig. I-5 and is almost identical to that proposed in ref.[3]. Eight additional γ-rays have been found which correspond to transitions GC, HG, TM, KG, NC, VE, JA, KA; but several of the weak transitions previously detected have been missed. In particular, no transitions from or to a level at 1973 keV have been found although the level has been assigned 3^-. There appears to be some confusion in the literature as both this state[4,16] and a state at 2000 ± 10 keV[13] (interpreted in this work as the level of energy 2005 keV) have been classified as the first octupole collective state of ^{112}Cd. The present results favour the assignment of the level at 2005 keV as the octupole vibrational state. The level energies tabulated in fig. I-5 are consistently greater by a small amount than those of ref.[2,3] with the result that the γ-ray cascade sums reported here are in better agreement.

The branches of the β-decay of ^{112}Ag to levels of ^{112}Cd have been deduced from the γ-ray intensity data with the assumption that 54% of the β-decay takes place directly to the ground state[11]. The log ft values shown in fig. I-5 range from 7.4 to 10.2 with a possible uncertainty of ~0.5. According to Gove[15], this does not necessarily exclude the possibility for some of these β-transitions to have an allowed character,

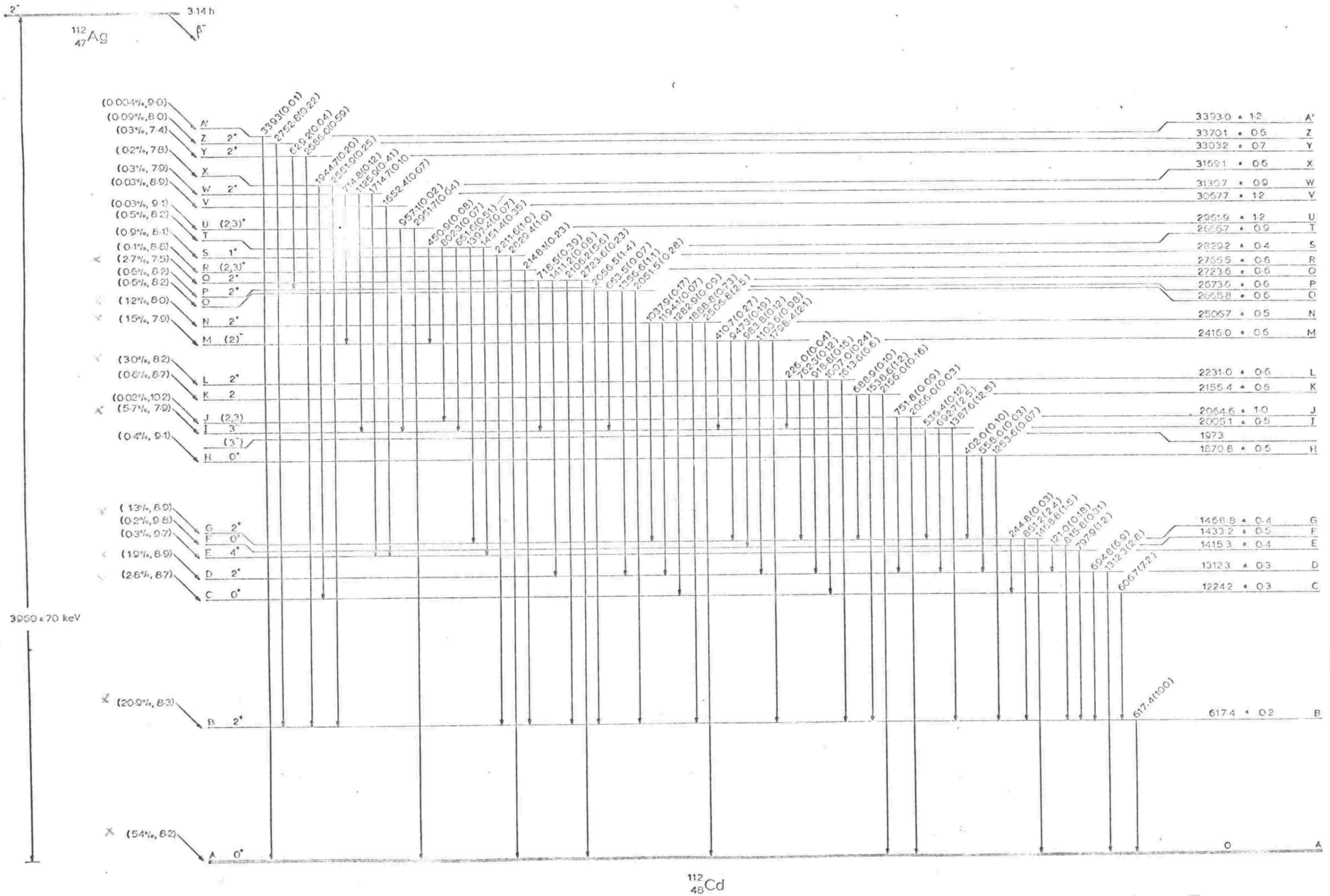

Fig. I-5. Decay scheme of ^{112}Ag to levels in ^{112}Cd.

although most of them will be first forbidden. The 2^- ground state of ^{112}Ag[14] arises most probably as a coupling $(P_{\frac{1}{2}})_\pi (d_{\frac{5}{2}})_\nu^{-1}$. Hence an allowed β-transition between the initial $(d_{\frac{5}{2}})^{-1}$ state to the final $(g_{\frac{9}{2}})$ state will be 1-forbidden and show a high log ft value. Spin and parity assignments for the levels populated by ^{112}Ag decay can therefore be from 0^+ to 4^+ and 1^- to 3^-. Macdonald and Sharma[3], and Lingeman et al.[2], have assigned many of the levels of ^{112}Cd on the basis of branching ratios of depopulation by γ-rays and this information, together with the present results, has been included in the decay scheme of fig. I-5. New conversion electron data and more extensive γ-γ angular correlation measurements with Ge(Li)-Ge(Li) systems would be necessary to finalise the nature of the levels of ^{112}Cd. Experiments investigating prompt γ-rays from reactions in which ^{112}Cd is a product could also be of value.

II THE DECAY OF ^{114}Ag

1. Introduction

^{114}Ag was first assigned[17] a 2 min β^--activity which was produced by the irradiation of fast neutrons on a ^{114}Cd sample. Alexander et al.[18] isolated a 5 sec β^-, γ-activity from fission products of ^{238}U, and this they assigned to ^{114}Ag. They repeated the experiment of Duffield and Knight[17] but failed to observe any 2 min decay in β^--radiation of energy above 3 MeV. The work reported here is an attempt to clarify and elucidate the decay of ^{114}Ag.

The level structure of ^{114}Cd has been the subject of many experiments, with charged particles[3,4], (n,γ) reactions[20,21] and ^{114}In decay[22], and has become firmly established below an excitation energy of 2 MeV. Level energies are known accurately through measurement of energies of conversion electrons[21] and bent crystal spectrometry of γ-rays[20].

2. Experiments and Results

2.1 Source Preparation

Sources of ^{114}Ag were made by (n,p) reactions on natural Cd and 97.8% enriched ^{114}Cd metal samples which were encapsulated in, or mounted on, polythene carriers. Sources suitable for use in β-ray detection were obtained by mixing the finely-divided metal with polystyrene dissolved in benzene, and thinly spreading the slurry on a flat surface of the carrier. Although this is not an ideal preparation for a β-ray source, because of the high endpoint energy expected, it was thought that reasonable estimates of endpoint energies and branching could be made in spite of some source absorption.

A pneumatic system[23], used to transport the carriers between irradiation and counting positions, and associated detection units were automated for recycling.

2.2 ^{114}Cd(n,p)^{114}Ag Cross Section

By irradiating mixtures of PTFE and Cd metal, a comparison of yields was obtained for the 558 keV γ-ray from the decay of ^{114}Ag and the 1.37 MeV γ-ray from ^{19}O decay[24]. As it was not possible to obtain the branching ratios of decay to ^{114}Cd states from the ^{114}Ag β-spectrum

(section 3.2), a measurement of the $^{114}Cd(n,p)^{114}Ag$ cross section could not be made. However, the statistical model of Gardner and Rosenblum[9] allows a realistic extrapolation of (n,p) cross sections between isotopes. At a neutron energy of 16.4 ± 0.4 MeV, the (n,p) cross section of ^{114}Cd was estimated to be 10.8 ± 2.0 mb from the measured value of 15.3 ± 2.0 mb of ^{112}Cd.* Assuming this value, the measurement of relative yields of γ-rays implies[25,8] that 10 ± 4% of the ^{114}Ag decay results in a 558 keV γ-ray. It is from this calculation that the β-decay branching shown in fig. II-5 has been deduced.

2.3 Half-Life Measurements

Using time durations of 6 sec irradiation, 2 sec delay and 40 sec counting, β-rays of energies greater than 1 MeV from the irradiated ^{114}Cd were analysed in a multiscale mode to determine the half-life of ^{114}Ag. Fig. II-1(a) shows the accumulated spectrum, a non-linear least-squares fit to which gives a half-life of 4.52 ± 0.03 sec. This is good agreement with the value, 4.5 sec, obtained by Poularikis et al.[26].

A similar experiment but with 2 min irradiation, 6.1 min counting and no discrimination in β-ray energy, failed to reveal any 2 min activity (fig. II-1(b)). A search for a 2 min activity in a γ-ray of energy 558 keV (expected since a high spin isomeric state would decay isomerically or through the 4^+ state of ^{114}Cd) also proved fruitless. The inference is that there is no such isomeric level in ^{114}Ag, a conclusion which is not unexpected when the sequence $^{112,114,116}Ag$ is compared with other similar sets of nuclei in neutron excess regions.

---

* see section 2.2 of ^{112}Ag decay (p. 50)

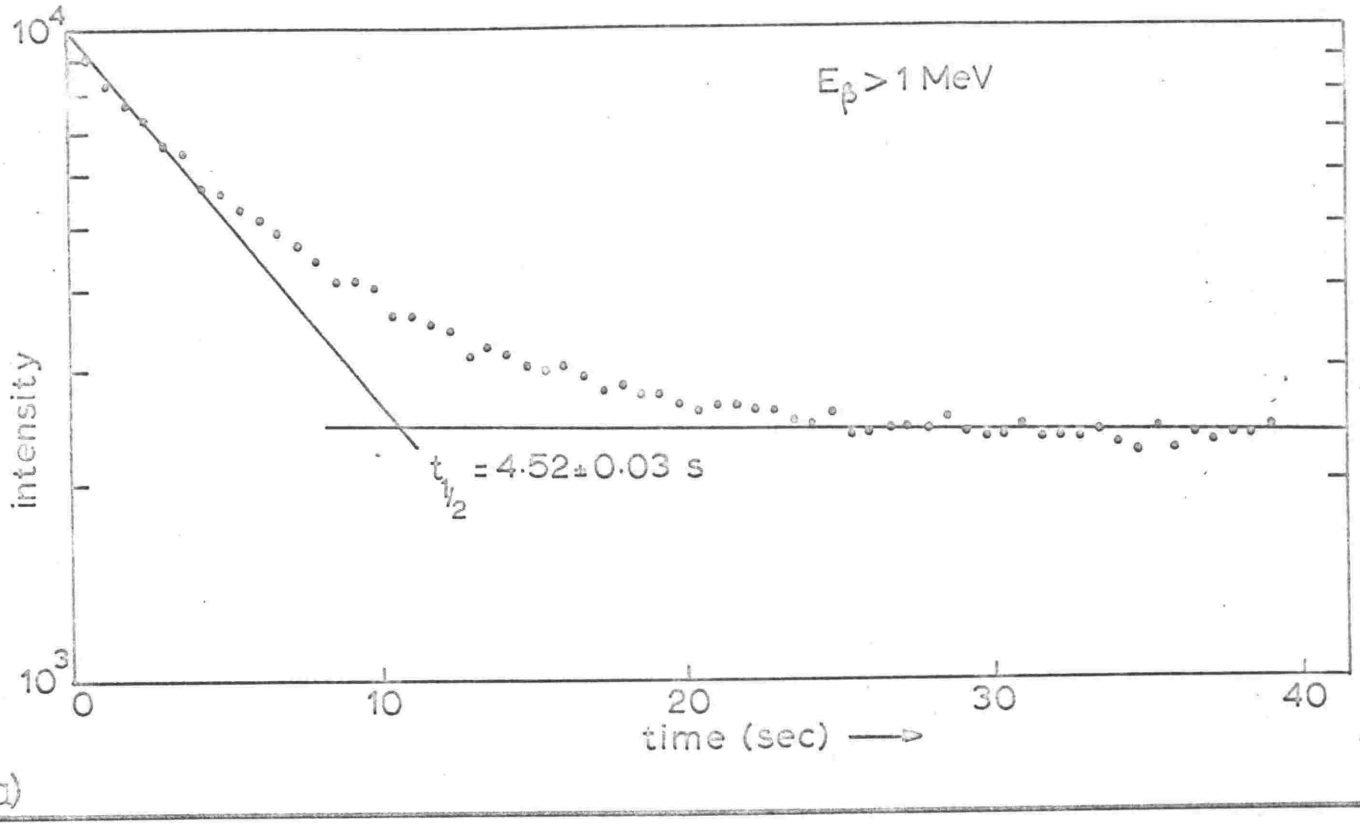

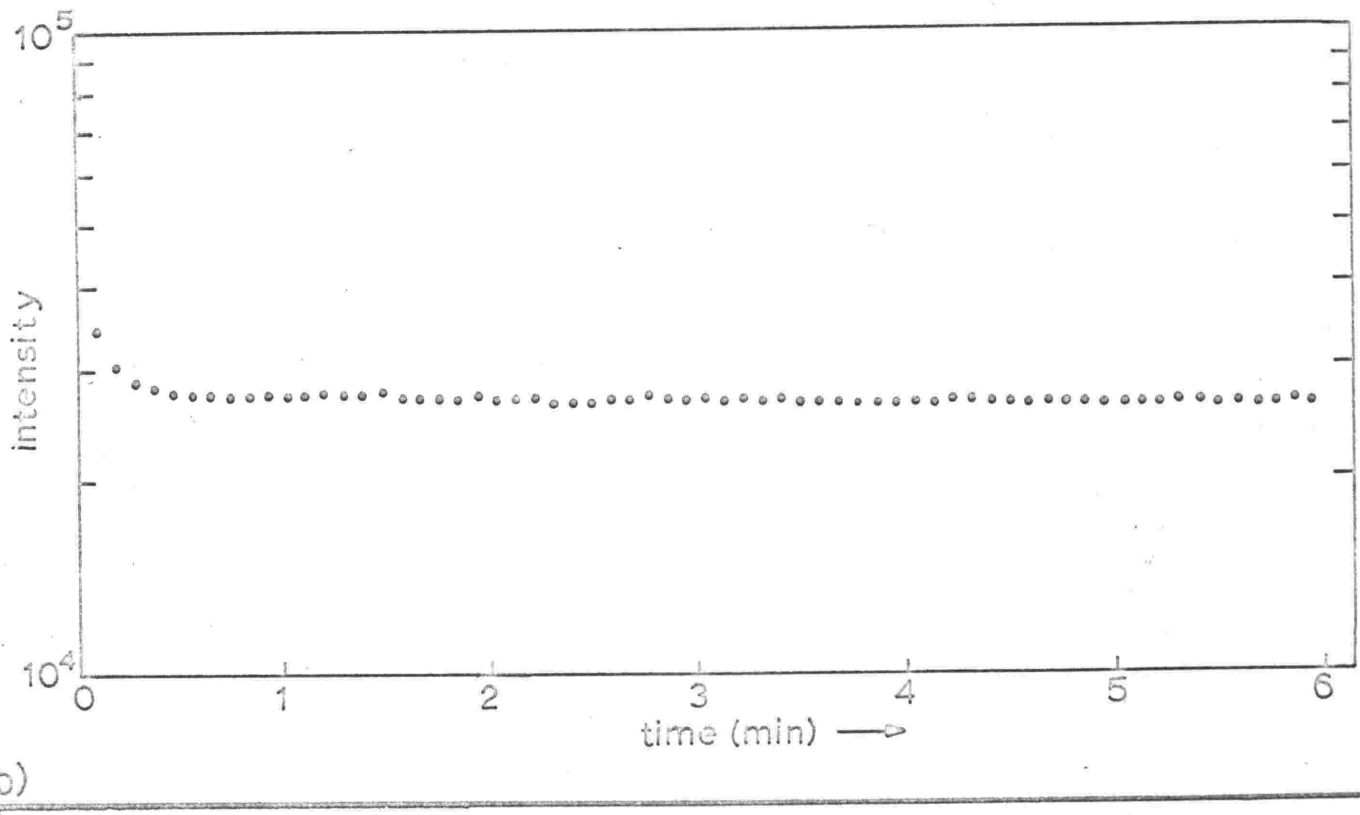

Fig. II-1. Decay of β-radiation produced by neutron activation of enriched ^{114}Cd sample.

2.4 γ-Ray Spectroscopy

The direct γ-ray spectra were taken with a 20 cm^3 coaxial Ge(Li) detector, which was fabricated at I.N.S., and the typical energy resolution obtained in an experiment was 7.8 keV (fwhm) at 1.332 MeV. Standard electronic instrumentation was used in pulse detection, and multichannel analysers included a Kicksort (4096 channels) and a Nuclear Data ND160-F dual ADC (1024 channels) interfaced to a PDP-8 computer which was programmed[27] to give a time sequence of spectra. Fig. II-2 shows relevant portions of a time sequence of spectra which identifies γ-rays from short-lived nuclides obtained by irradiating the enriched ^{114}Cd sample. Fig. II-3 is the total spectrum accumulated during the same time. Peaks attributed to ^{114}Ag decay are labelled by numbers corresponding to table II-1. Attempts at obtaining coincidence spectra failed because of low yields.

The spectra obtained were mostly analysed on a PDP-9/L computer using the techniques described by Routti and Prussin[12], the exception being that simple summing was employed for peaks of very low intensities. Energy and relative efficiency calibrations were derived from standard sources[24]. Since the spin and parity of the capture state of the $^{113}Cd(n,\gamma)^{114}Cd$ reaction[20,21] corresponds to the 1^+ ground state of ^{114}Ag, it is not surprising that the γ-rays detected from ^{114}Ag decay appear in the capture spectrum. The expected contaminants from (n,γ) and (n,α) reactions were found[28,29] and, where necessary, corrections were applied to ^{114}Ag γ-ray intensities. Not all γ-rays have been accounted for satisfactorily, and the appearance of ^{116m}In as a contaminant

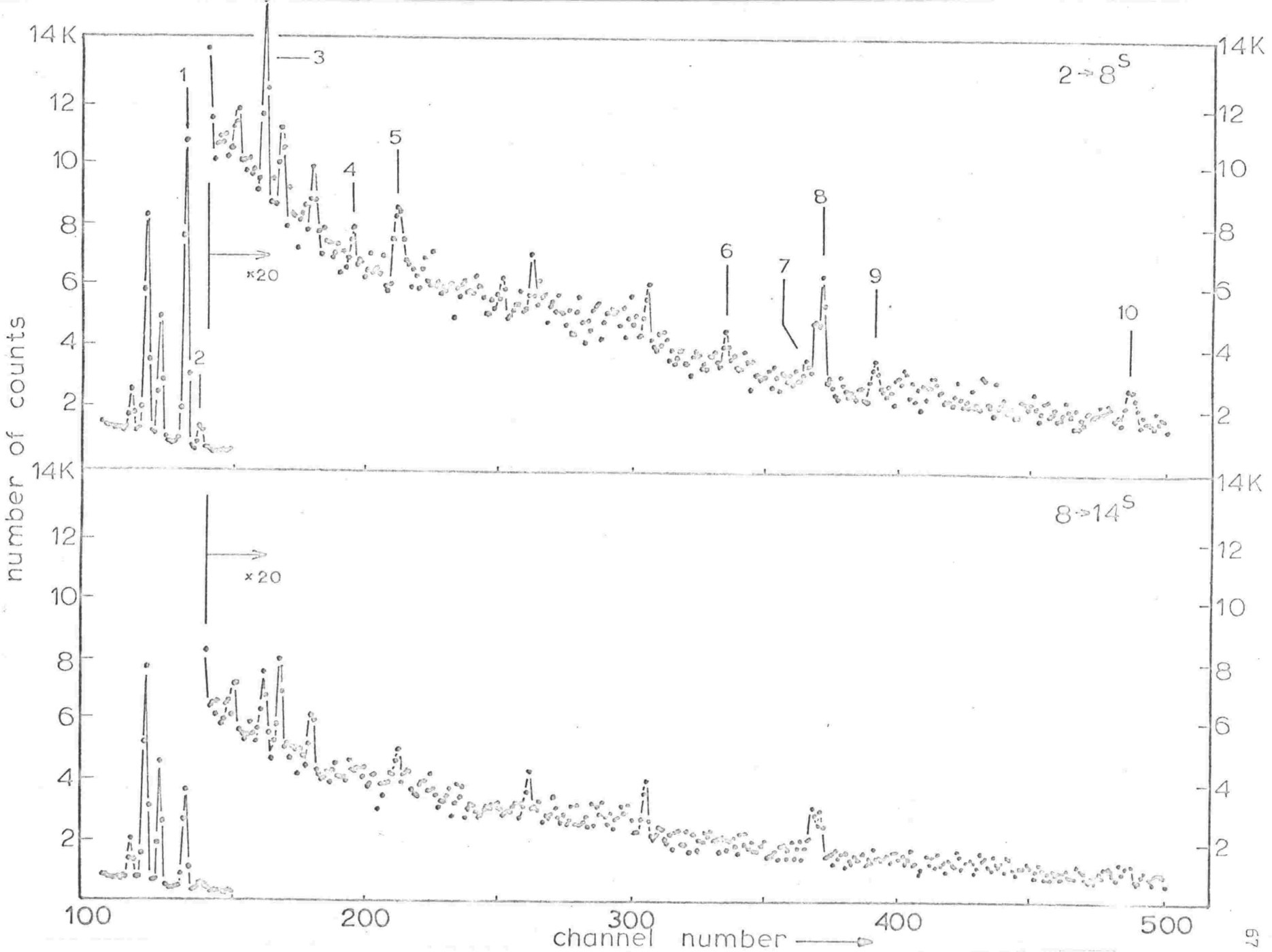

Fig. II-2. Time sequence of γ-ray spectra from activated ^{114}Cd sample, 2011 cycles.

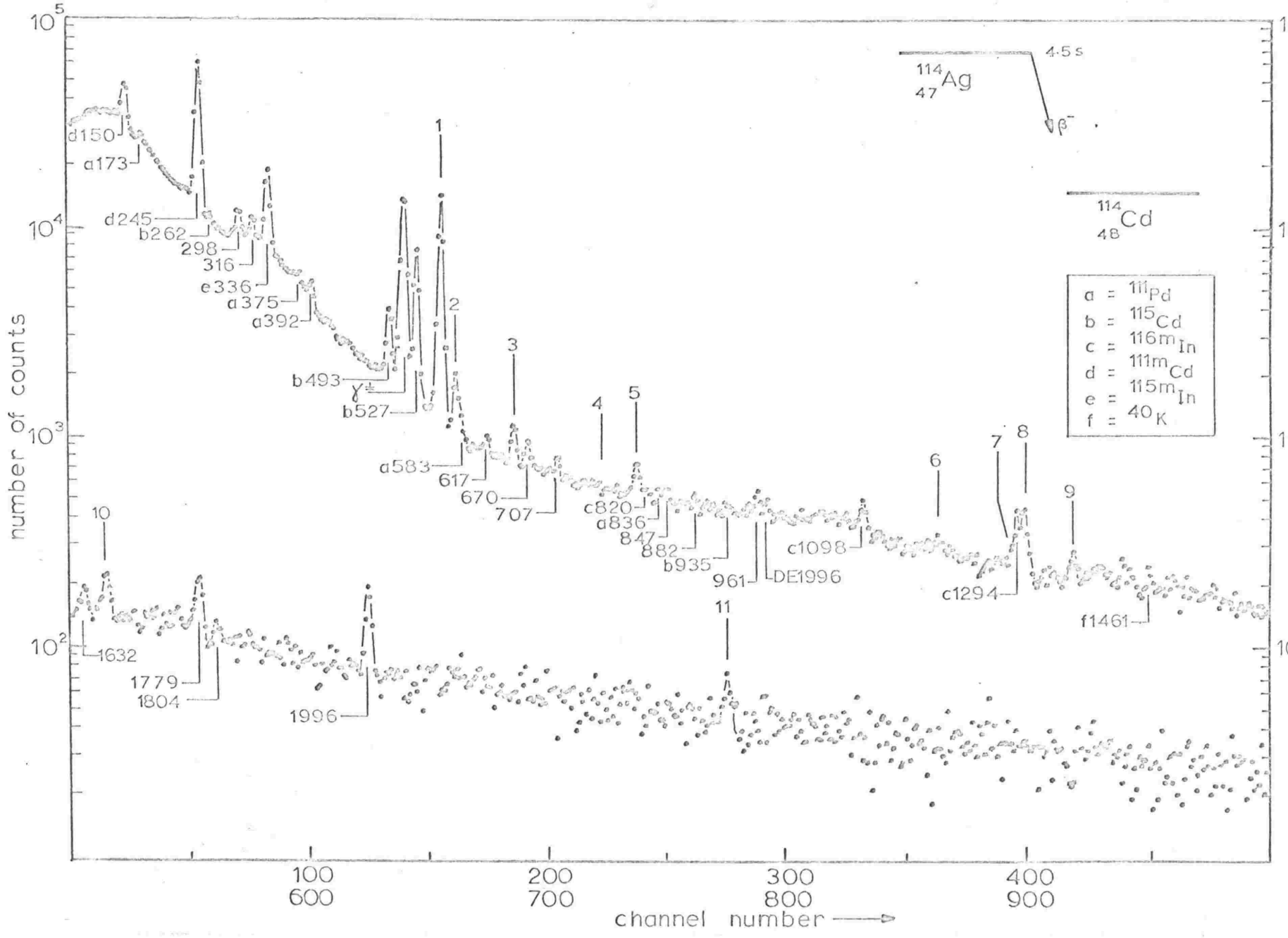

Fig. II-3. Total γ-ray spectrum from activated ^{114}Cd sample, 2011 cycles.

is unexpected as it indicates an elemental impurity.

2.5 β-Ray Spectroscopy

The short-lived activity produced by the irradiation of natural Cd was isolated by counting in two consecutive 10 sec interval, and subtracting the second from the first. Some ^{16}N contamination from the $^{16}O(n,p)^{16}N$ reaction was removed by using a spectrum obtained with an oxalic acid sample. Other energy calibration standards were ^{28}Al, ^{34m}Cl, ^{32}P, ^{24}Na and ^{207}Bi[24]. Samples for calibration purposes were mounted in the same manner as the Cd samples.

A 3" x 3" plastic scintillator (NE102) optically coupled to a photomultiplier (Dumont K1846) served as a β-detector. By using conversion electron peaks of ^{137}Cs and ^{207}Bi, the energy resolution of the system was found to be 13.4% at 1 MeV. The incident β-rays were collimated through 1 cm thick aluminium, and tailing and resolution corrections described by Slavinskas et al.[30] were applied to the accumulated spectrum. Fig. II-4 shows the corrected Fermi-Kurie plot obtained from the irradiated Cd sample. It is apparent that there are two groups of β-rays present, of endpoint energies 2.82 ± 0.19 and 4.90 ± 0.26 MeV. The former corresponds with the β^--decay of 24sec ^{110}Ag[24] and the latter is ^{114}Ag.

3. Discussion

3.1 γ-Ray Spectroscopy

11 of the γ-rays detected were assigned as being associated with the decay of 4.5 sec ^{114}Ag. All of them have been seen before as prompt γ-rays in the $^{113}Cd(n,\gamma)^{114}Cd$ reaction[20,21] and most of their energies are known accurately. 9 of the γ-rays are satisfactorily placed in the level scheme of Backlin et al.[21]

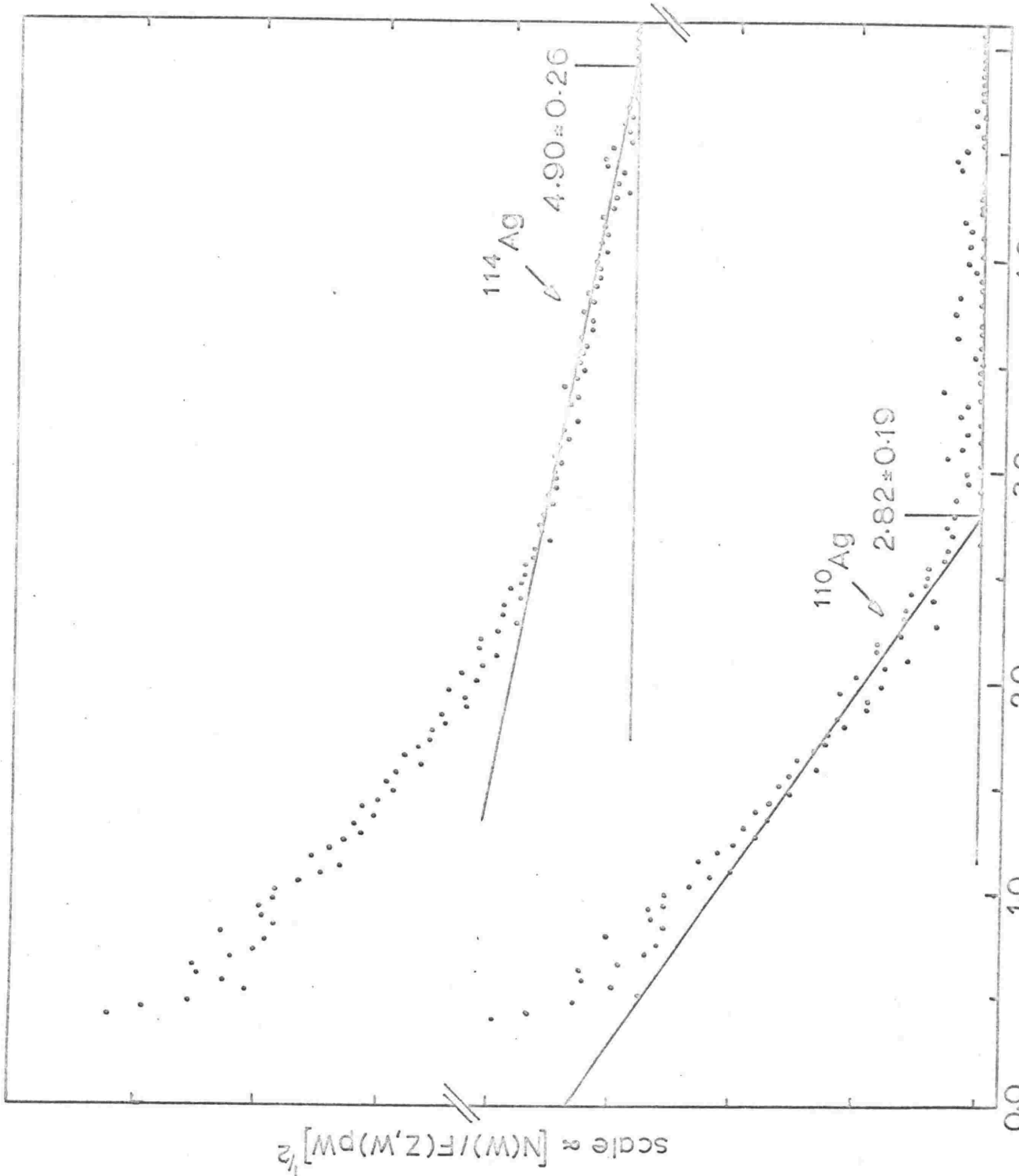

Fig. II-4. Fermi-Kurie plot of β-spectrum obtained by activation of natural Cd.

No.	E_γ (keV)	I_γ	assignment
1	558.0±0.4	100	BA
2	576.1±0.5	8.1±1.3	CB
3	651.3±0.6	3.3±0.5	DB
4	747 ±3	0.7±0.3	FB
5	808.2±0.7	3.0±0.5	GB
6	1208 ±3	1.5±0.5	DA
7	1286.4±2.7	0.7±0.4	IB
8	1302.9±0.6	5.5±1.0	
9	1363.8±1.2	1.8±0.4	GA
10	1660.6±0.9	3.0±0.5	LB
11	2454.8±1.7	1.7±0.5	

Table II-1. Energies and relative intensities of γ-rays occurring in the decay of ^{114}Ag.

3.2 β-Ray Spectroscopy

The Fermi-Kurie plot of the ^{114}Ag β-decay shows that most of the decay proceeds directly to the ground state of ^{114}Cd. This is in agreement with the estimate that 10% of the decay results in a 558 keV γ-ray. The measurement of endpoint energy, 4.90 ± 0.26 MeV, concurs with the value of 4.6 ± 0.4 MeV obtained by Alexander et al.[18]

3.3 The Decay Scheme of ^{114}Ag

The decay scheme is presented in fig. II-5 and the level structure shown is that of Backlin et al.[21]. The level energies used are those deduced from conversion electron studies[21] as they are of greater accuracy than the present work. The branches of the β-decay of ^{114}Ag to levels of ^{114}Cd have been deduced from the γ-ray intensity data with the normalisation imposed by the yield of the 558 keV transition. The log ft values shown in fig. II-5 range from 4.8 to 7.5 with a possible uncertainty of ~ 0.6, indicating that most branches are allowed transitions. As the

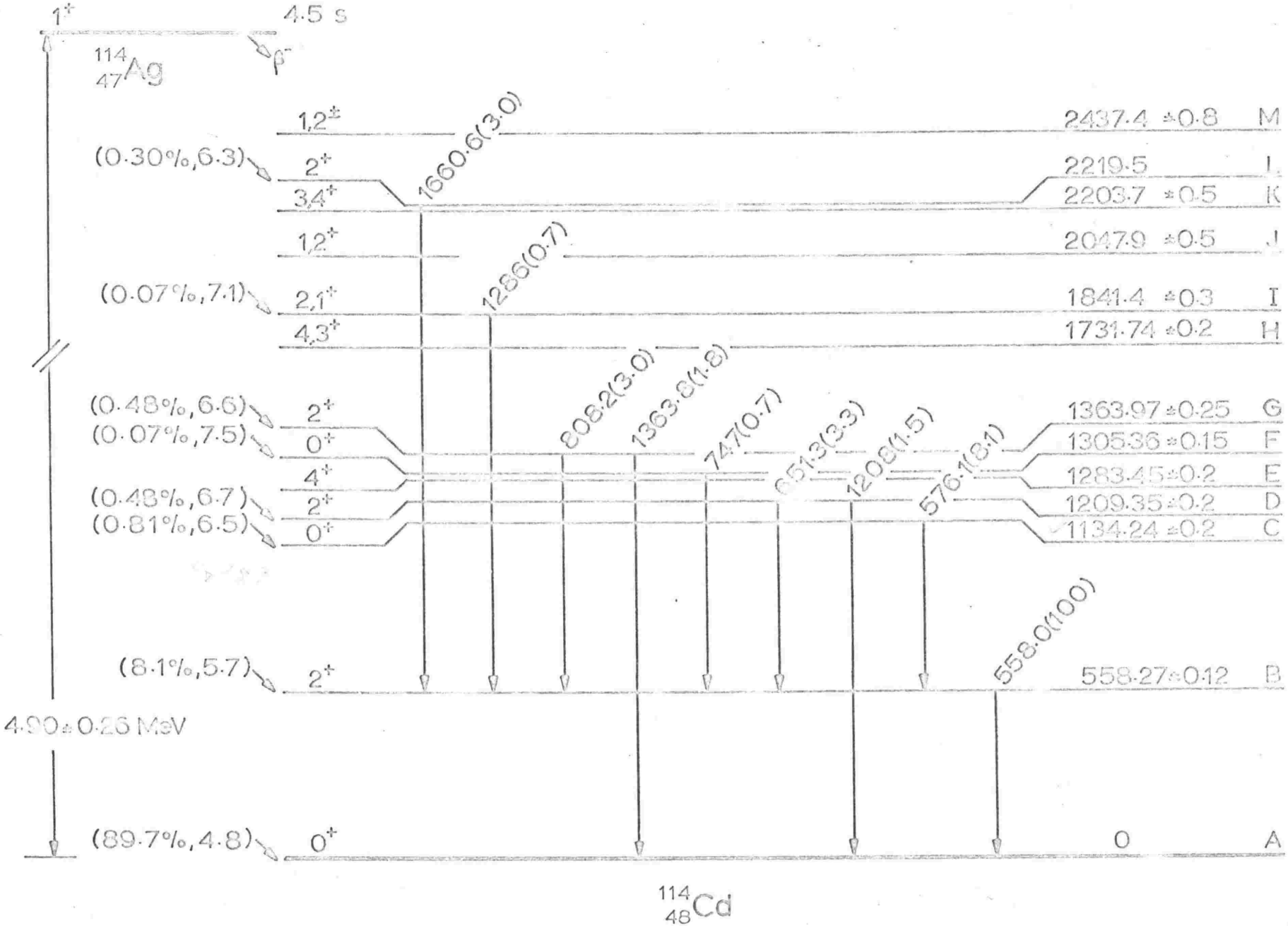

Fig. II-5. The decay scheme of ^{114}Ag. The level energies shown are those of ref.[21]

β-decay is confined to levels of spin and parity 0^+, 2^+, the expected assignment of 1^+, predicted by the Nordheim strong rule[31] from the coupling $(g_{\frac{9}{2}}^{-3})_{\frac{7}{2}^+}(d_{\frac{5}{2}}^{-1})$, is upheld.

The two γ-rays not accounted for had previously been assigned by Backlin et al.[21] as depopulating a level at an excitation energy of 2437 keV. The γ-ray of energy 2455 keV does not fit energetically, and the 1303 keV γ-ray presents difficulties when intensities are considered. If the latter γ-ray does arise from a level at 2437 keV, then a β-decay branch of 0.55% with a log ft value of 5.8 must feed the level. Even more unlikely is the consequence that there is no β-branch to the level of 1134 keV energy with which the 1302 keV transition would connect. Support for this argument exists in the lack of coincidence found by Smither[20] between the 1303 keV γ-ray and transitions of energies 558 and 576 keV. Although the 1303 keV γ-ray would make a reasonable energetic fit to the level at 1305, this level has been definitely shown to have spin and parity 0^+ by electron conversion measurements[21], and the transition would be forbidden. However, the log ft value of the β-decay to this level is surprisingly high for an allowed transition, and could be reduced to an acceptable value of 6.5 (with a β-branch of 0.62%) if the 1302 keV γ-ray was included in its decay. The suggestion of Smither[20] that a possible close doublet exists at a level energy of ~ 1305 keV therefore warrants some attention. Backlin et al.[21] has the level at 1305 keV also depopulating by a transition of 95.90 keV which gives an excellent energy fit with the 2^+ 1209.35 keV level and is strongly converted. Smither[20] has measured the intensity of the corresponding γ-ray, which was unobserved in the preceding work. Assuming a total conversion coefficient of

5.23×10^{-3} for the 558 keV E2 transition[32], the combined results of ref.[20] and[21] yield a measured total conversion coefficient for the 96 keV transition of 3.8. The theoretical value for the E2 transition is 1.7. Backlin et al.[21] has compared the intensity of this transition to that of the 747 keV transition, with which it is supposed to compete, and has stated that the 96 keV transition would appear to be enhanced by approximately 10^4 compared to the single-particle estimate.

This inconsistency would be removed if the 96 keV transition was assigned elsewhere, although there is no supporting evidence for this[21], or if a doublet of 0^+, 2^+ existed at an excitation energy ~1305 keV. The strong internal conversion transitions of 96 and 1305 keV would then result from the 0^+ level, and the 1303 keV γ-ray and most of the intensity of the 747 keV γ-ray would arise from depopulation of the 2^+ level. In this way, the β-decay of ^{114}Ag reported here could be satisfactorily explained since the decay from the 0^+ 1305 keV level would be mostly unobserved. High resolution coincidence studies of conversion electrons and γ-rays occurring in the ^{113}Cd(n,γ)^{114}Cd reaction would probably resolve the inconsistencies found.

III THE DECAY OF ^{116}Ag

1. Introduction

The decay properties of ^{116}Ag were first investigated by Alexander et al.[18] who isolated the isotope by chemical separation from fission products of ^{238}U. A more extensive study by Bahn[33] revealed 13 γ-rays

and 5 groups of β-rays which were associated with the decay. However, a decay scheme proposed from these results has not been published, and no further work on ^{116}Ag decay has been reported. The present experiments were undertaken to establish a more detailed and accurate decay scheme of ^{116}Ag using a high resolution Ge(Li) detector.

Complementary reaction studies of ^{116}Cd level structure, using inelastic proton scattering[19,34] and Coulomb excitation[7], have revealed spins and parities of levels up to an energy of 2.37 MeV.

2. Experiments and Results

2.1 Source Preparation

Sources of ^{116}Ag were made by (n,p) reactions on natural Cd and 98.14% enriched ^{116}Cd metal samples which were encapsulated in, or mounted on, polythene carriers. A pneumatic system[23], used to transport the carriers between irradiation and counting positions, and associated detection units were automated for recycling.

2.2 ^{116}Cd(n,p)^{116}Ag Cross Section

By irradiating mixtures of Si and Cd metals, a comparison of yields was obtained for the 513 keV γ-ray from the decay of ^{116}Ag and the 1.78 MeV γ-ray from the ^{28}Al decay[24]. As the decay scheme proposed in this work (fig. III-4) indicated poor agreement with the β-decay data given by Bahn[33], it was not possible to use the latter's branching ratios to determine a cross section for ^{116}Ag production. Attempts at evaluating the β-spectrum of ^{116}Ag by irradiating natural Cd (the enriched sample was too thick to be used reliably as a β-ray source) failed due to a very

low yield. However, the statistical model of Gardner and Rosenblum[9] allows a realistic extrapolation of (n,p) cross sections between isotopes. At a neutron energy of 16.4 ± 0.4 MeV, the (n,p) cross section of ^{116}Cd was estimated to be 2.9 ± 0.5 mb from the measured value of 15.3 ± 2.0 mb of ^{112}Cd*. Assuming this value, the measurement of relative yields of γ-rays implies[25,8] that 46 ± 12% of the ^{116}Ag decay results in a 513 keV γ-ray. It is from this calculation and the relative γ-ray intensities that the β-decay branching ratios shown in fig. III-4 have been deduced. The report by Bahn[33] quotes that the 513 keV transition represents 25% of the ^{116}Ag decay.

2.3 Half-Life Measurement

Using time durations of 2 min irradiation, 2 sec delay and 20 min counting, β-rays from the irradiated ^{116}Cd sample were analysed in a multiscale mode to determine the half-life of ^{116}Ag. Fig. III-1 shows the accumulated spectrum, a non-linear least-squares fit to which gives a half-life of 2.50 ± 0.02 min. This value concurs with previous measurements[18,33]. The decay data shown in fig. III-1 is slightly contaminated by an activity of 10 ± 4 sec, which has been attributed to 7.2 sec ^{16}N[24]. The possible presence of the (n,α) product, 1.5 min ^{113}Pd[35], was not apparent.

2.4 γ-Ray Spectroscopy

The direct γ-ray spectra were taken with a 32 cm^3 Ortec coaxial Ge(Li) detector; the typical energy resolution obtained in an

---

* see section 2.2 of ^{112}Ag decay, p. 50

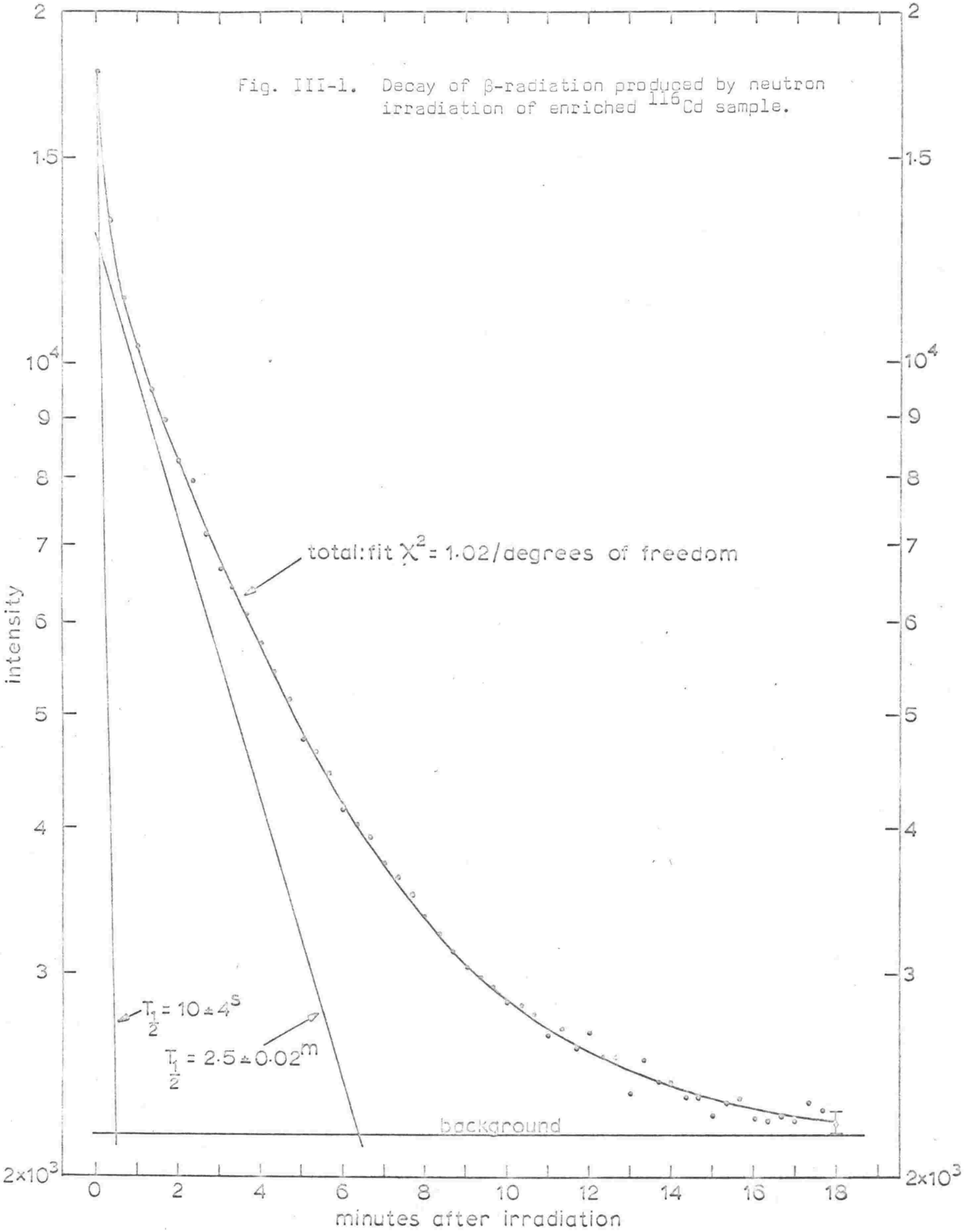

Fig. III-1. Decay of β-radiation produced by neutron irradiation of enriched ^{116}Cd sample.

experiment was 4.9 keV (fwhm) at 1.332 MeV. Standard electronic instrumentation was used in pulse detection, and multichannel analysers included a Kicksort (4096 channels) and a Nuclear Data ND160-F dual ADC (1024 channels) interfaced to a PDP-8 computer which was programmed[27] to give a time sequence of spectra. Fig. III-2 shows the total γ-ray spectrum accumulated by recycling 2.5 min irradiations of the enriched ^{116}Cd sample with periods of 8 min for counting. Peaks attributed to ^{116}Ag on the basis of their decay in the time sequence spectra (fig. III-3) are labelled by numbers according to table III-1. A 3" x 3" NaI(Tl) detector (Harshaw type 12S12) was added as a gating detector in Ge(Li)-NaI(Tl) coincidence experiments with the 513 keV transition. Typical timing resolutions were 70-100 ns. As the angle between detectors was 180° and because it was impossible to avoid gating on stray annihilation radiation which was present, the 511/513 keV radiation detected by the Ge(Li) was also gated. Coincidence between the two gates was then used to block annihilation radiation in the ^{116}Ag coincidence spectrum.

The spectra obtained were analysed on a PDP-9/L computer using the techniques described by Routti and Prussin[12]. Energy and relative efficiency calibrations were derived from standard sources[24]. The expected contaminants from (n,γ)[36] and (n,2n)[28] reactions were found and, where necessary, corrections were applied to the ^{116}Ag γ-ray intensities. A small amount of γ-radiation resulting from the daughter of the (n,α) product[37] was also detected. The measured contaminant intensities were generally in good agreement with the published values. The established energies and level relations of transitions from all reaction products were used in a subsequent energy recalibration in which the cubic

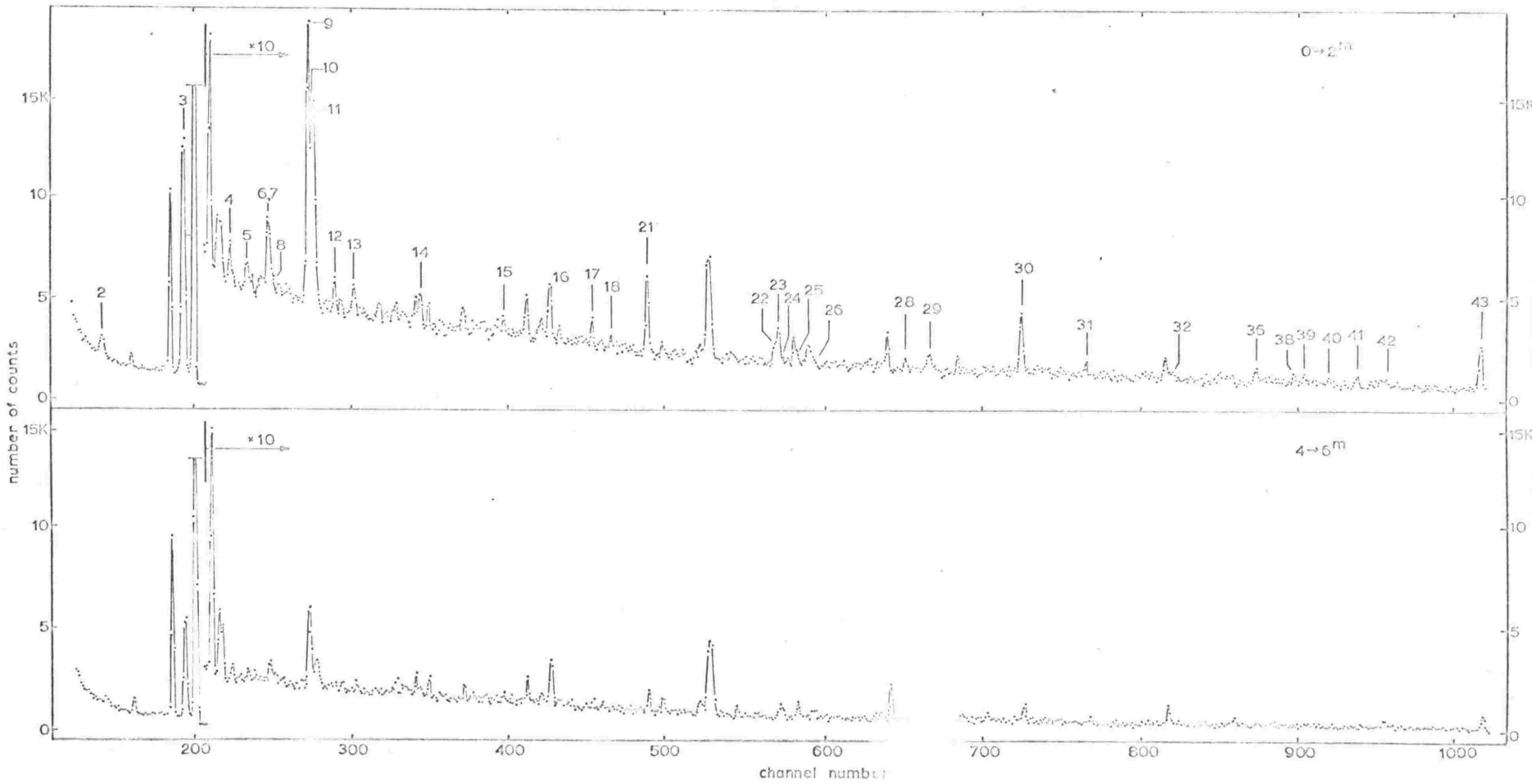

Fig. III-2. Time sequence of γ-ray spectra from activated ^{116}Cd sample.

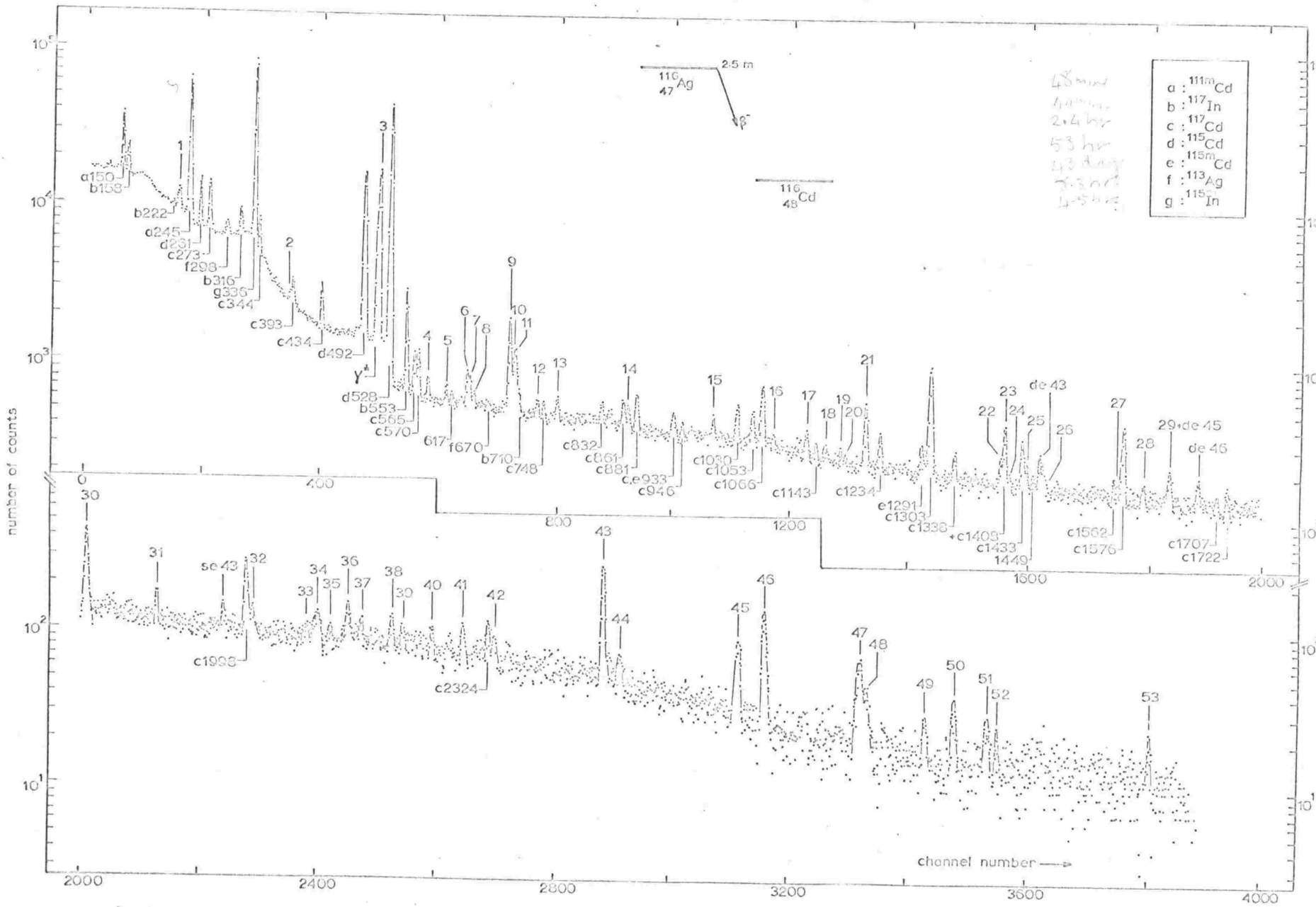

Fig. III-3. Total γ-ray spectrum from activated ^{116}Cd sample.

No.	E_γ (keV)	I_γ	assignment	No.	E_γ (keV)	I_γ	assignment
1	228.9±0.3	4.4		28	1603.8±0.9	1.4	
2	389.5±0.7	1.6	PM	29	1641.4±0.6	2.9	FA
3	513.4±0.3	100	BA	30	1778.5±0.4	12.	JB
4	583.8±0.4	1.7		31	1878.0±0.6	2.0	KB
5	609.9±0.5	1.3		32	2006.4±0.8	2.1	QC
6	640.0±0.4	3.1		33	2082.1±1.1	1.0	IA
7	643.6±0.5	2.4		34	2097.4±0.6	2.5	
8	649.4±0.5	1.1	JF	35	2112.2±1.2	0.99	MB
9	699.3±0.3	15.	CB	36	2135.5±0.7	2.4	RC
10	703.1±0.9	2.7	CC	37	2152.9±1.2	0.93	
11	706.5±0.4	7.3	DB	38	2193.6±0.6	2.4	
12	739.5±0.5	1.5	HC	39	2208.6±0.9	1.4	NB
13	768.8±0.5	1.8	NH	40	2248.3±0.9	1.8	
14	867.9±0.5	1.8	EB	41	2290.8±0.6	3.1	JA
15	994.8±0.6	1.7		42	2332.1±1.0	1.7	OB
16	1081.5±0.7	0.93	JC	43	2479.4±0.4	15.	LA
17	1129.1±0.6	2.2	FB	44	2502.5±0.8	1.8	PB
18	1156.1±0.9	1.0		45	2662.8±1.0	4.6	
19	1177.6±0.9	0.83	KC	46	2705.4±0.5	9.7	QB
20	1184.8±1.2	0.62		47	2835.0±0.6	4.6	RB
21	1212.6±0.4	8.5	CA	48	2843.5±0.9	2.2	OA
22	1402.4±0.5	2.3	GB	49	2921.4±1.1	1.7	
23	1408.2±0.4	5.0	MD	50	2960.3±0.8	2.0	
24	1414.8±1.0	0.82	MC	51	3003.3±1.2	1.2	
25	1438.7±0.6	2.0	HB	52	3016.4±1.7	0.38	PA
26	1461.6±0.5	2.5	OE	53	3218 ±2	0.80	QA
27	1569.4±1.4	0.83	IB				

Table III-1. Energies and relative efficiencies of γ-rays occurring in the decay of ^{116}Ag. Intensities above 1.0 are with an accuracy of about 10%. Below 1.0 the accuracy falls to 25%.

polynomial fit was bootstrapped to the level structure and escape peak relations found to be well-defined in the γ-ray spectrum.

3. Discussion

3.1 γ-Ray Spectroscopy

53 of the γ-rays detected were assigned as being associated with the decay of 2.5 min ^{116}Ag, and 36 of these have been placed in a level scheme involving 17 excited levels of ^{116}Cd. The energies of the major γ-rays roughly correspond to those found in the NaI(Tl) study of Bahn[33], but there is a lack of agreement when the relative intensities are compared. In particular, the intensity of the 513 keV transition relative to the other γ-rays appears to be decreased by a factor of about 4 compared with the present results and with the results of the earlier work reported by Alexander et al.[18]

The Ge(Li)-NaI(Tl) coincidence measurements revealed only the presence of peaks at 699 and 706 keV. However, cascade relationships of the 513 keV transition with higher energy γ-rays could not be discounted as their intensities would be much less.

3.2 The Decay Scheme of ^{116}Ag

The proposed decay scheme is presented in fig. III-4. The 4 lowest excited levels of ^{116}Cd have previously been established by reaction analysis[24], and further levels of energies 1.637, 1.90(3^-), 2.24(5^-) and 2.37(4^+) MeV have been found by inelastic proton scattering[19,34]. The 13 new levels deduced from this study have been constructed numerically and it would appear that levels at 1641 and 1915 keV correspond to the 1.637 and 1.90 MeV states of the (p,p') work. There is some ambiguity

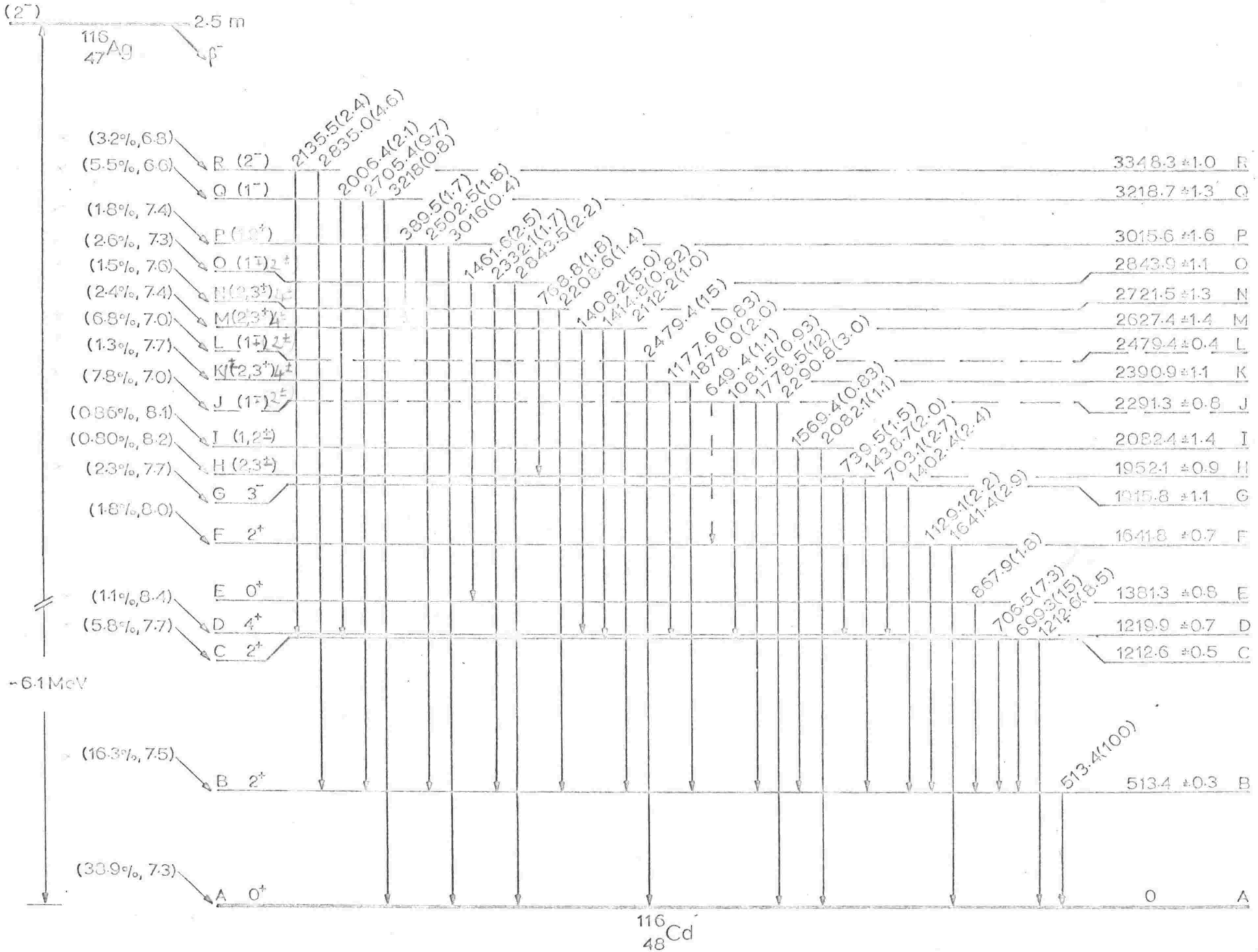

Fig. III-4. The decay scheme of ^{116}Ag.

in the levels depopulated by γ-rays of energies 1778.5 and 2479.4 keV as a reasonable energy fit for a level at about 2992 keV is obtained if these γ-rays were to arise from transitions from this level to the first and second excited states of ^{116}Cd. However, the agreement with other possible transitions for a level at 2291, and the β-ray branch to the 1212 keV level favour the system shown. No other γ-ray has been found to support the existence of a level at 2479 keV. A further level could exist at an energy of 2664 keV defined by γ-rays of energies 2663 and 2153 keV. This possible level was not included in the proposed decay scheme as the standard deviation of the energy sums involved was larger than that expected from the quoted errors. Several γ-rays with energies in the range 513 to 699 keV have not been assigned and it is possible that some of these result from states at an energy about that of the vibrational two-phonon triplet. Quintuplets of states at this position have been found in the even-even isotopes ^{112}Cd and ^{114}Cd[24].

The β-ray branches shown in fig. III-4 have been deduced from the γ-ray intensities and the assumed decay scheme with the normalisation imposed by the measured yield of the 513 keV γ-ray. The values disagree with measurements of Bahn[33] who found five β-ray groups with endpoint energies and intensities 5.12 (9%), 3.41 (21%), 2.58 (26%), 2.26 (33%) and 1.30 (11%) MeV. The γ-rays determined in this work cannot be matched to this β-decay. The log ft values, calculated with an endpoint energy assumed from mass formula predictions[38], range from 6.6 to 8.4 with a possible uncertainty of ~0.6. According to Gove[15], this does not necessarily exclude the possibility for some of these β-transitions to have an allowed character, although most of them will be first forbidden. The decay scheme is very similar to that of ^{112}Ag, and a ground state of

2^- for ^{116}Ag would be consistent with the proposed decay. This ground state probably arises as a coupling $(p_{1/2})_\pi\ (d_{3/2})_\nu^{-1}$, or $(p_{1/2})_\pi\ (d_{5/2})_\nu^{-1}$ which is the configuration found for ^{112}Ag[14]. Hence an allowed β-transition from an initial $(d_{3/2})$ or $(d_{5/2})^{-1}$ state to a final $(g_{9/2})$ state will be 1-forbidden and show a high log ft value. Spin and parity assignments for the levels populated by ^{116}Ag decay would therefore be from 0^+ to 4^+ and 1^- to 3^-. Tentative level assignments, based on log ft values and γ-ray branching, have been included in fig. III-4.

While the present results have led to a more detailed level structure of ^{116}Cd, there is a need for the β-spectrum from the decay of ^{116}Ag to be redetermined directly so that the assumption of a cross section value for the ^{116}Cd(n,p)^{116}Ag reaction can be eliminated. The proposed decay scheme of ^{116}Ag could then be put on a firmer basis.

IV DISCUSSION

The preceding investigations into the decay schemas of the three short-lived Ag isotopes have shown that ^{114}Ag is an apparent misfit in the triad with ^{112}Ag and ^{116}Ag. The decay character is substantially different and the reason for this is obviously due to the ground state spin and parity of this nuclide. To understand how a 1^+ ground state can interrupt a sequence of 2^- states, it is instructive to consider the single-particle configurations of nuclei adjacent to the odd-odd Ag isotopes as these may be chosen with only one odd nucleon (fig. IV-1).

Nilsson diagrams of single-particle eigenvalues for odd neutrons in

$|(1g_{9/2})^{-3}_{7/2}(d_{5/2})_{5/2}\rangle_{1+}$ $|(1g_{9/2})^{-1}_{7/2}(d_{5/2})^{3}_{5/2}\rangle_{1+}$ $|(g_{9/2})^{-3}_{7/2}(d_{5/2})^{-1}_{5/2}\rangle_{1+}$? ? ?

Fig. IV-I. States[24] due to single-particle configurations typical of the region studied.

the region $50 < N < 82$ are not to be found in the literature[24,39], and there is some uncertainty in the actual ordering of levels. The pairing energy of nucleons in the same shell is of particular importance as differences in level energy are small. The levels involved[40] (in the accepted order of increasing energy) in the Ag region considered are:

protons	$(2p_{1/2})$	$(1g_{9/2})$				(1)
total no.	40	50				
neutrons	$(2d_{5/2})$	$(1g_{7/2})$	$(3s_{1/2})$	$(2d_{3/2})$	$(1h_{11/2})$	
total no.	56	64	66	70	82	(2)

The low-energy level sequence of even-odd Cd nuclei (for which protons are coupled to spin zero) demonstrate all the neutron configurations possible with the single-particle levels shown above in a straight forward manner, and there are about four of these before collective states appear. The order of the levels vary, but the $s_{1/2}$ state generally forms the ground state. This indicates that the levels (2) are close together and that pairing of particles is very important. Possible proton configurations are illustrated by the odd-even Ag nuclei (neutrons coupled to spin zero) with A = 107, 109, 111 which all have $\frac{1}{2}^-$, $\frac{7}{2}^+$ for ground and first excited states. Higher energy $\frac{9}{2}^+$ states have also been found in ^{107}Ag and ^{109}Ag. The origins of the $\frac{1}{2}^+$ and $\frac{9}{2}^+$ states are obvious, but the $\frac{7}{2}^+$ can only come from an arrangement of the three $1g_{9/2}$ proton holes coupling to $\frac{7}{2}^+$ (allowed by the Pauli principle). This can similarly be found in the odd-odd Ag isotopes where a 6^+ isomeric state exists and is due to the $\frac{7}{2}^+$ state coupling with a $2d_{5/2}$ neutron hole (Nordheim's weak rule[31,41]). The 1^+ ground state of ^{106,108,110}Ag is most probably[41] the same configuration

$(g_{9/2}^{-3})_{7/2}\ d_{5/2}^{-1}$ but with spins anti-parallel (Nordheim's strong rule). A 2^- state which also appears to be common between the 1^+ and 6^+ states is the $p_{1/2}d_{5/2}^{-1}$ combination. It is this configuration which is most likely to be the reason for the 2^- ground state of $^{112}Ag^{41)}$. The 1^+ ground state of ^{114}Ag is probably a reversion back to the configuration of ^{110}Ag, although a $g_{9/2}g_{7/2}^{-1}$ coupling is possible, and the 2^- state of ^{116}Ag results from a new combination $p_{1/2}d_{3/2}^{-1}$. It would therefore seem that ^{112}Ag is the nuclide which interrupts a sequence of ground-state configurations and this may be due to a small change in spin-orbit coupling caused by the influence of the $3s_{1/2}$ sub-shell (if the $d_{5/2}$ hole was filled, a single neutron would occupy this level). The disappearance with ^{112}Ag of a sequence of 6^+ isomeric states in odd-odd Ag nuclei is also indicative of some change. The usual 1^+ ground-state in this case is only 18.5 keV above the 2^- state. The similarities found in the decays of the isotopes ^{112}Ag and ^{116}Ag remain since, although the ground states may arise from different configurations, the β-decay of the nuclides are both 1-forbidden as a d-neutron must change to a $g_{9/2}$ proton.

The low-energy level sequences of the even-even Cd nuclei are little changed as the neutron number increases, and the first few states certainly arise from collective quadrupole excitations. These will be examined in greater detail in the two following chapters. The salient similarity in the $^{112,114}Cd$ level structure is the quintuplet of states about the expected two-phonon triplet. This appears to be missing in ^{116}Cd but it is probable that the states exist. The present investigation could not confirm this as β-branching to them would be weak. Above about 1.5 MeV, the presence of noncollective states is apparent since they

represent changes in configuration. When these changes happen to resemble the decaying Ag isotope, relatively large β-branches feed them. Because of the closely-packed single-particle levels involved, interpretations of these states are difficult to make.

REFERENCES

1) D.T. Saskai, J.M. D'Auria and B.D. Pate, Nucl. Phys. A130 (1969), 687

2) E.W.A. Lingeman, J. Konijn and L.G.R. Mathot, Nucl. Phys. A122 (1968), ~~577~~ 557

3) J.A. Macdonald and H.D. Sharma, Nucl. Phys. A156 (1970), 321

4) M. Koike, Nucl. Phys. A98 (1967), 209

5) Y.S. Kim and B.L. Cohen, Phys. Rev. 142 (1966), 788

6) P.D. Barnes, J.R. Comfort and B.K. Bockelman, Phys. Rev. 155 (1967), 1319

7) W.T. Milner, F.K. McGowan, P.H. Stelson, R.L. Robinson and R.O, Sayer, Nucl. Phys. A129 (1969), 687

8) "Neutron Cross Sections" (2nd ed.), BNL 325, Vol. 1 and 2 (1964, 1966)

9) D.G. Gardner and S. Rosenblum, Nucl. Phys. A96 (1967), 121

10) V.N. Levkovskii, Soviet Phys. - JETP 18 (1964), 213

11) H. Inoue, J. Ruan, S. Yasukawa and Y. Yoshizawa, Nucl. Phys. 38 (1962), 50

12) J.T. Routti and S.G. Prussin, Nucl. Inst. and Meth. 72 (1969), 125

13) P.H. Stelson, J.L.C. Ford, R.L. Robinson, C.Y. Wong and T. Tamura, Nucl. Phys. A119 (1968), 14

14) J.W. Chan, W.B. Ewbank, W.A. Nierengerg and H.A. Shugart, Phys. Rev. 138 ~~1138~~ (1964), 1138

15) N.B. Gove, "Nuclear Spin-Parity Assignments", Academic Press (1961)

16) F.K. McGowan, R.L. Robinson, P.H. Stelson and J.L.C. Ford, Nucl. Phys. 66 (1965), 97

17) R.B. Duffield and J.D. Knight, Phys. Rev. 75 (1949), 1613

18) J.M. Alexander, U. Schindewolf and C.D. Corywell, Phys. Rev. 111 (1958), 228

19) M. Koike, I. Nonaka, J. Kokame, H. Kamitsubo, Y. Awaya, T. Wada and H. Nakamura, Nucl. Phys. A125 (1969), 161

20) R.K. Smither, Phys. Rev. 124 (1961), 183

21) A. Backlin, N.E. Holmberg and G. Backstrom, Nucl. Phys. 80 (1966), 154

22) F.E. Coffman and J.H. Hamilton, Nucl. Phys. A127 (1967), 586

23) P.J. Mathew, G.J. McCallum and R.M. Freeman, Phys. Lett. 28B (1968), 106

24) C.M. Lederer, J.M. Hollander and I. Perlman, "Table of Isotopes", Wiley and Sons (1967)

25) W.W. Givens, W.R. Mills and R.L. Caldwell, Nucl. Inst. and Meth. 80 (1970), 95

26) A. Poularikis, J. Cunningham, W. McMillan, J. McMillan and R.W. Fink, J. Inorg. Nucl. Chem. 13 (1960), 196

27) H.J. Hay, I.N.S. Report INS-R-59 (1968)

28) G. Graeffe, C.W. Tang, C.D. Corywell and G.E. Gordon, Phys. Rev. 149 (1966), 884

29) G. Berzins, M.E. Bunker and J.W. Starner, Nucl. Phys. A126 (1969), 273

30) D.D. Slavinskas, T.J. Kennet and W.V. Prestwich, Nucl. Inst. and Meth. 37 (1965), 36

31) L.W. Nordheim, Phys. Rev. 78 (1950), 294

32) R.S. Hager and E.C. Seltzer, Nuclear Data 4A, No's 1 and 2 (1968)

33) E.L. Bahn, Thesis, St Louis, Washington Univ. (1962)
Nucl. Science Abstracts 18: 4620 (1964)

34) H.F. Lutz, W. Bartolini and T.H. Curtis, Phys. Rev. 178 (1969), 1911

35) P.O. Aronsson, E. Ehn and J. Rydberg, Phys. Rev. Lett, 25 (1970), 590

36) V.R. Pandharipande, K.G. Prasad, R.P. Sharma and B.V. Thosar, Nucl.

Chapter Five

NUCLEAR MODELS FOR CADMIUM EVEN-EVEN NUCLEI

5.1 Introduction

Mathematical models proposed for the atomic nucleus fall into two broad categories, and most have some degree of success in predicting various properties of nuclei in different regions of the periodic table. A universal model is not yet in existence although some combinations of the two points of view (unified models) are proving to have more widespread applications.

The first category deals with a microscopic approach in which the nucleus is treated as being composed of distinct particles. The nucleons may be independent, as in the independent shell model, or may have some interaction with each other such as a two-body force (Hartree-Fock, RPA). This method generally becomes exceedingly complicated as the number of nucleons increases.

The other category is the collective model for which the approach is macroscopic: a quantised fluid is endowed with certain properties and subjected to boundary conditions in order to predict the gross characteristics of a system of nucleons. The eigenstates of the nucleus are then due to modes of motion of a liquid drop rather than individual particle excitation. This is the adiabatic approximation, and it is with this model that the low-energy level structure of Cd nuclei can be more easily interpreted. At higher energies it is probable that individual particle excitation would compete with collective motion, and so render the treatment invalid.

5.2 The Liquid Drop Model; Bohr's Collective Hamiltonian[1-4)]

With the nucleus considered to be a continuous drop of nuclear material, the surfaces of constant density may be described by equations

$$R = R_0 \left[1 + \sum_{\lambda=0}^{\infty} \sum_{\mu=-\lambda}^{+\lambda} \alpha_{\lambda\mu} Y_\lambda^\mu(\theta,\phi) \right] \tag{1}$$

where θ,ϕ are polar angles with respect to some arbitrarily chosen space-fixed axes. Imposing incompressibility upon the drop therefore implies that any collective motion will be described by variations of the coefficients $\alpha_{\lambda\mu}$ with time.

With the additional assumptions that nuclear fluid motion is irrotational and takes the form of small surface distortions about a spherical shape[1], the vibrational kinetic energy may be shown to be

$$T_{vib} = \tfrac{1}{2} \sum_{\lambda\mu} B_{\lambda\mu} |\dot{\alpha}_{\lambda\mu}|^2 \tag{2}$$

to a quadratic approximation, while the potential energy is

$$V = \tfrac{1}{2} \sum_{\lambda\mu} C_{\lambda\mu} |\alpha_{\lambda\mu}|^2 \tag{3}$$

The assumption that nuclear matter is incompressible demands that $\lambda = 0$ vibrations be ignored. The expansion term corresponding to $\lambda = 1$ describes motion of the centre of mass of the liquid drop in the lab. system and, since the nuclear Hamiltonian must be invariant under translation, is physically uninteresting. As only the first few excited states are to be considered, the following treatment will be confined to $\lambda = 2$ (quadrupole) vibrations. This restriction allows only positive parity eigenstates of spins 0,2,4... to be generated. The first few negative parity states (e.g., 3^-) are the result of $\lambda = 3$ (octupole) vibrations.

Hence (1) may be written

$$R = R_o \left[1 + \sum_{\mu} \alpha_{2\mu} Y^{\mu}_2(\theta,\phi) \right] \tag{4}$$

Should the nucleus possess a permanent deformation, and since θ,ϕ are measured relative to space-fixed axes, then, if the nucleus rotates, $\alpha_{2\mu}$ will again be functions of time. It would therefore be more appropriate to choose body-fixed axes (1,2,3) and constant nuclear shape, i.e.,

$$R = R_o \left[1 + \sum_{\mu} a_{2\mu} Y^{\mu}_2(\theta',\phi') \right]$$

with $$Y^{\mu}_2(\theta,\phi) = \sum_{\mu'} D^2_{\mu\mu'}(\Omega_i) Y^{\mu'}_2(\theta',\phi')$$

$$\therefore a_{2\mu'} = \sum_{\mu} \alpha_{2\mu} D^2_{\mu\mu'}$$

$D^2_{\mu\mu'}(\Omega_i)$ are the rotation matrices appropriate to the Euler angles Ω_i of the body-fixed axes. The choice of body-fixed axes as principal axes can be made such that it reduces the five coefficients $\alpha_{2\mu}$ to the two independent variables a_{22}, a_{20} which, together with the Euler angles, give a complete description of the system.

Defining the two new independent variables

$$\beta_0 = \beta\cos\gamma = a_{20}$$

$$\beta_2 = \beta\sin\gamma = \sqrt{2}\sqrt{a_{22}} = \sqrt{2}\sqrt{a_{2-2}} \tag{5}$$

then the constant density surface of the drop cuts the k-axes (body-fixed axes) at[15]

$$R_k = R_o \left[1 + (5/4\pi)^{\frac{1}{2}} \beta\cos(\gamma - 2\pi k/3) \right] \qquad k = 1,2,3 \tag{6}$$

and hence with $\gamma = (k-1)2\pi/3$ the nuclear shape is of a prolate spheroid, and oblate for $\gamma = (2k-1)\pi/3$. For a fixed value of γ, β-vibrations correspond to the nucleus preserving its axis of symmetry, whereas γ-vibrations destroy any axial symmetry.

In terms of the body-fixed components of angular velocity w_k, the nucleus will possess a rotational kinetic energy

$$T_{rot} = \tfrac{1}{2} \sum_{k'k} I^{(2)}_{k'k} w_{k'} w_k$$

where the components of the inertial tensor (for quadrupole deformation) are

$$I^{(2)}_{k'k} = B_{(2)} \sum_{\mu'\mu} a^{*}_{2\mu'} a_{2\mu} \langle 2\mu' \mid L_{k'} L_k \mid 2\mu \rangle \qquad (7)$$

for angular momenta $L_{k'}$, L_k about body-fixed axes k, k'. In the body-fixed system for which $a_{2\mu} = 0$ for μ odd, it can be shown that the inertial tensor, for either a rigid or non-rigid body, is diagonal.

The total kinetic energy of the system can then be put in the form (with $\hbar = 1$)

$$T = \tfrac{1}{2} \sum_{\mu\nu} B_{\mu\nu}(\beta_0, \beta_2)\, \dot{\beta}_\mu \dot{\beta}_\nu + \tfrac{1}{2} \sum_k I_k(\beta_0, \beta_2) w_k^2 \qquad (8)$$

where $\mu, \nu = 0, 2$ and $k = 1, 2, 3$. The addition of a potential term $V(\beta_0, \beta_2)$ completes the collective Hamiltonian due to Bohr

i.e. $\mathbf{H} = T + V \qquad (9)$

This equation forms the basis of most of the phenomenological models of

collective motion of nuclei, and in particular it is usually applied to even-even nuclei as it is generally assumed that these have spins of like particles paired off and that, for low-energy structure, none of the individual pairs are excited (i.e., the adiabatic approximation holds).

Although the six inertial coefficients entering into (8) are completely arbitrary, if deformations are small, they may be expressed in terms of a single constant B by the hydrodynamical formulae of Bohr[3]

$$I_k = 4B\beta^2 \sin^2(\gamma - 2\pi k/3)$$
$$B_{00} = B_{22} = B \; ; \; B_{02} = 0 \tag{10}$$

Calculations made with a pairing-plus-quadrupole model[1,5] indicate that the approximations are quite reasonable, and that it is the potential function which shows most diversity, the choice of which will be made later.

5.3 Analytical Solution of Collective Hamiltonian

With the definitions (10) and quantisation of (8) which is derived from classical considerations, the collective Schrödinger equation may be written

$$\left[-\frac{\hbar^2}{2B} \left\{ \frac{1}{\beta^4} \frac{\partial}{\partial\beta} \left(\beta^4 \frac{\partial}{\partial\beta}\right) + \frac{1}{\beta^2 \sin 3\gamma} \frac{\partial}{\partial\gamma} \left(\sin 3\gamma \frac{\partial}{\partial\gamma}\right) \right.\right.$$
$$\left.\left. - \frac{1}{4\beta^2} \sum_{k=1}^{3} \frac{I_k^2}{\sin^2(\gamma - 2\pi k/3)} \right\} + V(\beta,\gamma) \right] \Psi(\beta,\gamma,\theta_i) = E\Psi(\beta,\gamma,\theta_i) \tag{11}$$

The separation and subsequent solution of this equation depends upon the form of $V(\beta,\gamma)$, which has to be

$$V(\beta,\gamma) = V(\beta) + f(\gamma)/\beta^2 \tag{12}$$

Various simplifications, such as rigidity and symmetry, may be imposed[1,4]; however, the most general solution appears to that of Suárez[6], who assumes that vibrations are fast enough with respect to rotations to give sense to expressions like 'mean values of the moments of inertia' which are computed with the wave function of that part of the Hamiltonian which is a function of γ only.

With the potential operator

$$V(\beta,\gamma) = \tfrac{1}{2}C(\beta-\bar{\beta})^2 + \frac{\hbar^2}{2B}\frac{\Delta^2(\gamma-\bar{\gamma})^2}{\beta^2} \tag{13}$$

and wave functions

$$\beta^2\,|\sin 3\gamma|^{\frac{1}{2}}\,\Psi(\beta,\gamma,\theta_i) = \beta^2 F(\beta)\,|\sin 3\gamma|^{\frac{1}{2}} g(\gamma-\bar{\gamma})\,\psi_{n_I}(\theta_i) \tag{14}$$

the Schrödinger equation can approximately be separated into[6]

$$\left[\frac{d^2}{d(\gamma-\bar{\gamma})^2} - \Delta^2(\gamma-\bar{\gamma})^2 + L\right] |\sin 3\gamma|^{\frac{1}{2}} g(\gamma-\bar{\gamma}) = 0 \tag{15}$$

why is the $\frac{d}{d(\gamma-\bar{\gamma})}$ left out?

$$g(\gamma-\bar{\gamma}) \longrightarrow 0 \quad \text{for} \quad \gamma \longrightarrow \pm\infty$$

L^2 yes.

$$\left[\tfrac{1}{2}\cdot\sum_{k=1}^{3}\frac{I_k^2}{\left\langle\sin^2(\gamma - 2\pi k/3)\right\rangle} - \epsilon_{n_I}\right]\psi_{n_I}(\theta_i) = 0 \tag{16}$$

$$\left[\frac{\hbar^2}{2B}\frac{d^2}{d\beta^2} - \tfrac{1}{2}C(\beta-\bar{\beta})^2 + \frac{(\Lambda+2)\hbar^2}{2B\beta^2} + E\right]\beta^2 F(\beta) = 0 \tag{17}$$

why is the $\frac{d}{d\beta}$ term left out?

$$F(\beta) \longrightarrow 0 \quad \text{for} \quad \beta=0 \text{ and } \beta \longrightarrow \infty$$

The choice of limits for γ are rather strange when properties of the collective Hamiltonian are considered (section 5.4). However, they are no doubt chosen in this way so that (15) now corresponds to a harmonic oscillator, with solutions

$$|\sin 3\gamma|^{\frac{1}{2}} g(\gamma-\bar{\gamma}) = H_\lambda\left[\Delta^{\frac{1}{2}}(\gamma-\bar{\gamma})\right]\exp\left[-\tfrac{1}{2}\Delta(\gamma-\bar{\gamma})^2\right] \qquad (18)$$

$$L = (2\lambda+1)\Delta \qquad \lambda = 0,1,2.....$$

This gives for $\lambda = 0,1$

$$\langle \sin^2(j\gamma - 2\pi k/3)\rangle_{\lambda=0,1} = \tfrac{1}{2}\left[1-(1-\frac{2j^2\lambda}{\Delta})\exp(-j^2/\Delta)\cos(2j\bar{\gamma}- 4\pi k/3)\right] \qquad (19)$$

The eigenvalues L,ϵ_{n_I} and the separation parameter Λ are related

$$2(\Lambda+2) = \epsilon_{n_I} + 2L - \frac{9}{2}\left(\frac{1}{9} + \frac{1}{\langle \sin^2 3\gamma\rangle}\right) \qquad (20)$$

Eq. (16) corresponds to a rotor with eigenvalues

$$\epsilon_{n_I} = \left[\frac{1}{\langle \sin^2 3\gamma\rangle} + \frac{1}{\langle \sin^2(\gamma- 2\pi/3)\rangle}\right] J(J+1)/4$$

$$+ \left[\frac{1}{\langle \sin^2 3\gamma\rangle} - \frac{1}{\langle \sin^2(\gamma- 2\pi/3)\rangle}\right] \epsilon_\tau/4 \qquad (21)$$

where ϵ_τ is tabulated in ref.[7]. With relations (19), there seems to be no need for the normalisation factor graphed by Suárez[6]. The eigenfunctions of (16) are linear combinations of those of a rigid symmetrical top given in eq. (29), and the coefficients are independent of β,γ.

The solution of (17) is achieved by a truncated Taylor expansion

about $p\bar{\beta}$ i.e. the potential is approximated to an oscillator well with a minimum at $p\bar{\beta}$. This gives relations

$$p^3(p-1) = \hbar^2(BC\bar{\beta}^4)^{-1}(\Lambda+2) = \mu^4(\Lambda+2)$$
$$E(i\lambda nI) = \hbar w\left[(i-\tfrac{1}{2})(4-\frac{3}{p})^{\frac{1}{2}} + \frac{1}{2\mu^2}(2p-1)(p-1)\right] \qquad (22)$$

and the eigenfunctions are

$$\beta^2 F(\beta) = H_{i-1}\left[\delta^{\frac{1}{2}}(\beta - p\bar{\beta})\right]\exp\left[-\tfrac{1}{2}\delta(\beta - p\bar{\beta})^2\right] \qquad (23)$$

with $\delta^2 = \frac{BC}{\hbar^2}(4-\frac{3}{p})$ $\qquad w = (C/B)^{\frac{1}{2}}$

The eigenvalues E are adjusted to fit the level structure of a nucleus by variation of parameters $\bar{\gamma}$, μ and Δ. Suárez has tabulated best-fit parameters for a wide range of nuclei[6], and these show the general trend in collective features of nuclei.

Large values of Δ with small $\bar{\gamma}$ imply rotational level structure which can be expected with large ground-state quadrupole moments (i.e. nucleus possesses large permanent deformation). The moment of inertia about the 3-axis tends to zero so that the nucleus becomes symmetric about this axis and the spin K becomes a good quantum number, with eigenstates being classified according to K. This results in rotational bands being built on vibrational levels.

In the other extreme, $\Delta \longrightarrow 0$ and the level structure becomes that of a harmonic oscillator characterised by

$$E = (N+\frac{5}{2})\hbar w \qquad N = 0,1,2.... \qquad (24)$$

with angular momentum degeneracy because of a γ-independent potential operator (fig. 5.2). The quantum number K is not good and states are characterised by the phonon number N. These vibrational nuclei have small ground-state quadrupole moments (i.e., nuclei are close to being spherically symmetric). It is to this limit that the Cd nuclei under study tend.

To achieve the analytic solution, stringent requirements (eq. (12) and (13)) have to be placed upon the potential operator $V(\beta,\gamma)$ and these intuitively assume the separation of rotations and vibrations or the separation of β- and γ-motions. Furthermore, the form for $V(\beta,\gamma)$ given in eq. (13) does not adhere to the proper symmetry requirements of Bohr's Hamiltonian[2,3] (section 5.4). Although Suárez' treatment is an improvement over the static analysis of Davydov[4], the solution is still limiting, and the parameters are rather remote from those calculated from other considerations such as empirical mass formulae (liquid-drop model).

5.4 Numerical Solution of Collective Hamiltonian

Before formulating the numerical solution to the Bohr collective Hamiltonian, it is of interest to review the findings of Sakai[8] who has studied the transition from vibrational to rotational nuclei with large amounts of experimental data. He found systematic evidence to support a correspondence argument in which the 4^+, 2^+, 0^+ states of the vibrational two-phonon triplet gradually tend through a transitional region to form the 4^+ state of the ground band ($K=0^+$), the 2^+ head of the γ-vibrational band ($K=2^+$) and the 0^+ head of the β-vibrational band ($K=0^+$) of rotational nuclei respectively. Conversely, the level structure of

vibrational nuclei could be grouped into quasi-K bands resulting from the longitudinal co-ordination of excited levels in contrast to the lateral co-ordination of the phonon model. In fact, in many nuclei there appeared to be more than three quasi-bands. The success of Kumar's[9] analysis of band structure in ^{154}Sm suggests that the application of his numerical method would be of interest in the vibrational region.

The numerical technique differs from that of section 5.3 in that instead of substituting suitable wave functions into the Schrödinger equation and obtaining a set of coupled partial differential equations, the average energy $\langle\Psi|\mathbf{H}|\Psi\rangle$ is numerically found over a suitable mesh. A variation of this energy set equal to zero therefore reduces the Schrödinger system of differential equations to a set of linear algebraic equations. The integration is performed over the (β_0, β_2) plane and an investigation of symmetries shows that[1,2] the plane may be divided into 6 60^o wedges, each of which contains all possible quadrupole shapes. This arises since, for quadrupole collective motion, **H** must be invariant under rotation and that there are 24 ways of choosing the intrinsic frame such that it is right-handed. Symmetry also requires that the potential function $V(\beta_0, \beta_2)$ be composed from the two basic invariants

$$\beta^2 = \beta_0^2 + \beta_2^2 \quad ; \quad \beta^3\cos 3\gamma = \beta_0^3 - 3\beta_0\beta_2^2 \tag{25}$$

and that it must be completely smooth over the 60^o wedge.

After much reduction, the total collective energy may be expressed (with approximations (10))[2]

$$\langle\Psi_{\alpha IM}|V|\Psi_{\alpha IM}\rangle = \int d\tau' \sum_K |A_{\alpha IK}(\beta_0, \beta_2)|^2 V(\beta_0, \beta_2)$$

$$\langle\Psi_{\alpha IM}|T_{vib}|\Psi_{\alpha IM}\rangle = \frac{1}{2B}\int d\tau' \sum_{K\mu} \left|\frac{\partial A_{\alpha IK}}{\partial \beta_\mu}\right|^2 \qquad \mu = 0,2 \tag{26}$$

$$\langle \Psi_{\alpha IM} | T_{rot} | \Psi_{\alpha IM} \rangle = \int d\tau' \sum_{KK'} A^{*}_{\alpha IK} \langle \Phi^{I}_{MK} | T_{rot} | \Phi^{I}_{MK'} \rangle A_{\alpha IK'}$$

with

$$\langle \Phi^{I}_{MK} | T_{rot} | \Phi^{I}_{MK} \rangle = aI(I+1) + bK^2$$

$$\langle \Phi^{I}_{MK} | T_{rot} | \Phi^{I}_{M,K+2} \rangle = \langle \Phi^{I}_{M,K+2} | T_{rot} | \Phi^{I}_{MK} \rangle$$

$$= c\left[(1+\delta_{K0})(I+K+2)(I+K+1)(I-K)(I-K-1) \right]^{\frac{1}{2}}$$

$$d\tau' = \left| G(\beta_0, \beta_2) \right|^{\frac{1}{2}} d\beta_0 d\beta_2 \qquad (27)$$

$$G(\beta_0, \beta_2) = B^2 \prod_{k=1}^{3} I_k$$

The functions a, b and c are given by

$$a = (I_1^{-1} + I_2^{-1})/4$$

$$b = \tfrac{1}{2} I_3^{-1} - a$$

$$c = (I_1^{-1} - I_2^{-1})/8$$

The expansion of the wave function is written

$$\Psi_{\alpha IM}(\beta_0, \beta_2, \theta_i) = \sum_{K} A_{\alpha IK}(\beta_0, \beta_2) \Phi^{I}_{MK}(\theta_i) \qquad (28)$$

Where the sum runs over K even and ≥ 0, and

$$\Phi^{I}_{MK}(\theta_i) = \left[(2I+1)/16\pi^2(1+\delta_{K0}) \right]^{\frac{1}{2}} \left[D^{I}_{MK}(\theta_i) + (-)^{I} D^{I}_{M-K}(\theta_i) \right] \qquad (29)$$

The $D^{I}_{MK}(\theta_i)$ are the rotation matrices for Euler angles θ_i.

The mesh chosen[2] for numerical integration of (26) is shown in fig. 5.1 and is a series of equilateral triangles of side 2s. The 6 points specifying a triangle DEF are used to define a paraboloid, from which can be proved

$$\iint_{\Delta DEF} f(\beta_0,\beta_2)\,d\beta_0 d\beta_2 \doteq \tfrac{1}{3}(f_A+f_B+f_C)s^2/\sqrt{3} \tag{30}$$

implying that only the midpoints of the sides are required for integration. However, the vibrational kinetic energy involves derivatives of wave functions and so the vertices of the triangle enter into the problem. For the upright ΔDEF

$$\begin{aligned}
(\partial f/\partial\beta_0)_A &= \left[f_A-f_B-f_C+(f_D+f_F)\right]/s \\
(\partial f/\partial\beta_0)_B &= \left[f_F-f_D\right]/2s \\
(\partial f/\partial\beta_0)_C &= \left[f_A+f_B-f_C-\tfrac{1}{2}(f_D+f_F)\right]/s \\
(\partial f/\partial\beta_2)_A &= \left[f_A-f_B-f_C+\tfrac{1}{2}(f_D-f_F)\right]/s\sqrt{3} \\
(\partial f/\partial\beta_2)_B &= \left[2(f_A-f_B+f_C)\ -f_E-\tfrac{1}{2}(f_D+f_F)\right]/s\sqrt{3} \\
(\partial f/\partial\beta_2)_C &= \left[-f_A-f_B+f_C+f_E-\tfrac{1}{2}(f_D-f_F)\right]/s\sqrt{3}
\end{aligned} \tag{31}$$

and with the inverted triangles labelled as in fig. 5.1, the only difference in the above formulae is that the β_2 differentials should be negated.

The approximation to the collective energy which results from this procedure can therefore be written

$$\langle\Psi|H|\Psi\rangle \doteq \sum_{ii'} A_i H_{ii'} A_{i'} \tag{32}$$

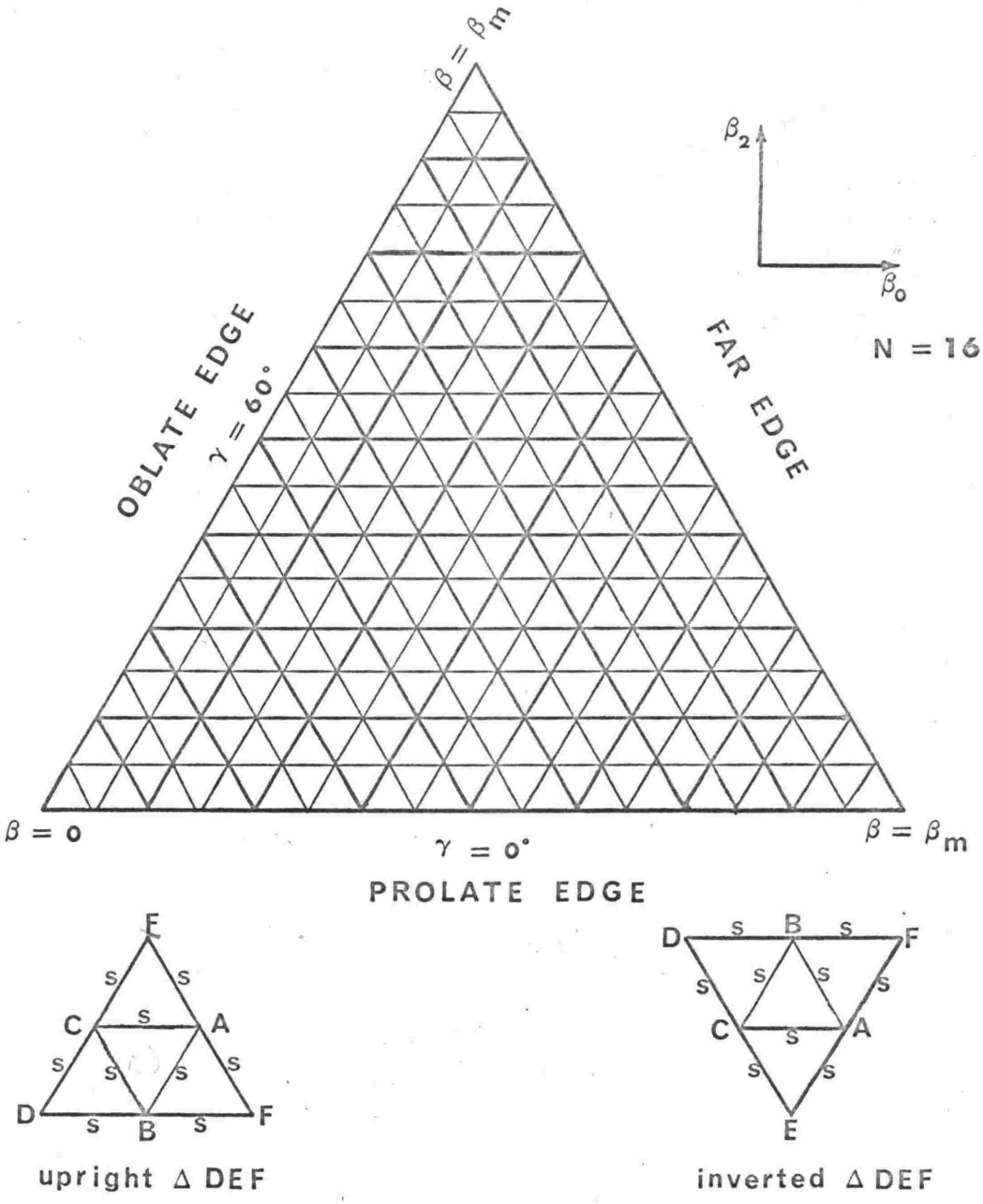

FIG. 5.1 Triangular mesh of (β_0, β_2) plane for numerical solution

- mesh size has been denoted by N from which the total number of points is $(N + 1)(N + 2)/2$.

the summation extending over all mesh points i, i'. The matrix $H_{ii'}$, obviously has many vanishing elements and, as the weight factor $|G(\beta_0, \beta_2)|^{\frac{1}{2}}$ is included in $H_{ii'}$, it vanishes on the prolate and oblate edges (γ = 0, 60^0 respectively). Hence wave functions on these edges enter into (32) only by vibrational kinetic energy terms. The solution of the Schrödinger equation is obtained by making (32) stationary, subject to the normalisation condition

$$1 = \int d\tau' \sum_K |A_{\alpha IK}|^2 \equiv \sum_i F_i A_i^2 \qquad (33)$$

and the result of the variation is the generalised eigenvalue equation

$$\sum_{i'} H_{ii'} A_{i'} = E F_i A_i \qquad (34)$$

Although the $A_{\alpha IK}$ could be expanded as a linear combination of, say, harmonic oscillator functions, the variational parameters are chosen as the values of $A_{\alpha IK}$ at the mesh points themselves, so that the method can easily be extended to cases where energy parameters are not analytically known. Certain boundary conditions exist for the mesh. The wave function will adjust itself to have zero normal derivative at the boundaries as in this way the kinetic energy will be minimised. All K = 0 components of the wave function must vanish on the prolate edge, as I_3 becomes infinite, and for odd I, all components vanish on the oblate edge. The effect of rotations yield relationships between K-components of even-I eigenfunctions on the oblate edge

$$A_{\alpha IK}(\beta, 60^0) = (-)^{K/2} \frac{M^I_{K0}}{M^I_{00}} A_{\alpha I0}(\beta, 60^0) \qquad (35)$$

which reduces the number of variational parameters. A boundary constraint must be imposed at the origin for $A_{\alpha 00}$ as (considering the first triangle DEF), wave functions at points B, C, D occur only in the vibrational kinetic energy at A, and then only the combination $(A_B+A_C-\frac{1}{2}A_D)$ enters. To solve for A_B, A_C and A_D the normal derivatives at B and C are made to vanish. $A_{\alpha IK}$ on the far edge may be forced to vanish, which it would do with large enough β_m - this can serve as a test to check that the edge has been placed far enough from the origin.

These boundary constraints may be included in the minimisation routine by writing them in the form

$$C_k(x) = \sum_i C_{i_k} x_i = 0 \qquad k=1,.....,m \text{ constraints}$$

with $$\sum_i C_{i_k} C_{i_{k'}} = \delta_{kk'}$$

The C_{i_k}'s are given in table 5.1.

The size of $H_{ii'}$ is dictated by the mesh size and the number of K-spins: for N=16 and I=4 (K=0,2,4), $H_{ii'}$ would be 459x459. However, the boundary conditions reduces these dimensions to 392x392. In the construction and subsequent solution of the Schrödinger equation, the present treatment ignores this and adds the boundary conditions in the minimisation routine. The largest number of non-zero elements in a row is 19 for the N=16 mesh.

5.5 Solution of the Eigenvalue Equation

The method of determining solutions of the generalised eigenvalue equation (34) is based on that of gradients. This is an iterative method in which a trial vector is modified in a prescribed manner until it

TABLE 5.1 - Boundary Conditions for Mesh

(i) Eigenfunction vanishing on a boundary

$$C_k = 1 \qquad \text{for point } k$$

(ii) K-components on oblate edge-relating corresponding points i

I	K			
	0	2	4	
2	0.86603	-0.5	--	C_{i_k}
4	0.83046	-0.55709	0.0	C_{i_k}
	0.41197	0.61413	-0.67315	$C_{i_{k'}}$

(iii) I = 0; vanishing normal derivatives at points B and C

points	D	B	F	C	A	E
C_{i_1}	-0.13608	0.54433	-0.27217	-0.54433	0.54433	-0.13608
C_{i_2}	-0.16731	0.44273	-0.19562	0.44273	0.66923	-0.30630

coincides with one of the eigenvectors of the given equation, and is particularly suitable for large matrices where only the first few eigenvectors are required.

The equation may be written in the form

$$\sum_j H_{ij} A_{jk} = E_k \sum_j F_{ij} A_{jk} \qquad (37)$$

with $$\sum_{ij} A_{ik'} F_{ij} A_{jk} = \delta_{k'k}$$

Solutions of (37) are determined by minimising the Rayleigh quotient

$$\mu(x) = h(x)/f(x)$$

with $$h(x) = \sum_{ij} x_i H_{ij} x_j \qquad f(x) = \sum_{ij} x_i F_{ij} x_j$$

and x is the trial vector

$$\partial\mu/\partial x_i = \frac{1}{f(x)} \left[\sum_j H_{ij} x_j - \mu(x) \sum_j F_{ij} x_j \right] = t_i/f(x) \qquad (38)$$

The vector t is in the same direction as the gradient of $\mu(x)$, and would determine the direction the trial vector x should be moved if no constraints were applied to x. However, x must be orthogonal to the boundary conditions and to any previous eigenfunctions.

Using Lagrangian multipliers λ_k and w_p, a new vector ξ determines the direction x should be moved

$$\xi_i = t_i - \sum_k^m \lambda_k C_{ik} - \sum_p' w_p A_{ip} \qquad (39)$$

where $\sum_p'$ is a summation over the lowest eigenvectors only. Obviously

the two types of constraint are orthogonal as the first (etc.) eigenvector was found orthogonal to the boundary conditions.

The new guess at the trial vector is then

$$\bar{x}_i = x_i - \gamma \xi_i \tag{40}$$

with the requirements

$$\text{(i)} \quad \sum_i C_{i_k} \bar{x}_i = 0 \qquad \text{i.e.} \quad \lambda_k = \sum_i C_{i_k} t_i$$

$$\text{(ii)} \quad \sum_{ij} \bar{x}_i F_{ij} A_{j_p} = 0 \qquad \text{i.e.} \quad w_p = \sum_{ij} t_i F_{ij} A_{j_p} = w_p(t) \tag{41}$$

The scalar γ determines how far the trial vector x should be moved in the direction ξ. The optimum value of γ is found by demanding the biggest possible reduction in $\mu(x)$. This is found by equating to zero the derivative of $\mu(\bar{x})$ with respect to γ, and solving:

$$\gamma_{opt} = \left[(b^2 + ac)^{\frac{1}{2}} - b \right] / a \tag{42}$$

where $$a = f(\xi) \sum_{ij} \xi_i H_{ij} x_j - h(\xi) \sum_{ij} \xi_i F_{ij} x_j$$

$$b = \tfrac{1}{2} \left[h(\xi) f(x) - f(\xi) h(x) \right] \tag{43}$$

$$c = f(x) \sum_{ij} \xi_i H_{ij} x_j - h(x) \sum_{ij} \xi_i F_{ij} x_j$$

It has been suggested[2] that the number of iterations can be reduced by

$$\gamma = 0.9 \gamma_{opt}$$

Unless one has a priori knowledge of the eigenvector required, an initial guess for the trial vector is

$$x_i = z_i - \sum_p{}' w_p(z) A_{i_p} \tag{44}$$

where $z_i = \left[f(x_i=1) \right]^{-\frac{1}{2}}$ for lowest solution, or $f(t)=0$

$= \left[f(t) \right]^{-\frac{1}{2}} t_i$ otherwise

and t is the vector obtained during the last iteration needed for determination of the p^{th} vector.

Iteration may stop when $|t| = |Hx-\mu Fx|$ is smaller than some desired limit (since this tests $x=A$, $\mu=E$) and the fractional change in μ is less than some limit. Experience revealed that both μ and $|t|$ would successfully converge to some fixed values, and that although μ decreased monotonically, $|t|$ tended to fluctuate in its convergence. The existence of a finite limit for $|t|$ is probably due to the imposed boundary conditions although computing round-off errors may also be present.

5.6 Electromagnetic Moments

As the solutions of the Schrodinger equation are stationary, good agreement between model eigenvalues and observed nuclear level structure is not a particularly sensitive test of the model description of a nucleus. Various predictions, such as electromagnetic transition probabilities, provided by model eigenfunctions yield much more stringent conditions on the validity of a model. In the numerical analysis, it is important to

realise that with the preceding treatment, the shape and hence the intrinsic state of the nucleus is free to change from one nuclear state to another. The collective wave function of each stationary state is in general a linear combination of many intrinsic wave functions.

A Electric Quadrupole Moments

The reduced transition probability associated with a radiative transition of multipolarity E2 is given by

$$B(E2;\ \alpha I \rightarrow \alpha' I') = (2I+1)^{-1} \left| \langle \alpha I \| M(E2) \| \alpha' I' \rangle \right|^2 \qquad (45)$$

In the lab. system, the E2 operators are written as

$$M(E2,m) = \sum_p e_p r_p^2 Y_2^m(\Omega_p) \qquad m=0,\pm 1,\pm 2 \qquad (46)$$

and r_p, Ω_p are the radial and angular co-ordinates of a particle outside the core. e_p is the effective charge of the particle. The corresponding relation in the intrinsic system is

$$M'(E2,k) = \sum_p e_p r_p^2 Y_2^k(w_p) \qquad (47)$$

with $M(E2,m) = \sum_k D^2_{mk}(\theta_i) M'(E2,k)$

The Wigner-Eckhart theorem gives the reduced matrix element of (45) as

$$\langle \alpha I, M=I \left| M(E2,0) \right| \alpha' I', M'=I \rangle = \begin{pmatrix} I & 2 & I' \\ -I & 0 & I \end{pmatrix} \langle \alpha I \| M(E2) \| \alpha' I' \rangle \qquad (48)$$

$\langle \alpha IM|$ being a stationary nuclear state.

After reduction, one obtains for the wave functions defined in (28) and (29)

$$\langle \alpha I \| M(E2) \| \alpha' I' \rangle$$

$$= \left[(2I+1)(2I'+1)\right]^{\frac{1}{2}}(-)^{I} \sum_{K\geq 0} \left[\begin{pmatrix} I & 2 & I' \\ -K & 0 & K \end{pmatrix} \langle A_{\alpha I K} | Q_0 | A_{\alpha' I' K} \rangle \right.$$

$$+ \sqrt{\tfrac{1}{2}(1+\delta_{K0})} \left\{ \begin{pmatrix} I & 2 & I' \\ -K-2 & 2 & K \end{pmatrix} \langle A_{\alpha I, K+2} | Q_2 | A_{\alpha' I' K} \rangle \right.$$

$$\left. \left. + (-)^{I+I'} \begin{pmatrix} I & 2 & I' \\ K & 2 & -K-2 \end{pmatrix} \langle A_{\alpha I K} | Q_2 | A_{\alpha' I', K+2} \rangle \right\} \right] \qquad (49)$$

from which the B(E2)'s may be found.

The spectroscopic quadrupole moment of a state $|\alpha I\rangle$ may also be expressed in terms of the reduced matrix element:

$$Q(\alpha I) = (16\pi/5)^{\frac{1}{2}} \begin{pmatrix} I & 2 & I \\ -I & 0 & I \end{pmatrix} \langle \alpha I \| M(E2) \| \alpha I \rangle \qquad (50)$$

The Q_μ are defined

$$Q_0(\beta,\gamma) = \langle X | M'(E2,0) | X \rangle$$

$$Q_2(\beta,\gamma) = \sqrt{2}\langle X | M'(E2,2) | X \rangle = \sqrt{2}\langle X | M'(E2,-2) | X \rangle \qquad (51)$$

where $\langle X|$ is an intrinsic wave function dependent on β,γ but not on the quantum numbers I,M and K. Assuming a uniform charge distribution and Bohr's definition of deformation (6)

$$Q_0(\beta,\gamma) = (3\pi/4)ZR_0^2\beta\cos\gamma \qquad (52)$$

$$Q_2(\beta,\gamma) = (3\pi/4)ZR_0^2\beta\sin\gamma$$

Alternatively, one could use Nilsson single-particle wave functions for a better approximation.

Where K is a good quantum number, the transition probability may be reduced to that given by Bohr[3] for collective transitions of a strongly coupled system

$$B(E2;\ I+2\rightarrow I) = (15/32\pi)e^2Q_0^2\,\frac{(I+1)(I+2)}{(2I+3)(2I+5)} \tag{53}$$

with $Q_0 = (9/5\pi)^{\frac{1}{2}}ZR_0^2\langle\beta\cos\gamma\rangle$

B Magnetic Dipole Moments

The reduced M1 transition probability is similarly

$$B(M1;\ \alpha I\rightarrow\alpha' I') = (2I+1)^{-1}\left|\langle\alpha I\|M(M1)\|\alpha' I'\rangle\right|^2 \tag{54}$$

with the expectation values of the operators M'(M1) in the intrinsic state written as

$$\langle X|M'(M1,\pm1)|X\rangle = \mp(3/8\pi)^{\frac{1}{2}}(g_{\mp}I_- + g_{\pm}I_+) \tag{55}$$

$$\langle X|M'(M1,0)|X\rangle = (3/4\pi)^{\frac{1}{2}}g_3I_3$$

$$I_{\pm} = I_1 \pm iI_2 \qquad g_{\pm} = \tfrac{1}{2}(g_1 \pm g_2) \tag{56}$$

I_k (k=1,2,3) is the component of the total angular momentum on the intrinsic axis k, and g_k is a gyromagnetic ratio dependent on k as well as β,γ. After reduction, one obtains

$$\langle\alpha I\|M(M1)\|\alpha' I'\rangle = \left[3(2I+1)(2I'+1)/4\pi\right]^{\frac{1}{2}}$$

$$\times(-)^{I}\sum_{K\geq 0}\Bigg[\Bigg\{\begin{pmatrix} I & 1 & I' \\ -K & -1 & K+1\end{pmatrix} R_{I'K} - \begin{pmatrix} I & 1 & I' \\ -K & 1 & K-1\end{pmatrix} R_{I',-K}\Bigg\}\langle A_{\alpha IK}|g_{+}|A_{\alpha' I' K}\rangle$$

$$-(1+\delta_{K0})^{\frac{1}{2}}\Bigg\{\begin{pmatrix} I & 1 & I' \\ -K-2 & 1 & K+1\end{pmatrix} R_{I'K}\langle A_{\alpha I,K+2}|g_{-}|A_{\alpha' I' K}\rangle$$

$$-\begin{pmatrix} I & 1 & I' \\ -K & -1 & K+1\end{pmatrix} R_{I',-K-2}\langle A_{\alpha IK}|g_{-}|A_{\alpha' I',K+2}\rangle\Bigg\}$$

$$+\begin{pmatrix} I & 1 & I' \\ -K & 0 & K\end{pmatrix} K\langle A_{\alpha IK}|g_{3}|A_{\alpha' I' K}\rangle\Bigg] \qquad (57)$$

where $R_{IK} = \sqrt{\tfrac{1}{2}(I-K)(I+K+1)}$

The reduced transition probabilities may then be obtained by substitution, and the spectroscopic magnetic dipole moment of a state $\langle \alpha I|$ is given by

$$\mu(\alpha I) = (4\pi^2/3)^{\frac{1}{2}}\begin{pmatrix} I & 1 & I \\ -I & 0 & I\end{pmatrix}\langle \alpha I\|M(M1)\|\alpha I\rangle \qquad (58)$$

These relations simplify if K is a good quantum number.

In the classical treatment of a liquid drop, Lipas[10] has demonstrated that, for even-even nuclei within the context of collective motion, the M1 multipole operator has no non-zero matrix elements between any two different nuclear states, implying that collective M1 transitions are strictly forbidden. The physical reason is just that there can be no M1 radiation because there is no precession of the dipole moment about the total angular momentum

$$\text{i.e. } \underline{\mu} = g_R \underline{I} \qquad g_R = Z/A \qquad (59)$$

where g_R is the gyromagnetic moment of the even-even core.

In fact, weak M1 transition are found in even-even collective nuclei, and although they can be accounted for by pair creation and annihilation in HRPA calculations[11] (implying a breakdown of the adiabatic approximation), there is an alternative explanation which is within the bounds of the collective model[12]. The two gross nuclear forces intuitively assumed in collective motion are quadrupole deformation and the pairing force. It is the latter that favours a spherical nuclear shape, and, as protons and neutrons have been found to have different magnitudes of pairing forces ($G_p > G_n$), it is reasonable to suppose the deformation of an assembly of protons would differ from that of neutrons. Since the dipole moment of an even-even nucleus is due to proton orbital motion, and the deformation of the protons is less than that of the total mass distribution, g_R becomes a spherical tensor, with components

$$g_+ \doteq g_R(1 - 2f)$$

$$g_- \doteq 2\sqrt{\tfrac{2}{3}}\, g_+ f \frac{\beta \sin\gamma}{\bar{\beta}}$$

$$g_0 = g_3 \doteq \frac{Z}{A}\left(1 - \frac{8}{3}f\right) - \frac{4}{3} g_+ f \left(\frac{\beta\cos\gamma - \bar{\beta}}{\bar{\beta}}\right) \qquad (60)$$

where $f = \dfrac{\bar{\beta} - \bar{\beta}_p}{\bar{\beta}} \doteq \dfrac{N}{A}\left(\dfrac{\bar{\beta}_n}{\bar{\beta}_p} - 1\right)$ since $\bar{\beta} = \dfrac{N\bar{\beta}_n + Z\bar{\beta}_p}{A}$

The subscripts n,p refer to neutron and proton, and the ratio of their deformations is derived from a quasi-spin model

$$\frac{\bar{\beta}_p}{\bar{\beta}_n} = \left[\frac{G_n}{G_p}\right]^{\frac{1}{2}} \doteq \left[\frac{20/A}{30/A}\right]^{\frac{1}{2}} \qquad (61)$$

The gyromagnetic ratios are derived with the assumption that the potential function used to describe the nucleus has its lowest minimum at $\beta=\bar{\beta}$ and $\gamma=0,60^{o}$ in the range $\beta\geq 0$ and $-180^{o}\leq\gamma\leq 180^{o}$. Heestand et al.[13] have found that these g-factors proposed by Greiner[12] gave the best agreement with experimental values of doubly-even nuclei.

The expressions for reduced transition probabilities may be used for both the analytic and numerical solutions, the relations between these being

$$A_{\alpha IK}(\beta,\gamma) = g(\gamma - \bar{\gamma})F(\beta)C_{n_{IK}} \tag{62}$$

where $C_{n_{IK}}$ are the coefficients of expansion of the eigenfunctions of (16) in terms of functions (29). These may be obtained by solution of (16) with relations (27). For the numerical solution,

$$\langle A_{\alpha IK}|Q_{\mu}|A_{\alpha' I' K'}\rangle = \sum_{a}\left[A_{\alpha IK}FQ_{\mu}A_{\alpha' I' K'}\right]_{a} \tag{63}$$

the summation being over points 'a' of the mesh and F is the normalisation integral given in (33).

5.7 Test for Accuracy; Numerical Solution

Relevant parts of the preceding sections were encoded in FORTRAN for the PDP-8 and PDP-9/L computers[15] and tested with the potential function

$$V(\beta,\gamma) = \tfrac{1}{2}C\beta^{2} \tag{64}$$

for which the Hamiltonian may be solved analytically. Solutions in the $(\beta,\gamma,\theta_{i})$ representation have been given by Kumar[2] and these are compared

TABLE 5.2 Numerical Eigenfunction Test

B(E2) values for the oscillator well specified in section 5.7 and calculated with

$Z = 50 \quad A = 125 \quad R_0 = 1.2A^{1/3}$ fm

initial state	final state	$B(E2;\alpha,I \rightarrow \alpha',I') \times 10^{-48}$ e^2cm^4	
		exact[2]	numerical
1,0	1,2	0.4616	0.4546
2,0	1,2	0.1847	0.1913
1,2	2,2	0.1847	0.1849
1,2	1,4	0.3324	0.3328
2,2	1,3	0.2770	0.2779
1,3	1,4	0.0791	0.0798

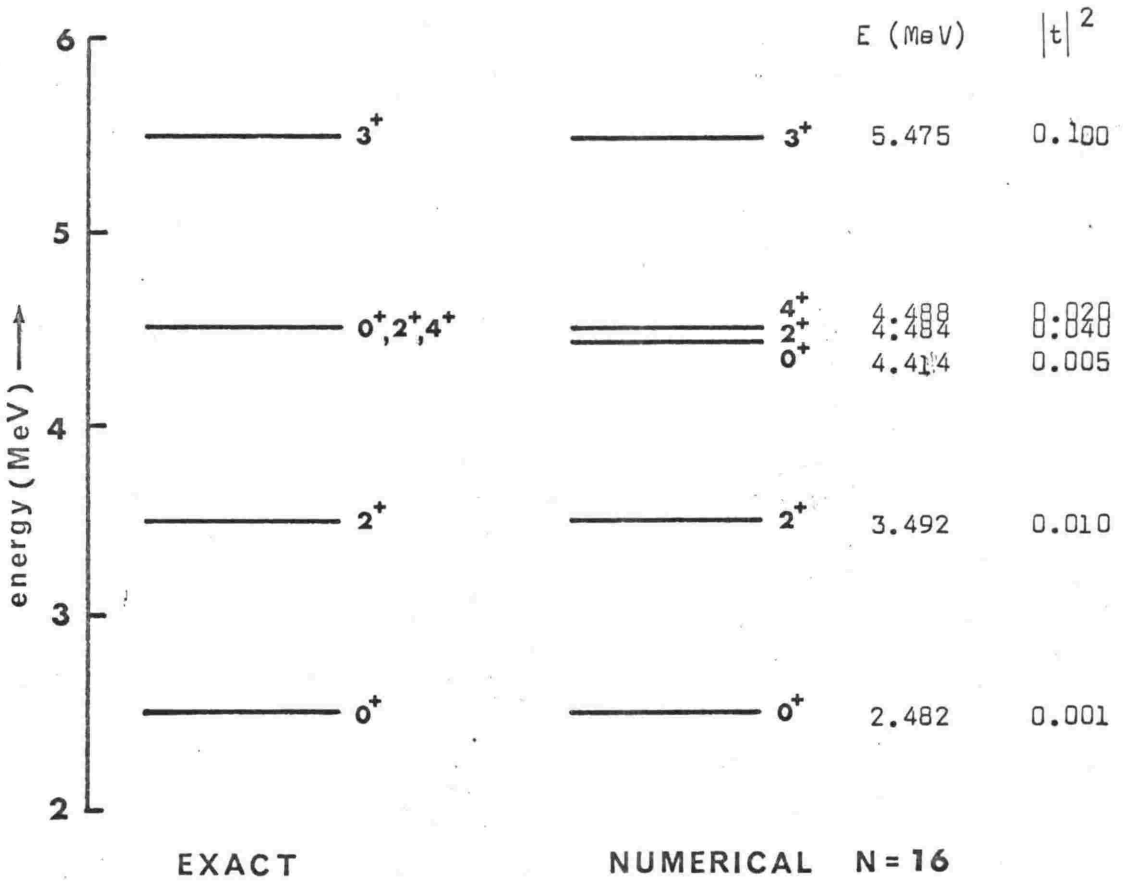

FIG. 5.2 Numerical Solution Test- Oscillator Potential

Parameters are

$C = 100$ MeV $B = 100$ MeV^{-1} $\beta_m = 0.45$ $\omega = (C/B)^{\frac{1}{2}} = 1$ MeV

and $A_{\alpha IK} \neq 0$ on the far edge.

$$|t|^2 = |HA_{\alpha IK} - E_{\alpha I} FA_{\alpha IK}|^2$$

with the present analysis in table 5.2 and fig. 5.2 for the parameters

$$C = 100 \text{ MeV} \qquad B = 100 \text{ MeV}^{-1} \qquad \beta_m = 0.45$$

Corresponding contour plots of wave functions are presented in fig. 5.3→ 5.7. The agreement obtained with the results of Kumar and those of the exact solution indicated that the programs were functioning correctly.

Contours of analytically and numerically determined eigenfunctions correspond very closely except for some lack of definition at maxima and a tendency for contours to arrange themselves perpendicular to the far edge, thereby minimising kinetic energy. The latter effect is present because, as $\beta_m \neq \infty$, the wave function does not vanish at the far edge.

REFERENCES

1 J.P. Davidson, "Collective Models of the Nucleus", Academic Press (N.Y.), 1968

2 K. Kumar and M. Baranger, Nucl. Phys. A92 (1967), 608

3 A. Bohr, Mat. Fys. Medd. Dan. Vid. Selsk. 26 (1952), no. 14

4 A.S. Davydov, Atomic Energy Rev. 6 (1968), no. 2, 3
Nucl. Phys. 8 (1958), 237

5 K. Kumar and M. Baranger, Nucl. Phys. A122 (1968), 273

6 J.F. Suárez, Nuovo Cimento 62B (1969), 109

7 C.H. Townes and A.L. Schalow, "Microwave Spectroscopy", McGraw-Hill (N.Y.), 1955

8 M. Sakai, Nucl. Phys. A104 (1967), 301

9 K. Kumar, Nucl. Phys. A92 (1967), 653

10 P.O. Lipas, Phys. Lett. 8 (1964), 279

11 T. Tamura and T. Udagawa, Nucl. Phys. 53 (1964), 33

12 W. Greiner, Nucl. Phys. 80 (1966), 417

13 G.M. Heestand, R.R. Borchers, B. Herskind, L. Grodzins, R. Kalish and D.E. Murnick, Nucl. Phys. A133 (1969), 310

14 J.M. Irvine, Report Prog. Phys. 31 (1968), 1

15 G. Wallace, I.N.S. Report INS-P-63 (1970)

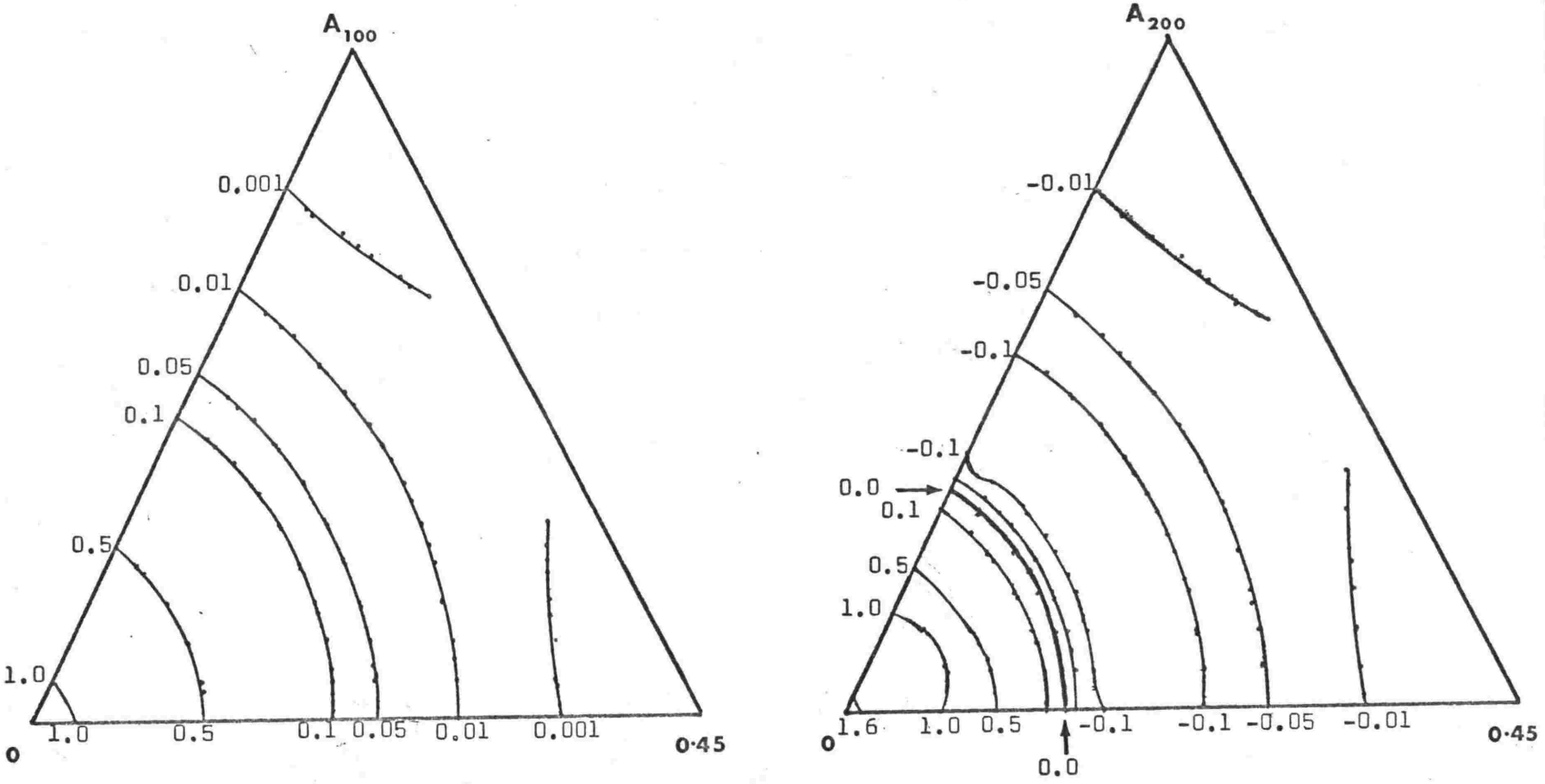

FIG. 5.3 Numerical Solution Test - ground and first-excited 0^+ states of harmonic oscillator.
Note the effect of finite β_m.

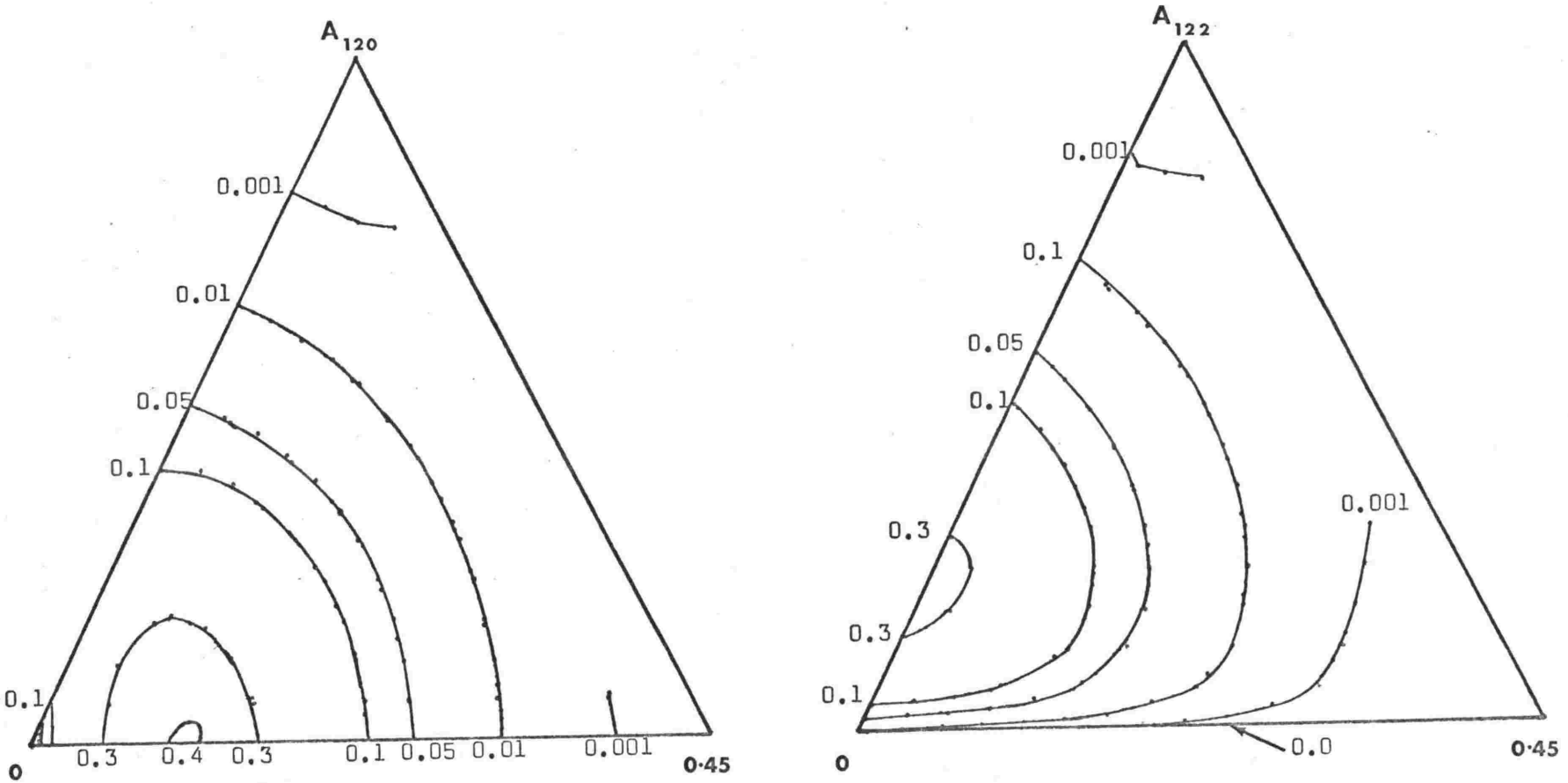

FIG. 5.4 Numerical Solution Test - 2^+ state of harmonic oscillator.

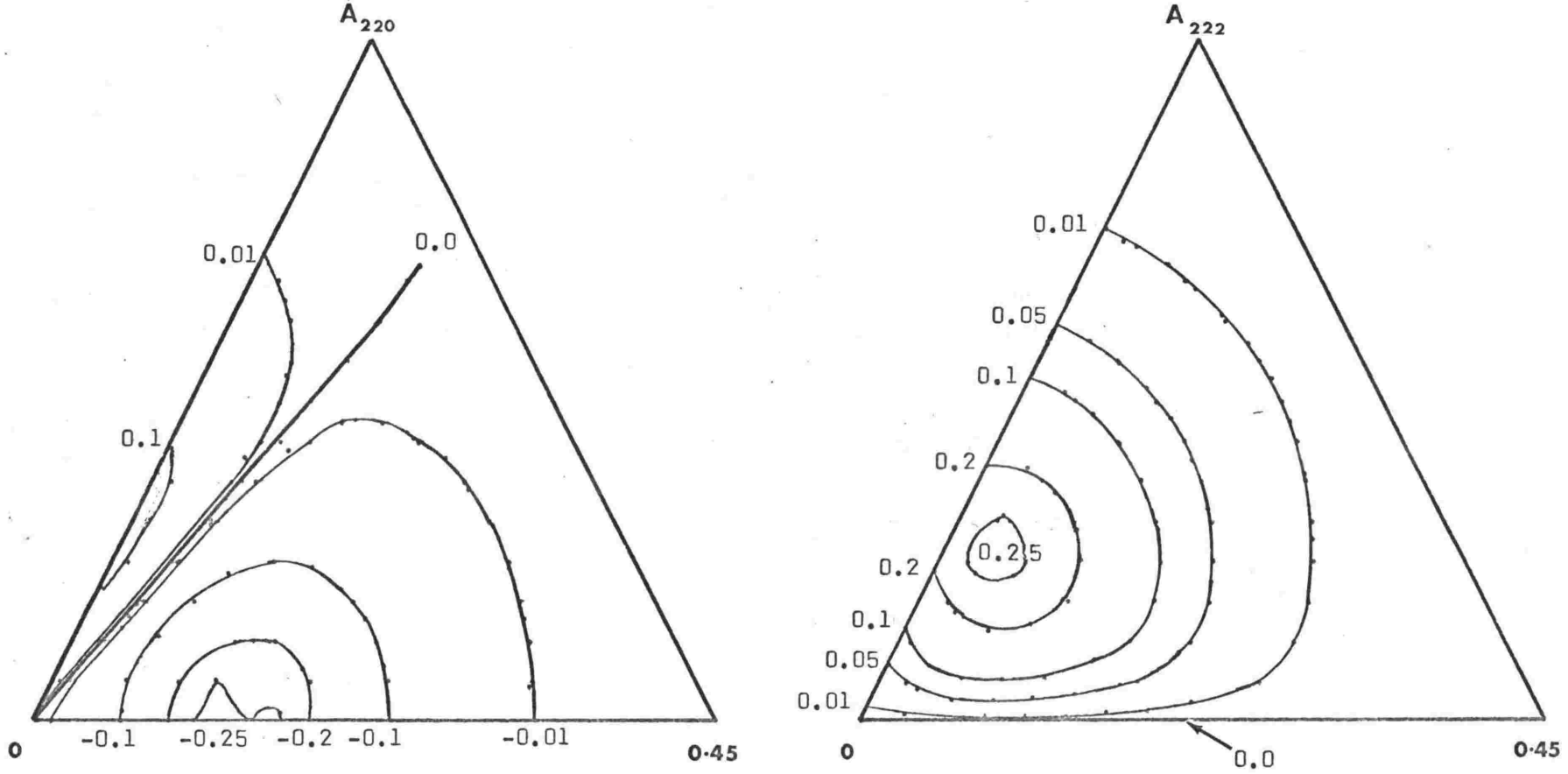

FIG. 5.5 Numerical Solution Test - $2^{+'}$ state of harmonic oscillator.

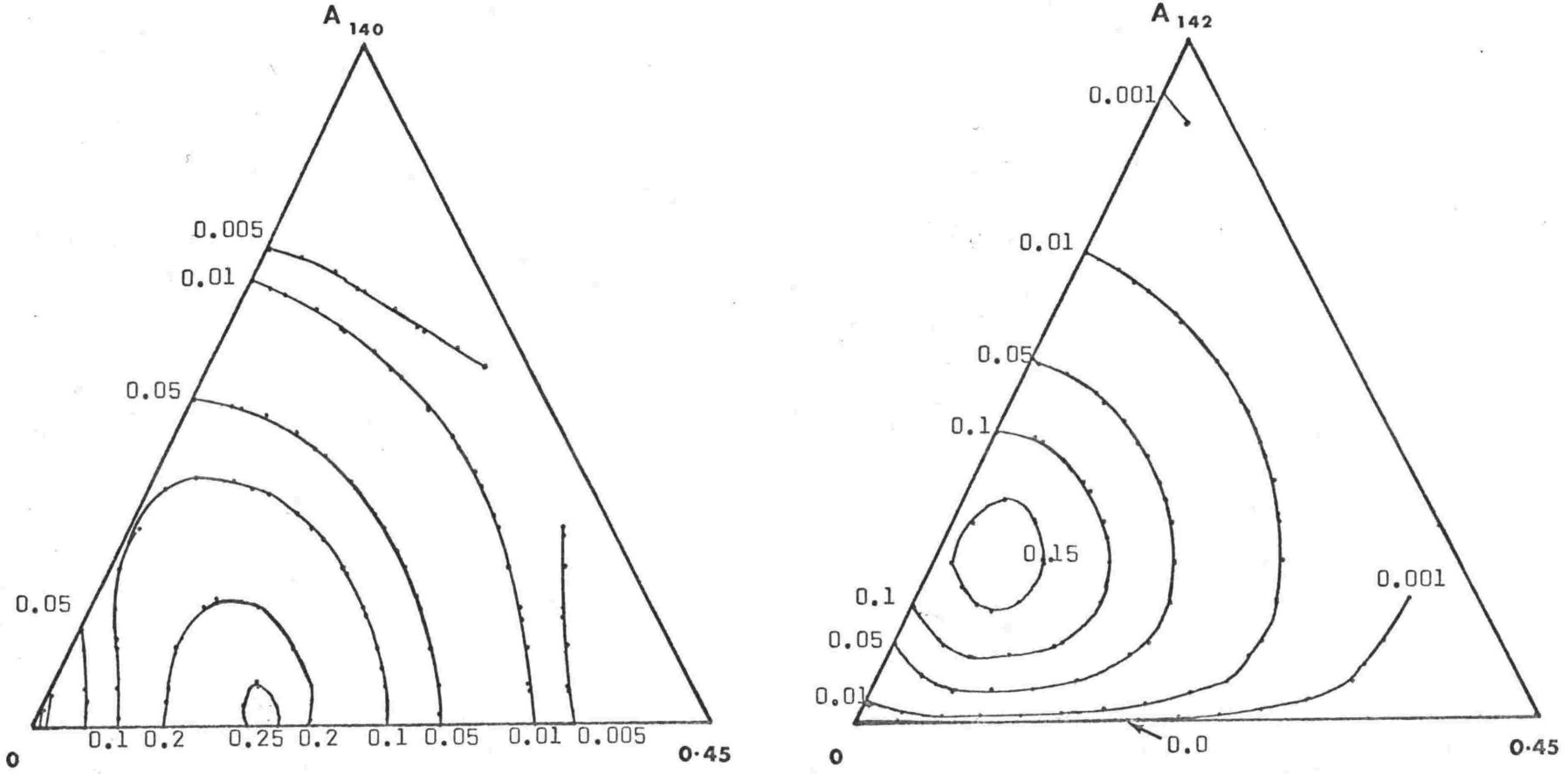

FIG. 5.6 Numerical Solution Test - 4^+ state of harmonic oscillator.

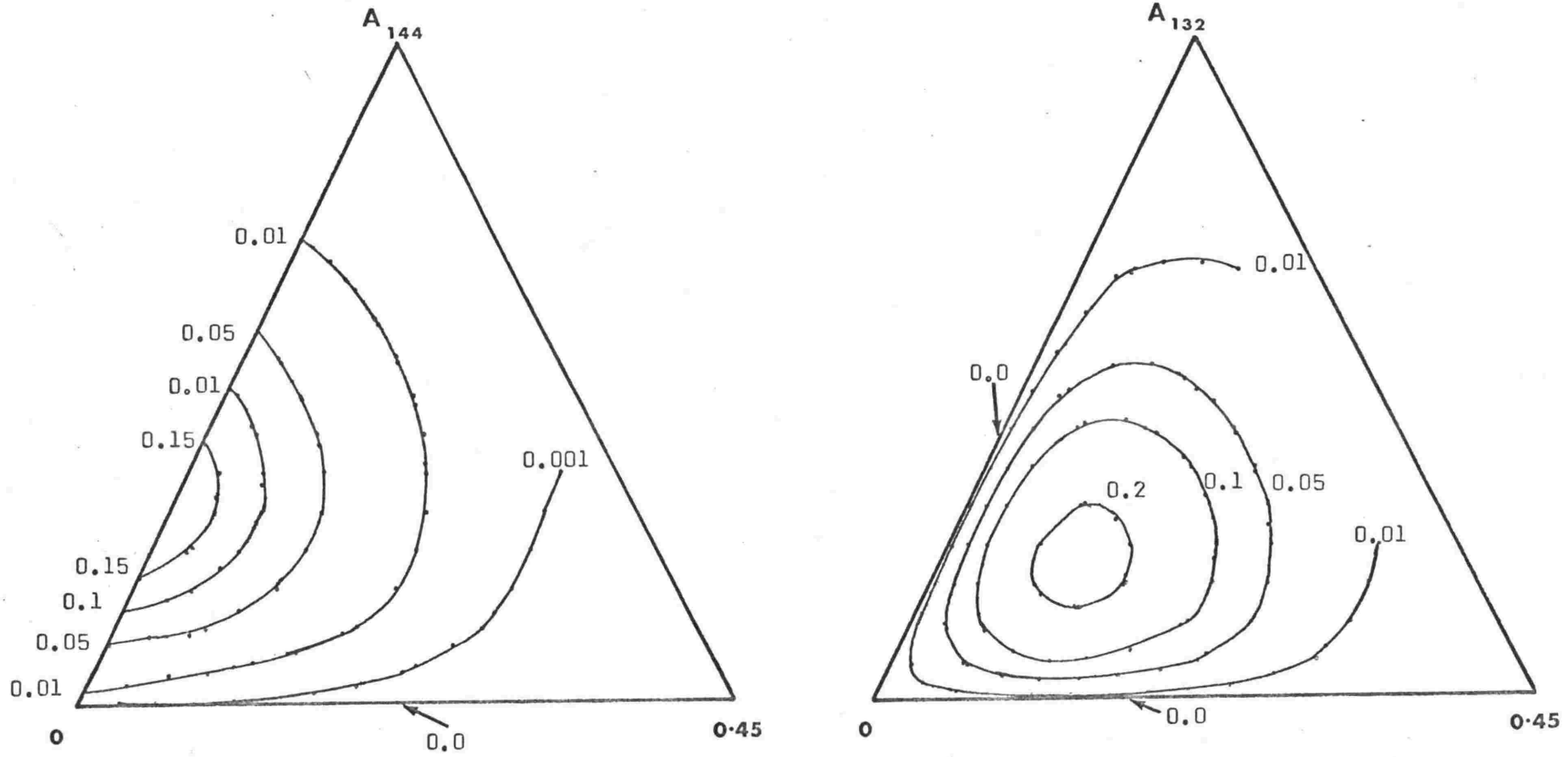

FIG. 5.7 Numerical Solution Test - 4^+ and 3^+ states of harmonic oscillator.

Chapter Six

APPLICATION OF COLLECTIVE MODELS TO EVEN-EVEN CADMIUM NUCLEI

6.1 Introduction

The Cd isotopes, and in particular ^{114}Cd, have long been considered as typical quadrupole-type vibrational nuclei. However, experimental measurements on ^{114}Cd have revealed properties with significant deviations from phonon model predictions, even though the nucleus is basically spherical[1]. In general, the ratios

$$R_1 = B(E2;\ 2^{+\prime} \longrightarrow 2^+)/B(E2;\ 2^+ \longrightarrow 0^+)$$
$$R_2 = B(E2;\ 2^{+\prime} \longrightarrow 0^+)/B(E2;\ 2^{+\prime} \longrightarrow 2^+) \qquad (1)$$

for even Cd nuclei differ considerably from the vibrational model values of 2 and 0 respectively. This model also predicts a zero static quadrupole moment for the first 2^+ state; however, this is found to be -0.50 ± 0.25 e.b for ^{114}Cd. Tamura and Udagawa[1] have shown that these electromagnetic properties do not imply that the Cd nuclei are excluded from the vibrational framework since, by treating the 2^+ levels as orthogonal linear combinations of one- and two-phonon harmonic vibrational 2^+ states $|1\rangle$ and $|2\rangle$

i.e. $$\psi(2^+) = a_1|1\rangle + a_2|2\rangle$$
$$\psi(2^{+\prime}) = -a_2|1\rangle + a_1|2\rangle \qquad (2)$$

one can prove

$$R_1 = 2(2a_1^2 - 1)^2/a_1^2$$
$$Q(2^+) = \frac{12}{5}\sqrt{\frac{1}{7\pi}}\ a_1 a_2 Z R_0^2\ \bar{\beta} \qquad (3)$$

and setting $R_1 = 0.7$[2], $\quad |Q(2^+)| = 0.71$ e.b (4)

The value estimated for the quadrupole moment (which is very close to the rotational model prediction) illustrates that the vibrational model is still applicable. Bès and Dussel[3] have extended this type of approach with addition of anharmonic effects and higher-phonon state mixing, and although achieving some success with electromagnetic properties, good agreement with level structure was not obtained.

The level sequence of the Cd triad closely resembles the phonon spectrum except for the addition of 0^+, 2^+ states close to the two-phonon triplet (in ^{112,114}Cd at least). These five states appear to be isolated from states of higher energy by a considerable gap. This feature should also be reproduced by a model description. The following sections describe attempts to synthesise Cd level structure using the prescriptions given in Chapter 5, with emphasis on the physical basis of the parameters involved.

6.2 Choice of Parameters

One of the main deductions which can be obtained from a discussion of different collective models is that it appears that the potential energy of deformation requires special consideration, and it is this operator which will be relied upon to introduce anharmonicities into the collective Hamiltonian. Suárez[5] has determined best-fit parameters for analytic solutions, and these will be adhered to, although they bear little relation to what one might expect from liquid drop considerations (see eq. (17)). Kumar[4] has developed a semi-empirical mass formula of Myers and Swiatecki (MS)[6] such that prolate-oblate differences are increased and axial symmetry may be destroyed. The basic features of the

MS-potential, such as fission properties, remain. In applying the numerical method to the deformed nucleus ^{154}Sm, Kumar made a detailed investigation of the effects of each term in the potential on the structure and properties of energy levels. The potential function is written

$$V(\beta,\gamma) = \tfrac{1}{2}C\beta^2 - f\beta^3\cos 3\gamma + \left[G_0 + (G_1+G_2\frac{\beta^3}{a^3}\cos 3\gamma)\frac{\beta^3}{a^3}\cos 3\gamma\right]\exp(-\frac{\beta^2}{a^2}) \qquad (5)$$

and coefficients are related to those of the MS mass formula by

$$C = \frac{2\beta^2}{\alpha_0^2}E \quad ; \quad f = (\frac{b}{\alpha_0})^3 F \quad ; \quad a = \frac{\alpha_0}{b} \quad ; \quad G_0 = S \qquad (6)$$

with $b = (5/4\pi)^{\frac{1}{2}}$ (α_0 is tabulated in ref.[6] as CONV)

Since the collective properties of low-energy nuclear structure involve small deformations (compared with fission), C and f should remain as defined in (6). However, exponential terms (which include shell effects) require modification to get good agreement with experimental data.

The Gaussian range, a, was treated as fixed since, as it determines the magnitude of nuclear deformation, small changes in a should not change the nature of the nuclear spectrum. As the deformation of the Cd nuclei was small, a was set to 0.25, only slightly larger than the value obtained from the MS tables ($\sim$0.2). An initial guess at the ground state deformation $\bar{\beta}$ can be obtained from the strong coupling formula of Bohr[7] and the experimental $B(E2;\ 2^+ \longrightarrow 0^+)$ value[2]

$$\bar{\beta} = \frac{4\pi}{3ZR_0^2}\sqrt{\frac{5B(E2;\ 2^+ \longrightarrow 0^+)}{e^2}} \qquad \text{with } R_0 = 1.2A^{\frac{1}{3}}\text{fm} \qquad (7)$$

Two further conditions may be reliably used to determine potential parameters. These are

$$\frac{\partial V(\bar{\beta},\ 0 \text{ or } \pi/3)}{\partial \beta} = 0 \tag{8}$$

and

$$V(\bar{\beta},\ 0 \text{ or } \pi/3) = S_E \tag{9}$$

where S_E is the shell effect, or difference between the experimental mass and liquid drop mass[6]. There is a supplementary condition when the depth of the potential well is considered (see fig. 6.1); for a deformed nucleus

$$V(0,0) \geqslant V(\bar{\beta},\ 0 \text{ or } \pi/3)$$

$$\therefore\ G_0 \geqslant S_E \tag{10}$$

It should be noted that values for $\bar{\gamma}$ have been restricted to 0, $\pi/3$ i.e., a nucleus is either prolate, oblate or a mixture of these shapes. This restriction on the potential minima has been enforced to obtain agreement with single-particle calculations[8] but it may well be that the position of minima for these calculations is a reflection of the wave functions used.

Unfortunately, to gain a reasonable deformation ($G_0 > S_E$), one finds when using the potential of eq. (5) that large values for the γ-asymmetry terms G_1, G_2 need to be applied. The single-particle calculations of ref.[8,9,12,13], the value of C_{expt} ($\sim \frac{1}{2} C_{MS}$) and the proximity of the 2^+, and 4^+ states of the Cd nuclei[10] all indicate the contrary. To achieve deformations without large γ-asymmetry, the following expression was added to the potential function (5)

$$+\left[(1 + \delta\exp(-\beta^2/a^2))G_3(\beta^2/a^2)\right]\exp(-\beta^2/a^2) \tag{11}$$

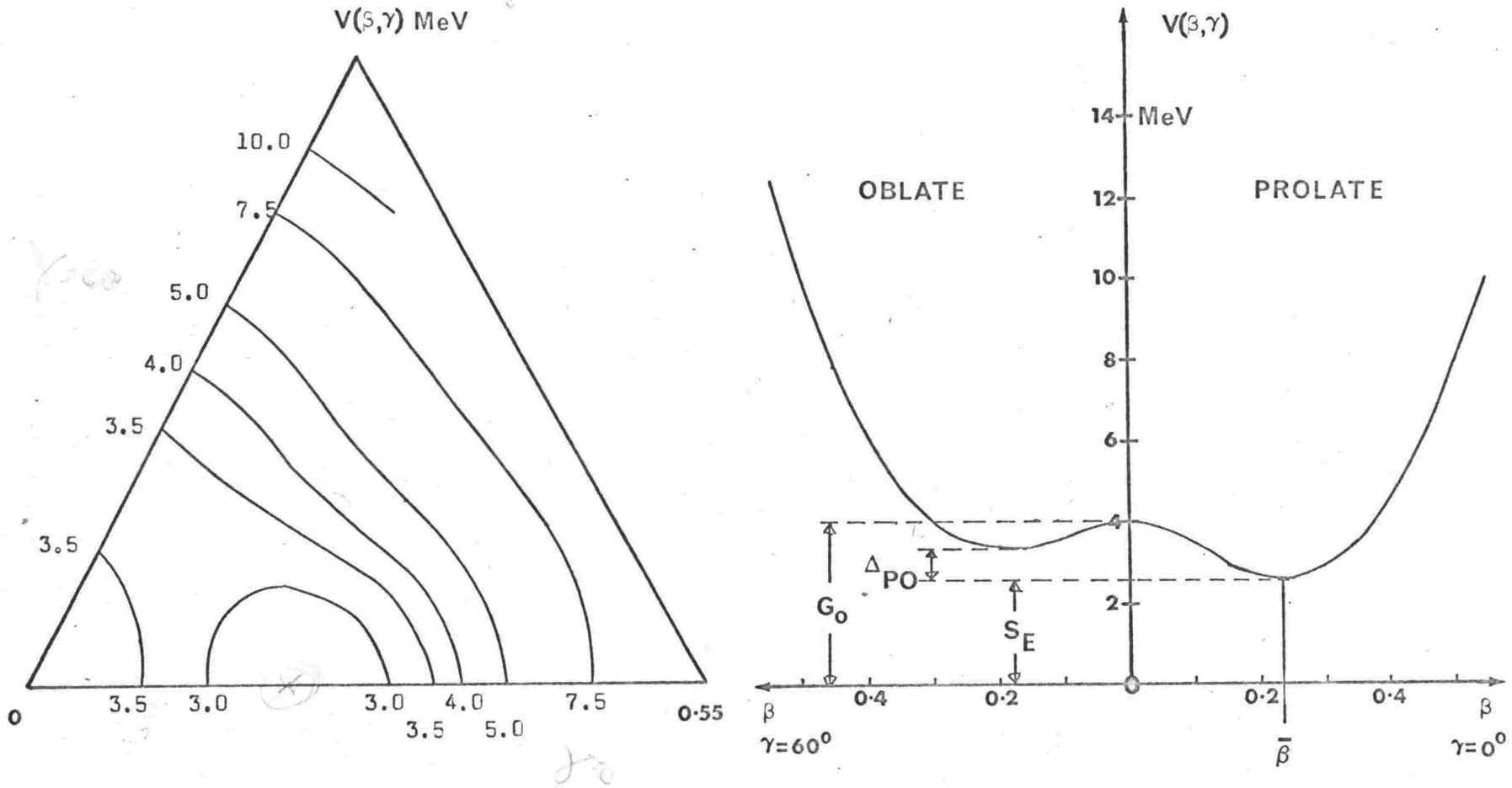

FIG. 5.1 Typical prolate potential function used in Cd numerical calculations.

C = 78.5, f = 7.283, G_0 = 4, G_1 = 0.964, G_2 = -0.750, G_3 = 1.287, S_E = 2.745, Δ_{PO} = -0.5 MeV
a = 0.25

and to reduce the number of undetermined variables, conditon (8) was made independent of G_1 and G_2, an approximation which is reasonable when single-particle calculations are examined. The potential difference between prolate and oblate edges at $\beta = \bar{\beta}$ was utilised to fix G_1 and G_2

$$\text{i.e.} \quad \Delta_{PO} = 2G_1(\bar{\beta}/a)^3 \exp(-\bar{\beta}^2/a^2) \tag{12}$$

so only two free parameters exist in the potential function, viz. G_0 and Δ_{PO}. Fig. 6.1 shows a typical potential function used in the Cd calculations.

The inertial parameter B may be estimated from the semi-empirical relation of Grodzins[11] for the transition probabilities

$$T(E2;\ 2^+ \longrightarrow 0^+) = 3.10^{10}\ E^4 Z^2/A\ \text{sec}^{-1} \qquad (E \text{ in MeV}) \tag{13}$$

Coupling this with the rotational model (in the notation $\hbar = 1$) one obtains for $R_0 = 1.2A^{\frac{1}{3}}$ fm

$$B = 0.9621.10^{-3}\ A^{7/3} \quad \text{MeV}^{-1} \tag{14}$$

Alternatively, the vibrational model gives

$$(BC)^{\frac{1}{2}} = 2.405.10^{-3}\ EA^{7/3} \tag{15}$$

where E is the excitation energy of the first 2^+ state.

6.3 Numerical Solution

After some preliminary investigation, a systematic study was made of the effects due to the G_0 and Δ_{PO} variables of the potential function. Conditions (8), (9) and (12) were adhered to in the determination of other parameters, and the various constants required were those applicable to ^{114}Cd.

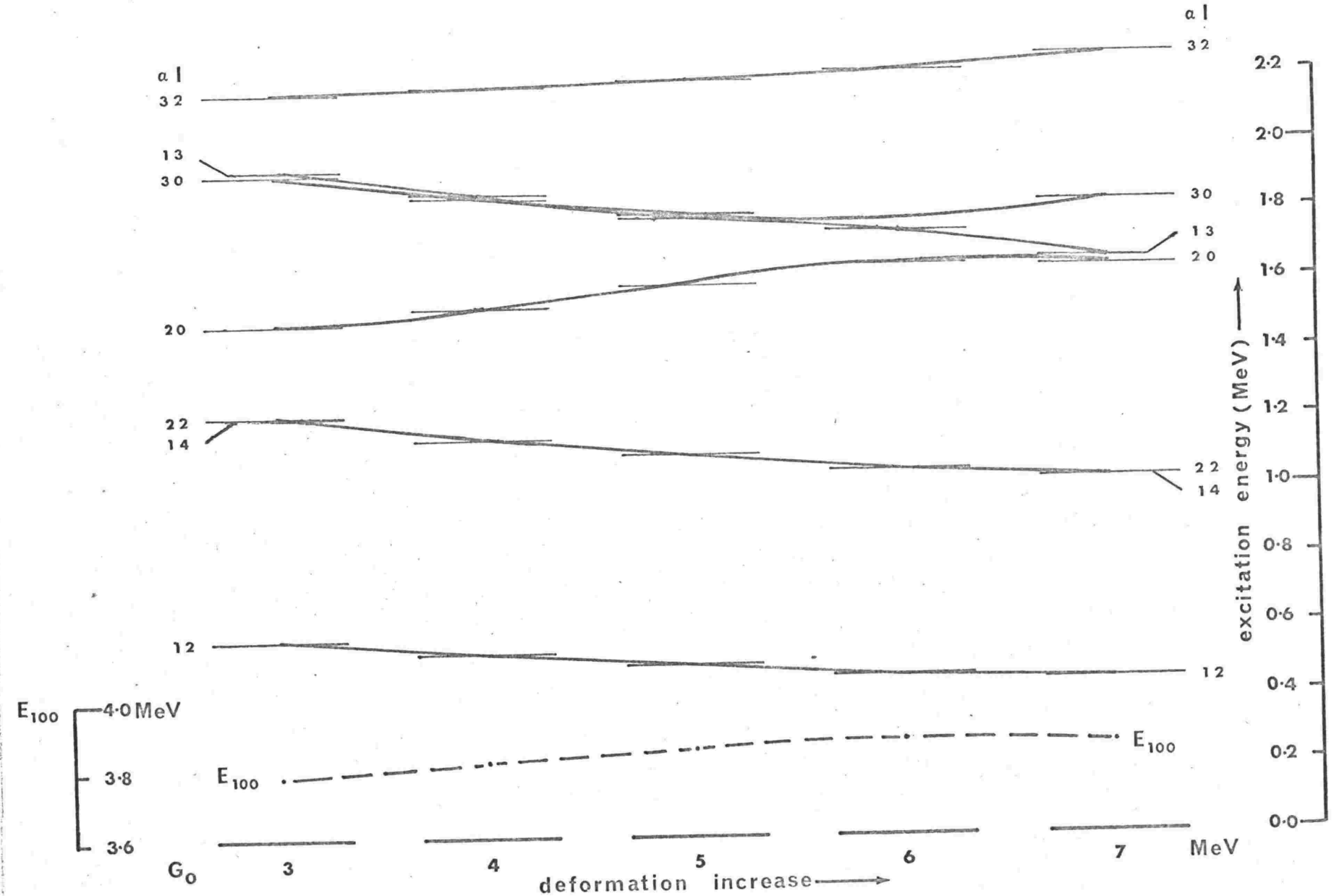

FIG. 6.2 Variation of eigenvalues with G_o in numerical solution.

C = 78.5, f = 7.283, S_E = 2.745, Δ_{p0} = 0 MeV; a = 0.25, $\bar{\beta}$ = 0.1955; B = 91.2 MeV^{-1}

Fig. 6.2 shows the variation of eigenvalues of states (αI) with G_0. This is in conflict with a similar study with Kumar's potential[8], eq. (5), and is due to the enforcement of condition (9). Without the addition of (11), condition (9) cannot be maintained (with $G_1 = G_2 = 0$), and an increase in G_0 is merely an effective decrease in the parameter C. The γ-independent potential (except for the f term) of fig. 6.2 allows degeneracy of the (22) and (14) states, as expected[10]. The effect of changes in G_0 upon the properties of the eigenfunctions is very small and regular. There is virtually no change in relative intensities of K-components of wave functions and the electromagnetic properties corresponding to those tabled in 6.1 undergo only slight increases with G_0.

The effect of different values for Δ_{p0} is much more interesting. The variation of eigenvalues with Δ_{p0} (fig. 6.3) demonstrates that it is possible to get two excited 0^+ levels close together, although to the detriment of the $0^+ - 2^+$ spacing. Figs 6.4 and 6.5 illustrate the wave function change in going through the point of closest approach of E_{20} and E_{30}. At this value of Δ_{p0} the prolate and oblate maxima in intensity will be equal so that A_{200} and A_{300} roughly resemble each other. One finds that the position of the secondary maximum of A_{200} always follows the potential minimum (while preserving its orthogonality property - radial node at $\sim \bar{\beta}$) and that of A_{300} (orthogonality demonstrated roughly by an angular node at $\sim 30^o$) opposes it. There is no crossing of levels. This verifies an assumption of Kregar and Mihailović[9] that 0^+, states may correspond to oblate ground states. In view of the small effect that the f term of the MS-potential had in fig. 6.2, it seems unlikely that

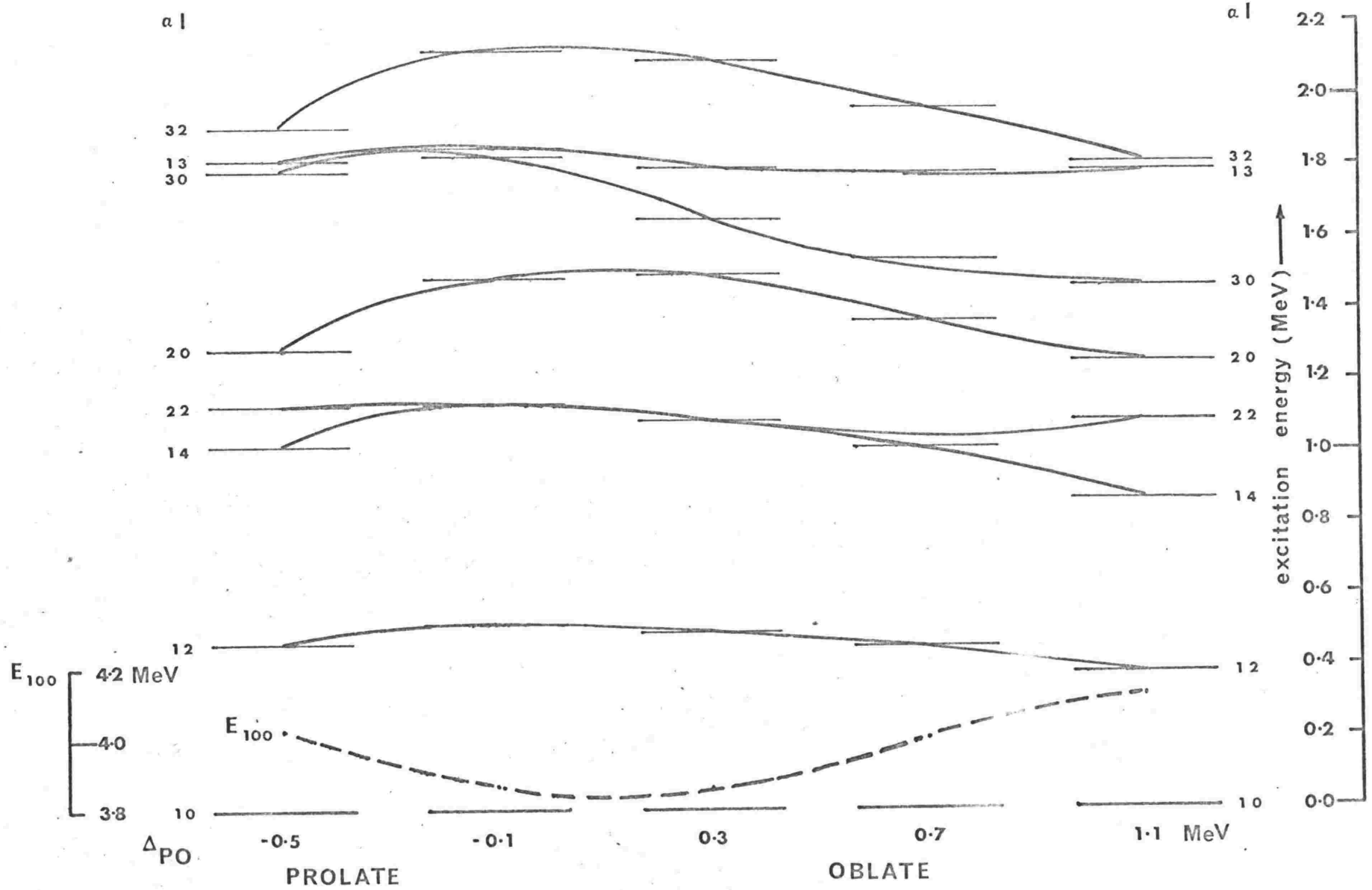

FIG. 6.3 Variation of eigenvalues with Δ_{PO} in numerical solution.

C = 78.5, f = 7.283, S_E = 2.745, G_0 = 4 MeV; a = 0.25, $\bar{\beta}$ = 0.1955; B = 91.2 MeV^{-1}

B(E2; 12 $\longrightarrow$ 10)	16.029	15.331	16.126	16.562	17.730	$.e^2.10^{-50}$ cm^4
B(E2; 22 $\longrightarrow$ 10)	0.167	0.006	0.094	0.273	0.721	$.e^2.10^{-50}$ cm^4
B(E2; 22 $\longrightarrow$ 12)	23.560	26.063	26.658	24.850	17.522	$.e^2.10^{-50}$ cm^4
R_1	1.470	1.700	1.653	1.500	0.988	
R_2	0.007	0.000	0.003	0.011	0.041	
Q(12)	-0.380	-0.107	0.121	0.339	0.642	$.e.10^{-24}$ cm^2
	K-intensities					
state αI						
12 K = 0	0.863	0.764	0.663	0.567	0.425	
K = 2	0.137	0.236	0.337	0.433	0.575	
22 K = 0	0.238	0.310	0.417	0.519	0.686	
K = 2	0.762	0.690	0.583	0.481	0.314	
32 K = 0	0.813	0.782	0.750	0.653	0.476	
K = 2	0.187	0.218	0.250	0.347	0.524	
14 K = 0	0.818	0.720	0.590	0.461	0.284	
K = 2	0.143	0.214	0.282	0.327	0.362	
K = 4	0.039	0.066	0.128	0.212	0.354	
Δ_{PO}	-0.5	-0.1	+0.3	+0.7	+1.1	MeV
	PROLATE			OBLATE		

TABLE 6.1 Some numerical eigenfunction properties from ^{114}Cd parameters.

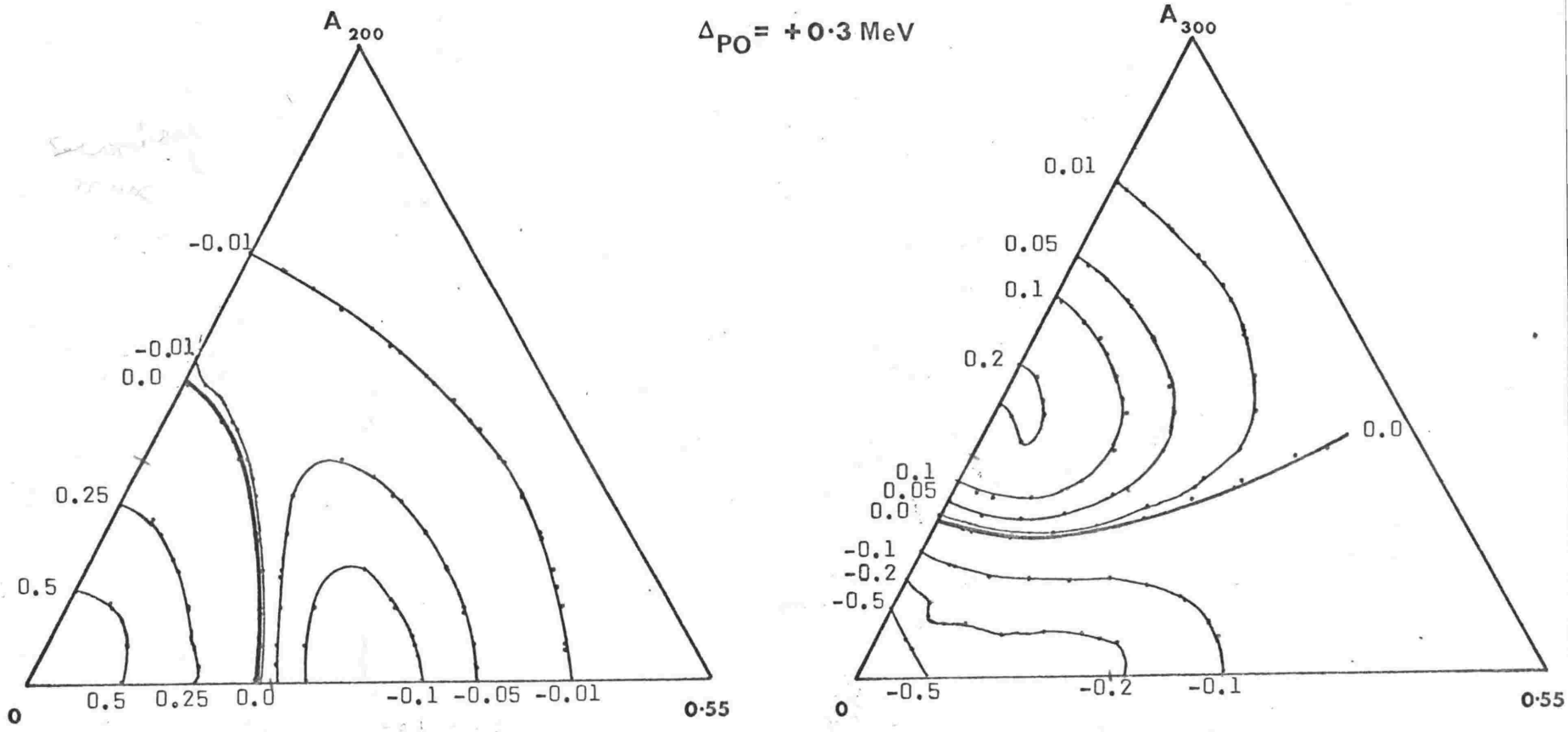

FIG. 6.4 $0^{+}{}'$ and $0^{+}{}''$ eigenfunctions of numerical solution corresponding to fig. 5.3.

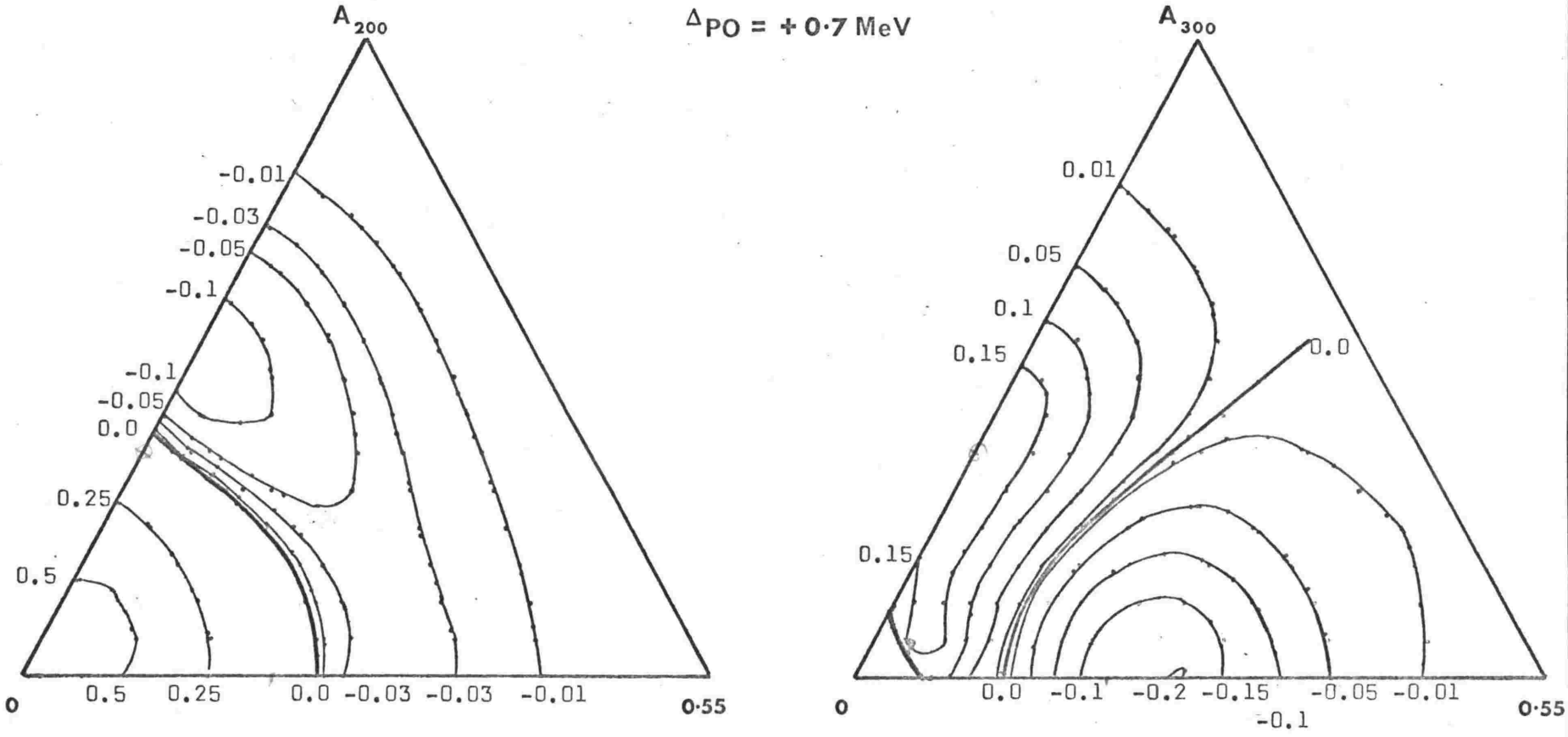

FIG. 6.5 $0^{+}{}'$ and $0^{+}{}''$ eigenfunctions of numerical solution corresponding to fig. 5.3.

the asymmetry in shape transition is due to it. The ground state A_{100} remains little changed by small variations in Δ_{PO}, and corresponds to that of the harmonic oscillator (fig. 5.3).

The mechanism of change with Δ_{PO} in the case of spin 2 eigenfunctions is different. As can be seen in figs 5.4 and 5.5 of the oscillator case, these eigenfunctions possess distinct prolate (K = 0) and oblate (K = 2) components and, as one would expect, changes in Δ_{PO} are accompanied by shifts in intensities of K-components. This is demonstrated in table 6.1 where, after the electromagnetic properties, intensities of different K-components are given for states (αI). Table 6.2 contains extreme model values for these intensities and one can see that the transitions to the extreme models is smooth. It is evident that α = 1,3 for I = 2 corresponds to the potential shape whereas the (22) state opposes it. Again, as in the spin 0 cases, a prolate shape is preferred. Interplay between K-components of spin 4 is similar. From the analysis, it is apparent that the correspondence argument of Sakai[14] (section 5.4) holds although the quasi-K spin formalism is not obvious. In particular, the value of B(E2; 2,2$\rightarrow$1,2) which is zero for good K (interband transition) reduces rather slowly with Δ_{PO}, and is disproportionately much larger than B(E2; 1,2$\rightarrow$1,0) when compared to ^{114}Cd values (see table 6.3). It could well be that the quasi-K bands result from some other effect.

Although the preceding analysis leads to an understanding of various nuclear properties, it should now be evident that the application of the model to the Cd triplet is not going to reproduce good results. The requirements of electromagnetic properties and level structure are in conflict with each other as well as within themselves, and although this

TABLE 6.2 Intensities of K-components for models

state (αI)		prolate rotator	harmonic vibrator	oblate rotator
12	K = 0	1.0	0.725	0.250
	K = 2	0.0	0.275	0.750
22	K = 0	0.0	0.339	0.750
	K = 0	1.0	0.661	0.250
32	K = 0	1.0	0.725	0.250
	K = 2	0.0	0.275	0.750
14	K = 0	1.0	0.618	0.140
	K = 2	0.0	0.275	0.313
	K = 4	0.0	0.107	0.547
Δ_{PQ}		-ve	0	+ve

point will be discussed later (section 6.6), the application of this model to the Cd nuclei will not be pursued.

6.4 Analytic Solution

The following values for analytic solution parameters which are given by Suárez[5] were used to generate the level structure and nuclear properties shown in fig. 6.6 and table 6.3.

	$\bar{\gamma}$	μ	Δ
^{112}Cd	20^{o}	0.5	4.0
^{114}Cd	18^{o}	0.5	3.5
^{116}Cd	18^{o}	0.5	4.5

(16)

The level structure is normalised to the spacing of the first excited (1012) state.

It appears that the eigenvalues obtained yield a structure more closely allied to the experimentally determined spectrum than the numerical analysis, a fact which is surprising when one compares the relative numbers of approximations made. In particular, the 4^{+} (1014) state can easily be made considerably higher in energy than the $2^{+}{}'$ (1022) state, a feat which other models find impossible or have limited success with. One other salient feature of the analytic solution is the close proximity of a 3^{+} (1013) state to levels which are near the two-phonon triplet. The electromagnetic properties shown in table 6.3 are reasonable although agreement for the $B(E2;\ 2^{+}{}' \rightarrow 0^{+})$ value is bad.

Because the analytic solution and its form of potential operator (and similar treatments such as the Davydov model[18]) has been widely

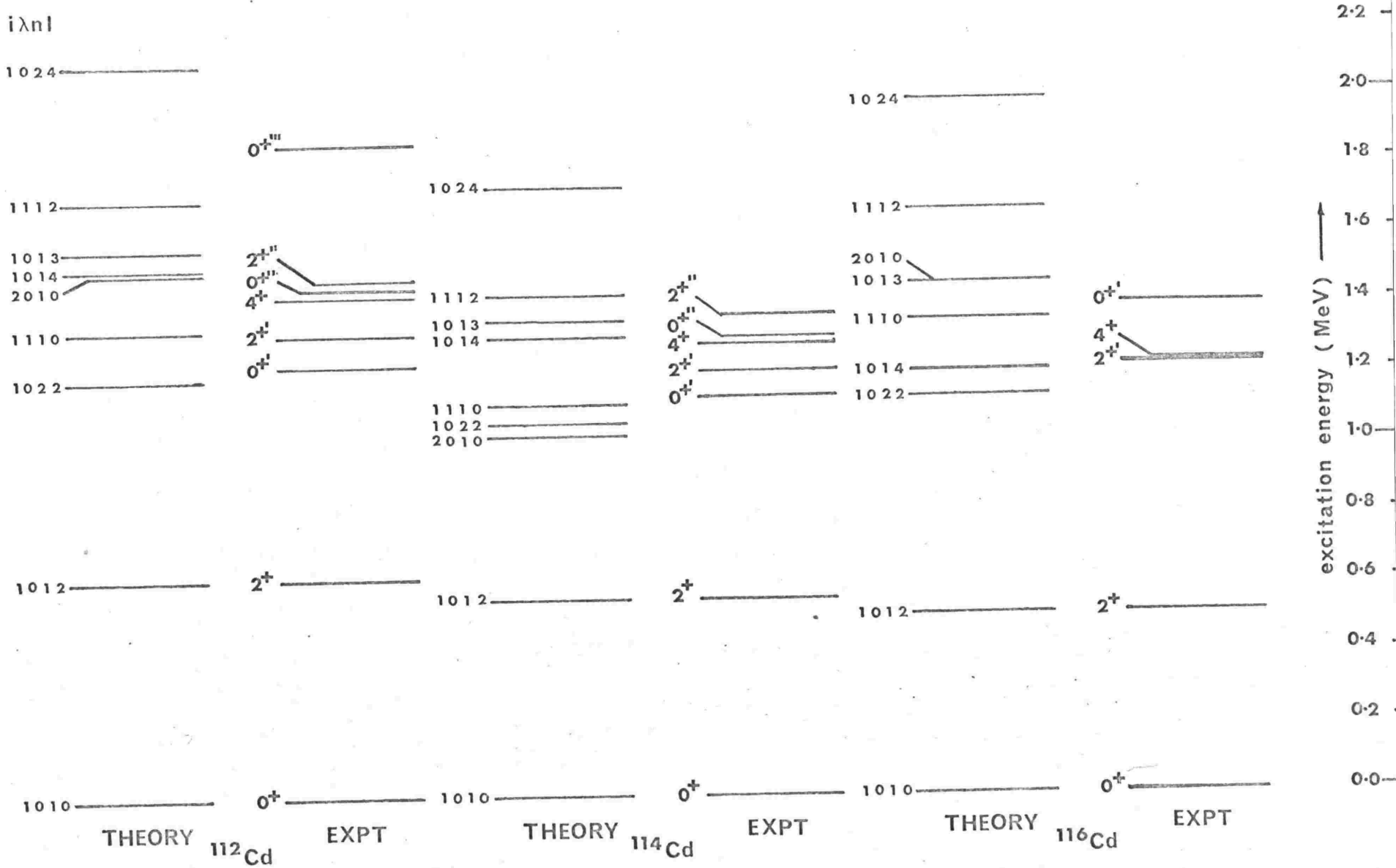

FIG. 6.6 Analytic solution for Cd isotopes.

	^{112}Cd		^{114}Cd		^{116}Cd	
	THEORY	EXPT	THEORY	EXPT	THEORY	EXPT
$B(E2;\ 2^+ \rightarrow 0^+)$	19.00	10.48±0.42	18.55	11.52±0.46	22.32	11.62±0.46
$B(E2;\ 2^{+\prime} \rightarrow 0^+)$	1.83	0.21±0.30	1.50	0.19±0.03	1.85	0.38±0.06
$B(E2;\ 2^{+\prime} \rightarrow 2^+)$	6.81	14.78±1.61 6.92±1.08	5.39	8.12±2.27	5.52	7.30±2.00
R_1	0.36	1.41±0.21 0.66±0.13	0.29	0.70±0.23	0.25	0.63±0.20
R_2	0.27	0.01±0.02 0.03±0.05	0.28	0.02±0.01	0.34	0.05±0.02
Q(12)	-0.40		-0.48	-0.49±0.23 [19]	-0.53	-0.93±0.23 [20]

TABLE 6.3 Comparison of analytic and experimental electromagnetic properties. The B(E2) values are in units of $e^2.10^{-50}$ cm^4 and experimental results are taken from ref.[2]. The Q(12) moments are in $e.10^{-24}$ cm^2 units.

used, it is important that it should be fully investigated. The numerical method should be valuable in this respect.

6.5 Comparison of Analytic and Numerical Solutions

The potential operator (eq. 5.13) used in the analytic solution of the collective Hamiltonian does not conform strictly to the symmetry requirements adhered to in the numerical method. However, the application of the numerical technique to a Hamiltonian with the analytic potential should still produce meaningful results regarding the assumptions and approximations inherent in the analytic procedure. This has been tested with the potential operator applicable to ^{114}Cd. With the parameter values given in (16), the equivalent parameters for use in the numerical solution are (with $\hbar = 1$)

$$C = E_{2^+}/(\mu\bar{\beta})^2 = 58.40 \text{ MeV}$$

$$B = C/E_{2^+}^2 = 187.56 \text{ MeV}^{-1} \tag{17}$$

with the assumption that the excitation energy of the first 2^+ state is given by

$$E_{2^+} = (C/B)^{\frac{1}{2}} \text{ MeV} \tag{18}$$

The potential operator takes the form

$$V(\beta,\gamma) = \tfrac{1}{2}C\left[(\beta-\bar{\beta})^2 + (\mu\bar{\beta})^4\Delta^2\,\frac{(\gamma-\bar{\gamma})^2}{\beta^2}\right] \tag{19}$$

and the prolate-oblate difference for ^{114}Cd is

$$\Delta_{PO} = -0.375 \text{ MeV} \tag{20}$$

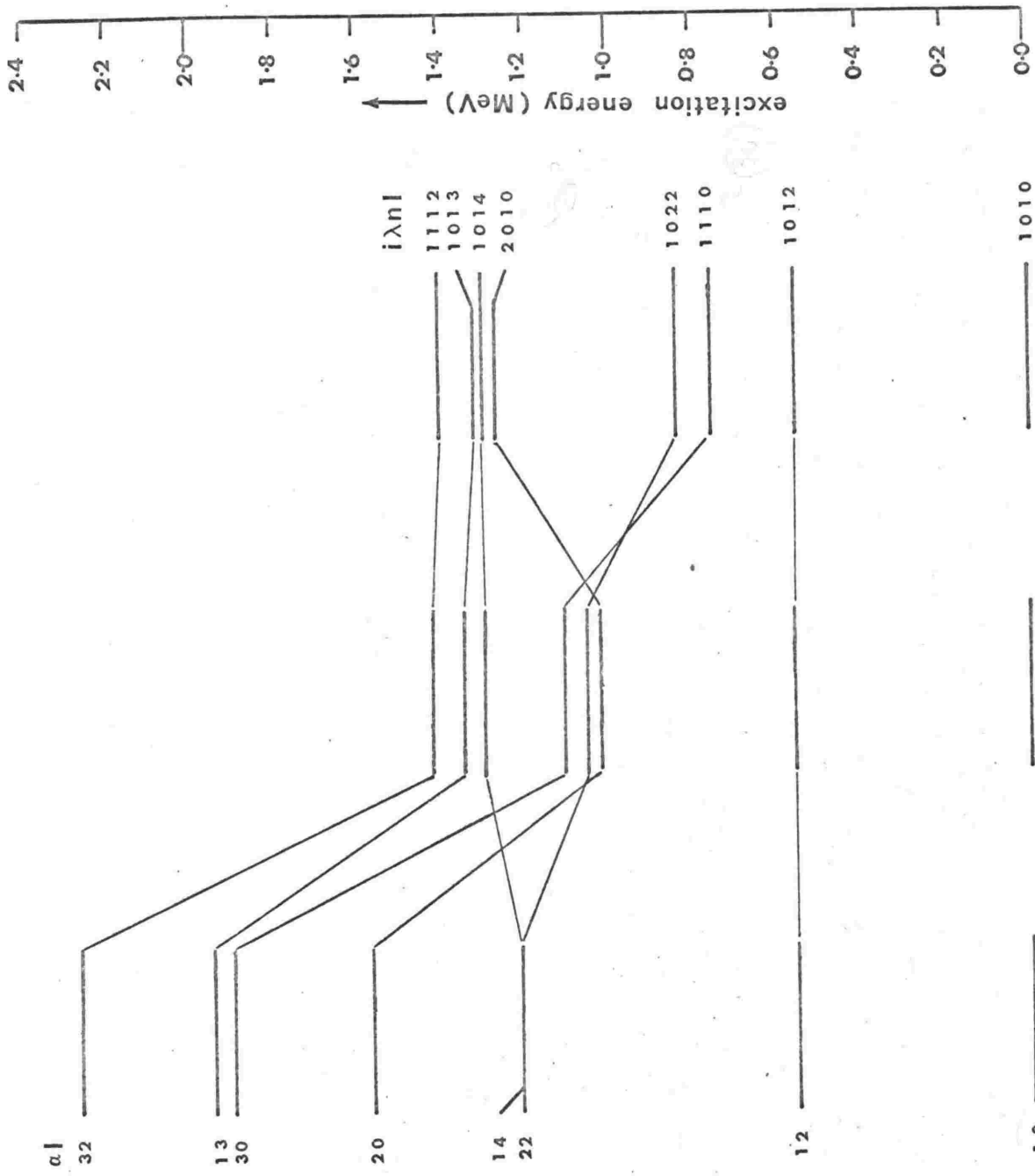

FIG. 6.7 - see text for explanation.

state		intensities of K-components					
αI	(iλnI)	K = 0		K = 2		K = 4	
10	(1010)	1.000	(1.000)				
12	(1012)	0.743	(0.943)	0.257	(0.057)		
22	(1022)	0.325	(0.000)	0.675	(1.000)		
14	(1014)	0.623	(0.564)	0.270	(0.435)	0.106	(0.001)
20	(2010)	1.000	(1.000)				
30	(1110)	1.000	(1.000)				
13	(1013)			1.000	(1.000)		
32	(1112)	0.739	(0.806)	0.261	(0.194)		

B(E2; 12 ⟶ 10) = 16.45 (18.55) B(E2; 22 ⟶ 10) = 0.007 (1.50)

B(E2; 22 ⟶ 12) = 23.39 (5.39) Q(12) = 0.040 (-0.48)

TABLE 6.4 Numerical and analytic solution comparison for ^{114}Cd. Figures in parenthesis are those obtained in the analytic procedure; others result from use of the analytic potential function in the numerical method. The B(E2)'s are in $e^2.10^{-50}$ cm^4 units and Q(12) is in e.b units.

In the analysis, the γ-dependent part of the potential operator was made to vanish at $\beta = 0$.

The resulting level structure, normalised to E_{2^+}, is shown in fig. 6.7(a) and some eigenfunction properties are listed in table 6.4. For comparison, fig. 6.7(b) is the ^{114}Cd analytic solution which was first given in fig. 6.6 and the figures in parenthesis of table 6.4 are corresponding eigenfunction properties. It is immediately apparent that the level structure and properties of eigenstates closely resemble those given in fig. 6.3 and table 6.1 for comparable values of Δ_{PO} and that the analytic solution of fig. 6.5 is misleading. This casts doubt upon the validity of the approximations used in the analytic method, and prompts an examination of these.

The success of the truncation of the Taylor expansion of the β-dependent potential plus the separation term

$$V_\Lambda(\beta) = \tfrac{1}{2}C(\beta-\overline{\beta})^2 + \frac{\hbar^2(\Lambda+2)}{2B\beta^2} \qquad (21)$$

is highly susceptible to the variable p, which is tabulated in table 6.5. These values, corresponding to the analytic solution shown in fig. 6.6 vary from 0.9 to 1.25 for ^{114}Cd eigenstates and, as can be seen from fig. 6.8, the resulting oscillator well differs considerably from the original well for $p<1$ (i.e., $(\Lambda+2) < 0$). The lines drawn across the well indicate the mean amplitude of β-vibrations and hence the position of the eigenstate. If $V_\Lambda(\beta)$ given in eq. (21) was used for $p<1$ cases (1010 and 2010 eigenstates), the eigenvalues would be reduced and the 2010 state would appear lower in the normalised structure. Obviously, this is not the reason for the inconsistencies between fig. 6.7(a) and 6.7(b).

state $i\lambda n I$ (αI)	$\langle \sin^2(\gamma - 2\pi k/3) \rangle$ k = 1	k = 2	k = 3	$\langle \sin^2(3\gamma) \rangle$	p
1010 (10)	0.8432(0.9502)	0.4609(0.2763)	0.1959(0.2735)	0.5118(0.6592)	0.9025(0.9895)
1012 (12)	0.8432(0.9494)	0.4609(0.2815)	0.1959(0.2691)	0.5118(0.6588)	1.0688(1.1285)
2010 (20)	0.8432(0.9508)	0.4609(0.2836)	0.1959(0.2655)	0.5118(0.6574)	0.9025(0.9889)
1022 (22)	0.8432(0.9489)	0.4609(0.2708)	0.1959(0.2803)	0.5118(0.6579)	1.1823(1.1867)
1110 (30)	0.6471(0.9018)	0.4832(0.2872)	0.3697(0.3109)	0.4512(0.3846)	1.1935(1.1712)
1014 (14)	0.8432(0.9494)	0.4609(0.2774)	0.1959(0.2732)	0.5118(0.6608)	1.2307(1.2712)
1013 (13)	0.8432(0.9740)	0.4609(0.2630)	0.1959(0.2630)	0.5118(0.8056)	1.2398(1.2744)
1112 (32)	0.6471(0.9480)	0.4832(0.2872)	0.3677(0.2647)	0.4512(0.6456)	1.2527(1.2883)

TABLE 6.5 Numerical and analytic solution comparison for ^{114}Cd.

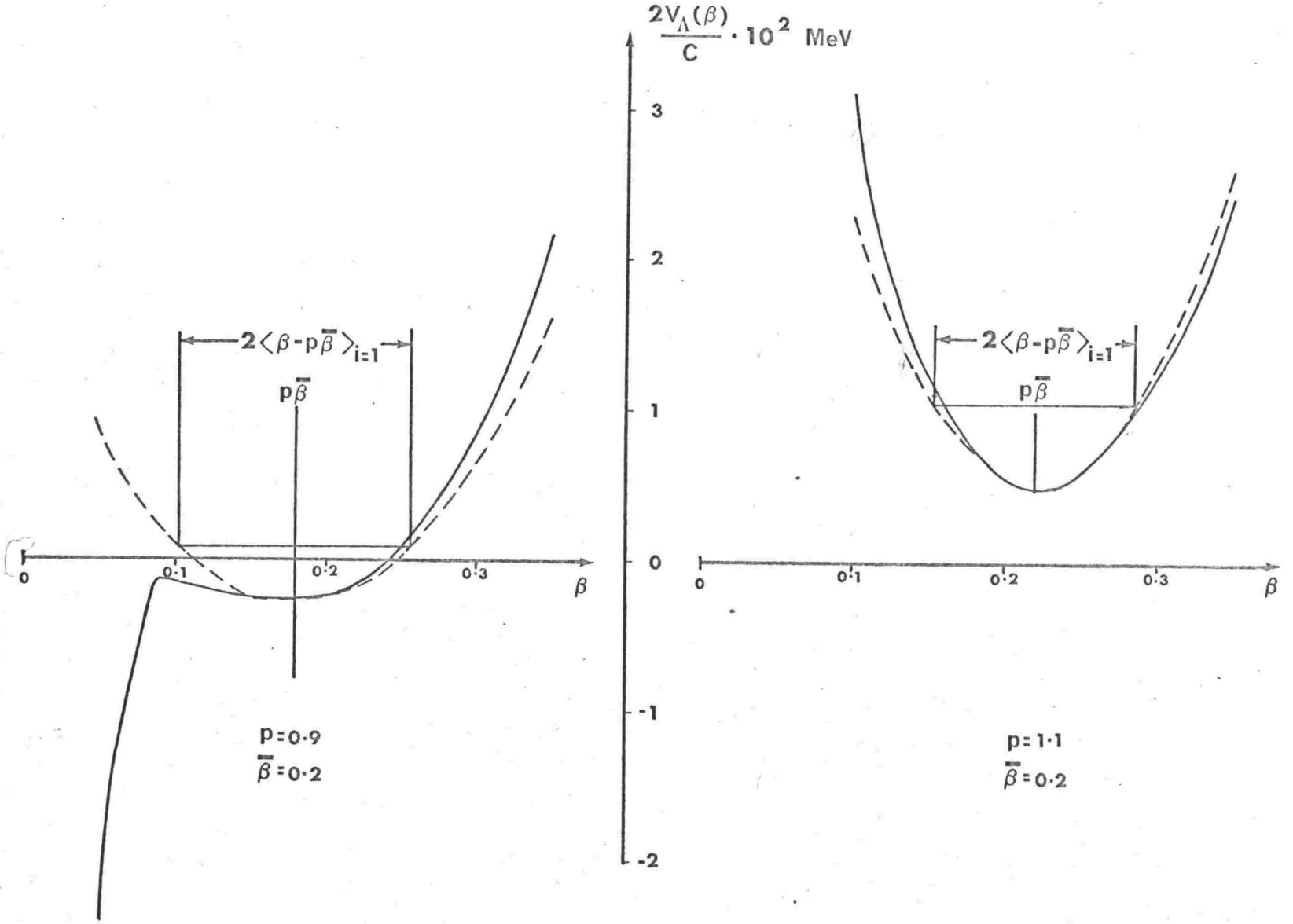

FIG. 6.8 Truncated Taylor expansion of analytic potential with separation term.

Also listed in table 6.5 are expectation values for moments of inertia used in the analytic solution, and, for comparison, moments calculated with the numerically determined eigenfunctions (and potential operator (19)) are tabulated in parenthesis. The latter expectation values are consistent with the potentials of section 6.3, and one might therefore expect that inaccurate expectation values of moments of inertia could destroy the equivalence of solutions. In the logical extension of this idea, the numerically determined expectation values of moments were substituted into the analytic method and eigenvalues computed. The resulting level structure is fig. 6.7(c) and the corresponding values of p are given in parenthesis in table 6.5. As well as the unrealistic level structure obtained, the K-component intensities of the eigenfunctions disagree even more with those of the full numerical analysis.

It is surprising that the expectation values of moments of inertia obtained with the numerical eigenfunctions are almost constant. If expressed in terms of a fixed angle $\bar{\gamma}$, the value of the angle $\sim 26^{o}$ and this is equal to $\bar{\gamma}$ used in the Davydov model[15] for ^{114}Cd.

The main reason for the inconsistency of analytic and numerical methods must therefore lie in the separation of γ and θ_i (Euler angles) dependency in the eigenfunctions. Although both techniques separate the θ_i dependency, in the analytic treatment the coefficients of expansion of the rigid rotator wave functions are independent of (β,γ). The different K-components of numerically determined eigenfunctions clearly show that this is not justified. In the case of well-deformed prolate nuclei, the approximation would probably hold quite well and the analytic treatment could be used successfully. However, where K is a bad quantum number, the analytic model will be misleading if applied.

6.6 Conclusion

The present application of a collective model to the Cd nuclei has not been successful although the potential used in the numerical analysis provided a good approximation to those obtained from single-particle wave functions. To merely state that the approximations to mass parameters given in eq. (5.10) cannot be valid does not greatly improve certain aspects of level structure. In particular, Kumar and Baranger[8] have computed mass parameters from single-particle wave functions for heavy-mass vibrational nuclei (small Δ_{PO}) and have failed to raise the (1,4) state sufficiently higher in energy than the (2,2) state. However, the same analysis does predict non-zero Q(1,2) moments for zero Δ_{PO} and this must be a direct consequence of (β,γ) dependency of mass parameters. A recent paper[16], published while the preceding work was in progress, contains a re-examination of this analysis from which Kumar has stressed the importance of Δ_{PO} with regard to nuclear structure, and the deformation dependency of inertial parameters. It is probable that the dependency of these parameters is of particular importance for small values of Δ_{PO}, but doubtful that this extension will reproduce ^{114}Cd nuclear structure.

A further complication may be present in Cd nuclei as some of the states about the position of the two-phonon triplet may be a result of non-collective excitations (adiabatic approximation violation), such as pairing, or a mixture of excitation modes. If this is true, and one ignores the 0^+ and the lower 2^+ states at the triplet energy, then the results of a fermion-system calculation of Sorenson[13] would easily be reproduced by the numerical analysis of the Bohr Hamiltonian. However, the choice of non-collective states is not obvious and lacks experimental evidence.

Tamura and Udagawa[17] have applied the HRPA to particle-hole interaction for a two-phonon description of the ^{114}Cd level structure and, although some states are reversed in order, have obtained a quintuplet of states at the two-phonon triplet energy. They have also had reasonable success with the electromagnetic properties of the states. It would therefore seem that it is with this technique that a good model description of the Cd nuclei will be obtained.

REFERENCES

1 T. Tamura and T. Udagawa, Phys. Rev. 150 (1966), 783

2 W.T. Milner, F.K. McGowan, P.H. Stelson, R.L. Robinson and R.O. Sayer, Nucl. Phys. A129 (1969), 687

3 D.R. Bes and G.G. Dussel, Nucl. Phys. 135 (1969), 1

4 K. Kumar, Nucl. Phys. A92 (1967), 653

5 J.F. Suárez, Nuovo Cimento 62B (1969), 109

6 W.D. Myers and W.J. Swiatecki, Nucl. Phys. 81 (1966), 1
UCRL-11980 (1967)

7 A. Bohr, Mat. Fys. Medd. Dan. Vid. Selsk. 26 (1952), no. 14

8 K. Kumar and M. Baranger, Nucl. Phys. A122 (1968), 273

9 M. Kregar and M.V. Mihailović, Nucl. Phys. A93 (1967), 402

10 L. Wilets and M. Jean, Phys. Rev. 102 (1956), 788

11 L. Grodzins, Phys. Lett. 2 (1962), 88

12 G. Gneuss, U. Mosel and W. Greiner, Phys. Lett. 30B (1969), 397

13 B. Sorenson, Nucl. Phys. A142 (1970), 411

14 M. Sakai, Nucl. Phys. A104 (1967), 301

15 E.Y. de Aisenberg and J.F. Suárez, Nucl. Phys. A97 (1967), 529

16 K. Kumar, Phys. Rev. C, 1 (1970), 369

17 T. Tamura and T. Udagawa, Nucl. Phys. 53 (1964), 33

18 A.S. Davydov, Nucl. Phys. 24 (1961), 682

19 J.J. Simpson, D. Eccleshall, M.J.L. Yates and N.J. Freeman, Nucl. Phys. A94 (1967), 177

20 R.G. Stokstad, I. Hall, G.D. Symons and J. de Boer, Nucl. Phys. A92 (1967), 319

Chapter Seven

CONCLUDING REMARKS

7.1 Summary

The aims of the present investigations were to study the decay of the three odd-odd isotopes ^{112}Ag, ^{114}Ag and ^{116}Ag, and to relate the results obtained to predictions of nuclear models which have been successfully applied in other regions of the periodic table.

Because these Ag isotopes all have short half-lives, special experimental techniques have been adopted or developed to facilitate data acquisition and analysis. The isotopes have been produced by fast neutron irradiation. Since the neutron flux was low and the production cross sections small, a pneumatic system was used to transport samples from irradiation to counting positions. The transport system, plus a beam stop unit and associated detection devices, was automated to permit recycling of the irradiation-detection process. Methods adopted in the reduction of background count rates included the use of a lead castle, the beam stop and efficient neutron shielding.

Many of the principles and methods used in the analysis of experimental data have been outlined, with particular emphasis on the requirements of the present study. These descriptions have been oriented such that methods given in the sections on experimental results can, if necessary, be pursued in depth.

The measured half-life of ^{112}Ag was long enough to permit its activity to be chemically separated from the reaction products formed by fast neutron activation of natural elements of Cd and In. 76 γ-rays were detected from the subsequent decay of ^{112}Ag and all but 12 of these were assigned in a level structure of ^{112}Cd involving 26 excited states. The results of three other studies of the decay of ^{112}Ag (the first since

1962) were published while the present investigation was in progress and, as extensive Ge(Li)-Ge(Li) coincidence measurements were included, the work presented in this thesis was interpreted in the light of these reports. The present study has led to more accurate level energies and the assigning of 8 γ-rays as new transitions between levels of ^{112}Cd. γ-γ angular correlations have been measured for major γ-rays in coincidence with the 617 keV transition, and these have been used to predict spins and parities of some excited levels. Cross sections for the production of ^{112}Ag by (n,p) and (n,α) reactions were measured, and the ^{112}Cd (n,p)^{112}Ag value was compared to that expected from statistical model calculations.

The nuclides ^{114}Ag and ^{116}Ag were produced by (n,p) reactions on natural and isotopically-enriched Cd metal samples. As the measured half-lives were very short (4.5 sec and 2.5 min respectively) and their production cross section small, the irradiation-detection process had to be cycled many times to obtain statistically significant data. Because of low yields, γ-γ coincidence measurements gave no new information on the decay of these isotopes. The study of the decay of ^{114}Ag revealed 11 γ-rays, 9 of which were satisfactorily placed in a level structure previously determined by conversion electron and bent-crystal γ-ray spectrometry of the ^{113}Cd(n,γ)^{114}Cd reaction. This level scheme was adopted because of greater accuracy of these methods. However, the value of studying level structure populated by β-decay of nuclides, for which different selection rules are invoked, was demonstrated by the evidence found to suggest the existence of a possible level doublet (at 1305 keV) in the structure of ^{114}Cd. A measurement of the β-spectrum

of ^{114}Ag was made and because no branching in the transition was found, the measured γ-ray yield was combined with a (n,p) cross section interpolated from the ^{112}Cd(n,p)^{112}Ag value to normalise the feeding of the β-decay. The resulting decay scheme was consistent with a spin and parity of 1^+ for the ground state of ^{114}Ag.

The study of ^{116}Ag decay revealed 53 γ-rays, 36 of which were assigned in a scheme of 17 excited states which were mostly numerically constructed from the γ-ray data. Previous studies of ^{116}Cd level structure have determined 6 of the levels, but with low accuracy in the energy determination. Experiments designed to obtain the β-spectrum of ^{116}Ag decay failed because of low yields in the production of the isotope. A previous measurement of the β-decay was discounted because of the disagreement of the present γ-ray study with the quoted β- and γ-ray intensities. It therefore became necessary to obtain the β-ray branching using the same method employed for ^{114}Ag. The resulting decay scheme was similar to that for ^{112}Ag, and a consideration of log ft values of the β-decay has led to the assignment of 2^- for the ground state of ^{116}Ag.

A discussion of the ground state assignments for these odd-odd Ag isotopes in terms of the single-particle shell model revealed the complications of this region of the periodic table. No definite configuration could be chosen for ^{116}Ag, but the interruption of 2^- ground states by the 1^+ state of ^{114}Ag suggests a change of configuration from the ground state of ^{112}Ag.

Attempts to synthesise level structure typical of the Cd daughter nuclei with collective models failed, even though the low-energy structure is known to be vibrational. The more sophisticated model, based on a

numerical evaluation of collective energy, revealed that the cause was partially due to simplifications made for the inertial parameters. A simpler treatment, essentially an extension of the Davydov model, which apparently gave level structure in much better agreement, was shown to be misleading. When the additional assumptions inherent in this model were removed by combining the principles of the two models, a level scheme was obtained identical to the results of the numerical method. It is thought that the main reason for lack of success is due to the influence of non-collective excitations. However, the application of the numerical method to the nuclear potential function constructed for this study gave considerable insight into the transition between rotational and vibrational excitations, and the formation of band structure in the level schemes of nuclei.

7.2 Suggestions for Further Research

Requirements necessary to finalise the decay schemes of the three Ag isotopes studied have been discussed in the appropriate sections of this thesis. Briefly, the following conclusions can be drawn:

(i) knowledge of the ^{112}Ag decay is detailed, although a conversion electron study would be of value.

(ii) an investigation is necessary to check the possibility that the 0^+ level at 1305 keV of ^{114}Cd is a doublet.

(iii) the β-ray spectrum of ^{116}Ag should be measured directly, and coincidence measurements should be made of the γ-ray spectrum to confirm the proposed level scheme.

The second point could easily be satisfied by results of coincidence measurements on γ-rays and conversion electrons produced in the $^{113}Cd(n,\gamma)^{114}Cd$ reaction. The work indicated in the third requirement is more difficult because of the low yield associated with the production of ^{116}Ag. This could be overcome by using higher fast-neutron fluxes in the $^{116}Cd(n,p)^{116}Ag$ reaction. However, as the decay properties of the Ag isotopes are becoming firmly established, production by fission and fast chemical separation holds more promise. Although detailed numerical analysis and stringent experimental conditions would be necessary to isolate Ag activities from each other, the advantage of greater yields for these isotopes should prove rewarding. The method could also be extended to study the decay schemes of Pd isotopes that are the parents of the Ag nuclides investigated in this work. This could lead to a better understanding of the Ag nuclei in terms of the single-particle shell model.

Complementary studies of γ-rays produced in reactions such as $(x,x'\gamma)$ should be carried out, particularly as the operation of different sets of selection rules permit the excitation of levels not populated by β-decay. However, access to the Cd isotopes studied is limited because the number of stable isotopes suitable as targets decreases as the neutron number becomes larger. It is probable that the most detailed information about level structure in this region will be gained from continued investigation of decay schemes of radioactive nuclei.

ACKNOWLEDGEMENTS

During the course of this study, a great number of people have assisted the author in various ways. A record of appreciation is due to his supervisors for the help which they have freely given: Professor N.G. Chapman, who has provided encouragement and guidance; Dr R.M. Freeman (now of Institut de Recherche Nucleaire, Strasbourg) for the initial introduction to the work; Professor D. Walker who, as head of the Physics Department, Victoria University of Wellington, permitted most of the work to be done outside the University; and Dr T.A. Rafter, director of the Institute of Nuclear Sciences, for a willing release from normal duties and for the keen interest he has shown in the study.

The loan of equipment, particularly the Ortec Ge(Li) detector, from the Physics Department of Victoria University of Wellington, and the provision of isotopically-enriched Cd samples and tritium targets by the Department, is gratefully acknowledged, as is the encouragement received from members of the Nuclear Physics group.

The author is indebted to members of the staff of the Institute of Nuclear Sciences for their support during this work, and would particularly like to thank Mr G.J. McCallum, head of the Accelerator Physics section, who has provided assistance and guidance with practical details, and Dr M.R. Manning for valuable discussions on the theoretical aspects of the thesis.

It is a pleasure to thank Miss S. Stuart for her diligent typing of this thesis.